Continental rift formation and transition to oceanic seafloor spreading: a case study of the Afar triple junction

De vorming van continentale riftzones en de transitie naar mid-oceanische spreidingsruggen: een studie van de Afar driehoek

(met een samenvatting in het Nederlands)

Proefschrift

ter verkrijging van de graad van doctor aan de Universiteit Utrecht op gezag van de rector magnificus, prof.dr. G.J. van der Zwaan, ingevolge het besluit van het college voor promoties in het openbaar te verdedigen op vrijdag 30 juni 2017 des middags te 12.45 uur

door

Alessio Lavecchia

geboren op 14 mei 1985 te Terlizzi, Italië

Promotor:	Prof. dr. S. Cloetingh
Copromotoren:	Dr. F. Beekman Dr. S. Clark

This thesis was partly accomplished with financial support from Simula School of Research and Innovation, Fornebu, Norway.

"O frati," dissi, "che per cento milia
perigli siete giunti a l'occidente,
a questa tanto picciola vigilia
d'i nostri sensi ch'è del rimanente
non vogliate negar l'esperïenza,
di retro al sol, del mondo sanza gente.
Considerate la vostra semenza:
fatti non foste a viver come bruti,
ma per seguir virtute e canoscenza".

"O brothers!" I began, "woe to the west
'Through perils without number now have we reach'd;
'To this the short remaining watch, that yet
'Our senses have to wake, refuse not proof
'Of the unpeopled world, following the track
'Of Phoebus. Call to mind from whence ye sprang:
'Ye were not form'd to live the life of brutes,
'But virtue to pursue and knowledge high."

Dante, Divina Commedia, Canto XXVI, Inferno
Translated by Rev. H. Cary, 1819

Members of the Reading Committee:

Prof. dr. R. Buck	Earth Institute, Columbia University, Palisades, NY
Prof. dr. G. Corti	Università degli studi di Firenze, Italy
Prof. dr. D.Dingwell	Ludwig-Maximilians Universität München, Germany
Prof. dr. T. Gerya	Department of Earth Sciences, ETH Zürich, Switzerland
Dr. C. Thieulot	Faculty of Geosciences, Utrecht University, Netherlands

The research presented in this thesis was carried out at Simula Research Laboratory, Fornebu, Norway, and the Tectonics Research Group, Department of Earth Sciences, Faculty of Geosciences, Utrecht University, the Netherlands.

This is Utrecht Studies in Earth Sciences volume 131

ISBN: 978-90-6266-472-6

Printed in the Netherlands by Ridderprint (www.ridderprint.nl), typeset in LibreOffice Writer by the author.

Cover: Cross-section showing viscosity field in one of the numerical experiments described in this research study (see Figure 5.4).

Table of Contents

Acknowledgements

This thesis is the final result of dedication, efforts and both professional and personal growth. During the last four years I have been through experience that helped me to mature, in so many different ways that I could have never imagined. This shaped me in a very different person from who I was when I left Italy, and it would have never happened without the help and support of all the people that crossed their path with mine.

First, I need to express my gratitude to my supervisors Fred Beekman, Stuart Clark, and Sierd Cloetingh, for offering me the possibility of pursuing my research in two institutes of high scientific profile like Simula Research Laboratory and Utrecht University, and working on a very challenging but inspiring project. In addition, special thanks go to Cedric Thieulot, for giving me the opportunity to work with him. His help has been fundamental for finalize my thesis, and I learned a lot from our work together. They have been people that marked my professional and personal growth, and it was a privilege to work with them. I really hope that we will have further opportunities to work together in the future.

My appreciation goes to Bjørn Rasmussen, for promoting the collaboration between Simula Research Laboratory and Utrecht University, giving me the opportunity to work with such high-profile people and making this PhD successful.

I would like to commend the members of my reading committee, Prof. Roger Buck, Prof. Giacomo Corti, Prof. Donald Dingwell, Prof. Taras Gerya and Dr. Cedric Thieulot. Their feedback greatly contributed in improving the quality of my thesis.

I would also like to thank professors Alfredo Caggianelli and Giorgio Ranalli, not only for the fruitful discussion that resulted in a significant improvement of my first paper relative to my PhD, but also because, thanks to their support in the past years, I fully realized that geosciences are much more than a job for me. I believe that any professional achievement I will reach in my life will be at least partly due to them, and for this I can never thank them enough.

During these four years I have shared experience with many different people, both in Oslo and in Utrecht. First of all, a special thanks to Johannes and Vamsi, with whom I shared an apartment and many pool games. Living with them was very fun, and even if they never managed to convince me to try cross country skiing, I really appreciated the effort. A special thank goes also to Badr Ghorbal, for all the support he gave me, and for introducing me to Sierd Cloetingh.

A big thank you to all the people with whom I shared my days at Simula Research Laboratory and Utrecht University: Antoine, Anouk, Attila, Damien, Dimitrios, Elisa, Ernst, Eszter, Inge, Jeremie, Jeroen, Jon, Julia, Katharina, Kristof, Liviu, Lukman, Lyudmyla, Magdala, Marcus, Milos, Nevena, Preben, Rui, Sagar, Shang Yu, Stefano, Thomas, Viviane and many others I am surely forgetting right now. All of you contributed in my growth during these years, and I will always be thankful for the opportunity I had to meet you all.

In the last year I met a very important person, who supported me in so many different ways, I could have never imagined. Thank you very much Kasia, for being at my side when I needed, supporting and pushing me to take out the best of myself. Everything would have proven much more difficult without you.

Acknowledgements

Un grazie enorme va ai miei genitori ed a mio fratello Fulvio. Questi anni lontano da casa sono stati duri senza di voi. Ma il vostro supporto ha reso possibile il raggiungimento di tutti i traguardi che mi ero prefissato, incluso questo. Perciò, sarò sempre grato a tutti voi.

Summary

Lithosphere extension, thinning and breakup are fundamental processes in geodynamics. During rift development, both the lithosphere and the mantle are involved in a coupled system in which the main mechanisms are heat transfer, active and passive mantle flow, far-field forces, viscous coupling between lithosphere and mantle flow, and magmatism. These mechanisms and the forces associated with them often vary during the rift evolution. Consequently, lithosphere rifting should be considered as an integrated thermo-mechanical process, involving a coupled lithosphere-mantle system, where different mechanisms act mutually and simultaneously. The presence of areas of lithospheric heterogeneities may determine variations in rifting location and style, but mantle plumes may also exert an important role.

Both features occur in Afar Rift, a region characterized by the transition from continental rifting features to seafloor spreading westwards. The Afar Rift is part of the East Africa Rift system, and represents the triple junction among the Main Ethiopian Rift, the Gulf of Aden and the Red Sea, separating the Nubia, Arabia and Somalia plates. The crystalline basement is composed of Neoproterozoic rocks, assembled and metamorphosed between 800 and 650 Ma, whose structure eventually influenced rifting location and evolution. The presence of a mantle plume has long been recognized in the region as an important factor influencing the tectonic activity and the extensive volcanism since the mid-Tertiary. The plume is considered as a part of the complex system called the African superplume.

The work presented in this thesis aimed at providing new insights in the role of lithospheric structure and mantle plumes on the development and evolution of rifting areas, with particular regard to the Afar Rift region. I included the study of Main Ethiopian Rift in my work, due to its greater structural simplicity compared to Afar Rift. The quantitative analysis of the area has been carried out by constructing numerical models where different physical interacting mechanisms are taken into account, with the aim to clarify specific aspects related to the initial and current phases of the Afar Rift evolution. The results of this work might also be applied to other rifting areas and contribute to give a better comprehension of breakup processes in the lithosphere, especially where rifting is accompanied by a marked volcanism.

The models constructed for this thesis are both thermo-rheological and thermo-mechanical, with particular emphasis to the effect of melts on the rheology of host rocks, at various depth in the lithosphere. The thermo-rheological model simulates the temperature variations in layered crustal sections, induced by melt emplacement. Of particular importance are the development and incorporation of novel methods that simulate metamorphism and crustal anatexis, induced by thermal perturbations. The combined effect of temperature and petrological variation and anatexis determines viscosity and rheological variations in the crust. I applied the model to the study of Main Ethiopian Rift, to better understand the evolution of the Ethiopian continental crust during the development of magma segments characterizing the axial rifting area. The thermo-mechanical model examines the evolution pattern of a continental lithosphere subject to extension, where the lithosphere is characterized by the presence of heterogeneities and impinged by a mantle plume. In this model I incorporated the partial melting of mantle materials in response to pressure and temperature variations. The aim of this model is to assess the importance of melts during the

evolution of rifting areas and distinguish the most favorable conditions that maximize their effects.

The results highlight the importance of lithospheric structure in the first phases of rifting development, whereas further stages may be more effectively influenced by the presence of mantle plumes, either in further focusing deformation along the lithosphere-controlled extension or in determining a diversion of previous rifts. An important conclusion is that under appropriate conditions melt presence may enhance the effectiveness of plume control.

In the East African area, the inherited basement structure may have exerted a primary control on initial rift location, even in presence of a melt-intruded and weakened lithosphere . This occurs in the case of Afar and Main Ethiopian Rift, where rifting areas are located in proximity of, but not directly above the estimated plume impact location against the lithosphere. Moreover, due to the uplifting of both rift shoulders (more accentuated in the Nubian Plateau than in the Somalian plateau), I suggest that the mantle plume impacted first the lithosphere in the Nubian Plateau region and subsequently spread across the whole area, thus also affecting the Somalian Plateau. The observations on volcanic activity in Afar highlight a beginning of volcanism in the Nubian Plateau region, followed by a migration toward the rift axis area. This fits the model of plume partial melting that I developed. However, the observed southeastward migration of volcanism is better explained by a variable topography of the lithosphere-asthenosphere boundary, with a thicker lithosphere in the Nubian region and a thinner lithosphere in the Somalian area.

The effect of lithosphere heterogeneities on rift axis localization occurs in combination with the melt-induced weakening of the crust and the lithosphere. This also explains the increased seismic activity on the rift areas. However, crustal anatexis cannot explain the widespread acidic volcanism in Afar, which can be explained better by processes of fractional crystallization of mafic, underplated melts, further contaminated by crust-derived melts.

At present day, the highest mantle thermal anomaly is located in the N-MER and may determine a further progression of the extensional tectonics towards continental breakup and seafloor spreading conditions. Based on the obtained results, I expect a further evolution of the area into conditions of seafloor spreading, in the same way as the Danakil microplate experiences today.

Samenvatting

Het uitrekken, verdunnen en opbreken (“riften”) van de lithosfeer zijn fundamentele geodynamische processen in de plaattektoniek. In de ontwikkeling van een rift speelt de interactie tussen lithosfeer en mantel een belangrijke rol, maar deze is nogal complex door dynamische variaties van de thermo-mechanische krachten en de rheologische processen die daarbij een rol spelen. De locatie en wijze van rifting wordt beïnvloed door zowel onregelmatigheden in de structuur van de lithosfeer als door de aanwezigheid van mantelpluimen.

Continentale rifting vindt momenteel plaats in de Afar Rift, een regio die geologisch gekenmerkt wordt door de overgang van de laatste fase van continentale opbreken naar de vorming van nieuwe oceanische lithosfeer. De Afar Rift vormt een driehoek tussen de Ethiopische Rift, de Golf van Aden en de Rode Zee, en is tevens de scheiding tussen de tektonische platen Nubia, Arabia en Somalia. Onder de Afar is ook een mantelpluim aanwezig, waarvan vermoed wordt dat die een invloedrijke rol speelt bij het optreden van de intense tektonische activiteit en de wijdverbreide vulkanische activiteit.

Het doel van deze studie was het met behulp van computermodellen bestuderen van de ontwikkeling van continentale rift zones, met de Afar Rift als studiegebied, en daarbij dan met name het analyseren en kwantificeren van de rol van pre-existente onregelmatigheden in de structuur van de lithosfeer en van de interactie tussen korst en lithosfeer als gevolg van de mantelpluim onder de Afar. Een nieuw aspect ten opzichte van eerdere modelstudies is de numerieke simulatie van rheologische veranderingen van korstgesteente als gevolg van metamorfisme, anatexis en het partieel smelten van onderliggend mantelgesteente. Met de nieuw ontwikkelde computermodellen zijn simulaties gemaakt van de interactie tussen de fysische, thermische en chemische processen die plaats vinden in de korst en bovenmantel van de rift zone onder extensie, met specifiek aandacht voor de effecten van de rheologische processen in de korst.

De resultaten laten zien dat de pre-existente (onregelmatige) structuur van continentale lithosfeer en de aanwezigheid van externe spanningsvelden van kritisch belang zijn voor de eerste fase van de ontwikkeling van de Afar Rift, en dat latere fasen meer beïnvloed worden door de aanwezigheid van de mantelpluim. De al aanwezige gelaagde structuur van de lithosfeer lijkt in sterke mate te bepalen waar de rift zich ontwikkelt in het Afar en Ethiopisch gebied, ook in het geval van een lithosfeer die lokaal aanzienlijk verzwakt is door hete smelt intrusies vanuit de mantel. De modellen voorspellen ook correct dat vulkanische activiteit begint in de Nubian Plateau regio en daarna verschuift richting de centrale as van actieve rifting. De waargenomen zuidoostwaartse migratie van vulkanisme wordt het best verklaard door een heterogene lithosfeer-asthenosfeer grens, met daarbij een dikkere lithosfeer in de Nubische deel van de Afar en een dunnere lithosfeer in het Somalische deel.

De plaats waar de rift zone zich vormt wordt gecontroleerd de heterogene structuur van de lithosfeer in combinatie met (mechanische) verzwakking van de korst door smelt vanuit de bovenmantel. De verzwakking verklaart ook de verhoogde seismische activiteit in de rift zones. Het uitgebreide vulkanisme in de Afar kan worden verklaard als zijnde het gevolg van

kristalfractionatie van smelt op het grensvlak van korst en mantel, die vermengd zijn met smelten afkomstig uit de korst.

Op dit moment bevindt de grootste thermische mantelanomalie zich onder de noordelijke Ethiopische Rift, en kan daar leiden tot voortgaande rifting die uiteindelijk zal resulteren in het geheel breken van de continentale lithosfeer en het begin van vorming van een nieuwe oceanische spreidingsrug. Deze situatie is vergelijkbaar met de huidige fase van rifting in de Danakil regio in de Afar driehoek.

1. Introduction

Lithosphere extension, thinning and breakup are fundamental processes in geodynamics. They represent pivotal elements in global plate tectonics theory and are processes that require more understanding. The complexity of rifting stems from the many different processes associated with plate rupture and drifting. It has been long recognized that rifts are commonly associated with volcanism, high heat flow, seismicity and anomalous crustal and mantle structure (e.g. Ziegler and Cloetingh, 2004; Koptev et al., 2015a, b), which reflects the number of distinct processes acting simultaneously during rift evolution. The interaction between different processes is often not easy to predict, and may result in ambiguous interpretations on the geodynamic causes of lithosphere extension and breakup.

During rift development, both the lithosphere and the mantle are involved in an integrated system, in which the main mechanisms are heat transfer, active and passive mantle flow (i.e. the mantle flux driven by composition and/or temperature related buoyancy, and the mantle flux induced by the necking of the extending lithosphere), far-field forces, viscous coupling between lithosphere and mantle flow, and magmatism (e.g. Koptev et al., 2015b, and ref. therein). These mechanisms and the forces associated with them are often subjected to variations during the rift evolution. As an example, tensional slab pull forces associated to subduction may become progressively greater, spreading extension and rifting to adjacent areas (Schubert et al., 2004).

The relationships between these processes and consequent feedback effects are still not well understood and are matter of debate. For instance, mantle flow influences the distribution and thickness of the lithosphere, but at the same time the lithosphere exerts a profound effect on mantle flow: previous studies have demonstrated that convection cells, temperature and flow regime in the mantle are affected by the thickness and distribution of continents (e.g. Guillou and Jaupart, 1995; Trubitsyn et al., 2003; Lenardic et al., 2005; Coltice et al., 2007; Phillips and Coltice, 2010). Consequently, lithosphere thinning and breakup should be considered as an integrated process, involving a coupled lithosphere-mantle system, where different mechanisms act mutually and simultaneously.

1.1 Continental rifts: general aspects

Many continental rifting areas have been recognized around the world (Figure 1.1). A recent example is constituted by the European Cenozoic Rift System, which is a continuous system of rifting structures traversing the lithosphere across the western and central Europe for some 1000 km, developing simultaneously with the main and late Alpine Orogeny from Eocene to Recent (Ziegler, 1992). Another area of interest is constituted by the Rio Grande Rift, which is part of a broad region, also including the Basin and Range province, where lithospheric thinning and extension are credited from the middle to late Cenozoic (Baldridge et al., 1995). Among the paleorifts, we can mention the Oslo Rift, part of a more complex system of rifts and grabens that developed in the Skagerrak – North Sea – Norwegan and Greenland Sea from Carboniferous to Cretaceous time (e.g. Ziegler 1978, 1982).

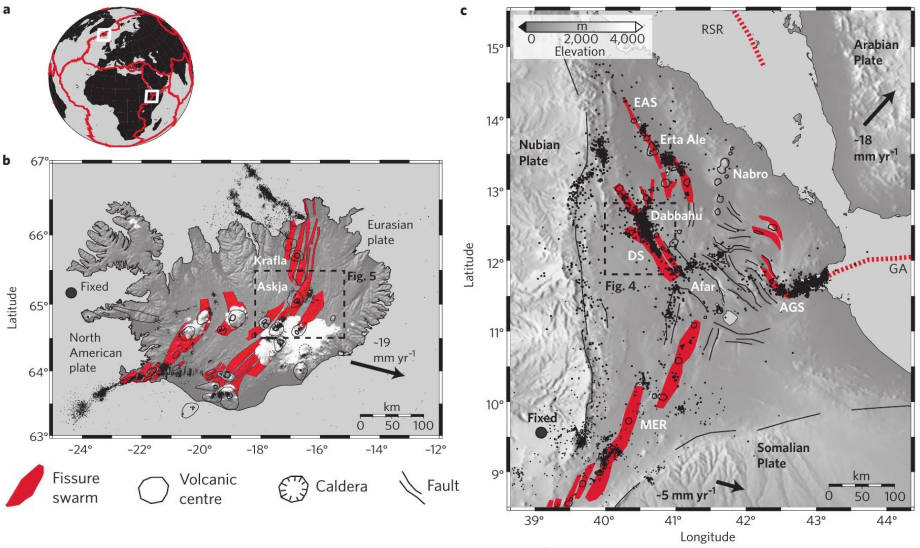

Figure 1.1 – Location of rifting areas in Iceland and Ethiopia. a) Overview map showing plate boundaries. b) Tectonic map of Iceland. c) Tectonic map of the Afar region. Black dots represent earthquake centers (from Wright et al., 2012).

The study of rifts is a key step in understanding the global plate tectonics theory, and proves fundamental for the comprehension of the interactions between mantle and lithosphere. However, other aspects of tectonic evolution are also important in the study of extensional areas. For example, trap layers extruded during rifting and coincident with plume events (Sleep et al., 2002; Lin and van Keken, 2005; Burov et al., 2007) greatly contributed to continental crust accretion (Boher et al., 1992) at the boundaries between the West African and the Australian craton and were accompanied by the "Archean metallogenic crises" (i.e. episodes of marked increase in metallogenic production). In addition, magmatism related to the Siberian Traps (Lin and van Keken, 2005) and, to a lesser extent, to the Emeishan Traps (e.g. Zhou et al., 2002) extrusion has been suggested as the cause for a massive greenhouse-gas emissions during the Permian. This caused a climate catastrophe and led to the Permian-Triassic (P-Tr) extinction event (Sobolev et al., 2011).

1.2 Magmatic and amagmatic riftings, active and passive

One of the aspects that is characteristic for several rifting areas is the presence of extended magmatic activity. Passive margins like e.g. the North Atlantic margins, the south-western Africa-Florida, Norway, west India and East Greenland (Buiter and Torsvik, 2014, and ref. therein), and areas like the aforementioned Siberian Basin, the Columbia River Flood Basalt Province (Bryan et al., 2010) and the Ontong Java Plateau (Coffin and Eldholm, 1994; Fitton et al., 2004) are characterized by massive amounts of volcanic deposits. These deposits are of both basaltic and silicic composition, and due to their large volumes (> 1000 km^3 dense rock equivalent) and areal extension (10^4 –10^5 km^2) the areas where they extrude are named Large Igneous Provinces (LIPs). During rifting episodes, melts are present at various depths in the lithosphere (e.g. Morgan, 1971; Menzies et al., 2002). It has already been suggested by analytical/numerical studies (e.g. Buck, 2004; 2006; Bialas et al., 2010) and field evidences (e.g. Björnnson et al., 1977; Hjartardóttir et

al., 2012; Keir et al., 2006; Wright et al., 2006; 2012) that rifting evolution and melt emplacement may exert a mutual influence (for example, when block gaps due to extension are accommodated by magma filling).

On the other hand, continental extension and breakup are not always associated with the presence of significant volcanic activity (e.g. Franke, 2013). Examples are the Iberia-Newfoundland and the East Antarctica-Australia magma-poor passive margins (e.g. Buiter and Torsvik, 2014, and ref. therein).

Consequently, it has been suggested (e.g. Buiter and Torsvik, 2014, and ref.therein) that a primary influence on rifting initiation and development is exerted by the lithosphere setting, in particularly by preexisting block sutures.

Sutures are favorable locations for lithosphere extension, thinning and breakup for different reasons:

1. Active mountain chains areas are in isostatic disequilibrium; consequently, gravity driven flows of over-thickened crust, or delamination of the crustal root or the thermal boundary layer may occur (e.g. Houseman et al., 1981; Dewey, 1988; Platt and England, 1993) and initiate extension. This process starts during or shortly after the orogenic phases, leading to a short interval time between collision and extension. This can be observed in the Norwegian basins, where the Silurian collision predates the development of the extensional basins during the Devonian (Andersen and Jamtveit, 1990).
2. The thickened crustal root in an orogen enhances crustal radiogenic heat production, with subseqent weakening of rocks due to the temperature increase (England and Thompson, 1984; Cloetingh et al., 1995; Ryan and Dewey, 1997). As a result, the thermally weakened orogen could localize subsequent extension, although the time delay between suture and rifting is significantly longer than the previously mentioned mechanism (hundreds of Myr, Buiter and Torsvik, 2014).
3. Inherited thrust faults can weaken active margins over long time spans and, where present, result in localization of deformation (Audet and Bürgmann, 2011).

Another criterion adopted for rifting classification is the localization of extensional stress fields; this allows to distinguish between active and passive rifting(e.g. Sengor and Burke, 1978; Turcotte and Emerman, 1983, Wilson, 1989; Olsen and Morgan, 1995) (Figure 1.2). In active riftings, thinning and extension are driven by force fields generated by mantle plumes impinging at the base of the lithosphere (Bott and Kusznir, 1979; Spohn and Schubert, 1982), whereas in passive riftings tensional stresses are result of movement and interaction of plates (e.g. Cloetingh and Wortel, 1986). It was suggested (e.g. Huismans et al., 2001) that not all evidences may fit into these two distinct end-member models. Instead, active and passive components may act simultaneously and be dominant one another at different extension and breakup stages. This is particularly true in the case of extensional far field forces associated with slab pull, which become progressively greater with subduction proceeding (Schubert et al., 2004). Thus, although we can still envisage “active” and “passive” components, their meaning must be reviewed (Ziegler and Cloetingh, 2004).

1.3 Mantle plumes, relationships with rifting areas

Many different forces control plate dynamics and may influence rift evolution. There is a wide consensus on the important role played by slab pull and roll-back, ridge push or frictional resistance (e.g. Forsyth and Uyeda, 1975; Bott and Kusznir, 1979; Bott, 1982, 1991; Ziegler, 1993). However, other factors and processes may strongly influence style and evolution patterns of rifting areas. Among these, the presence of mantle plumes has long been recognized as capable

in playing an important role during lithosphere extension (e.g. Buck, 2004). Plumes are focused upwellings of plate-scale mantle material, driven by temperature- and composition-related density differences (e.g. Burov et al., 2007, and ref. therein). Closely related to plumes (although distinct in meaning) is the concept of 'hot spots', described as topography swellings spatially and temporally associated with volcanism (e.g. Ito and van Keken, 2007, and ref. therein).

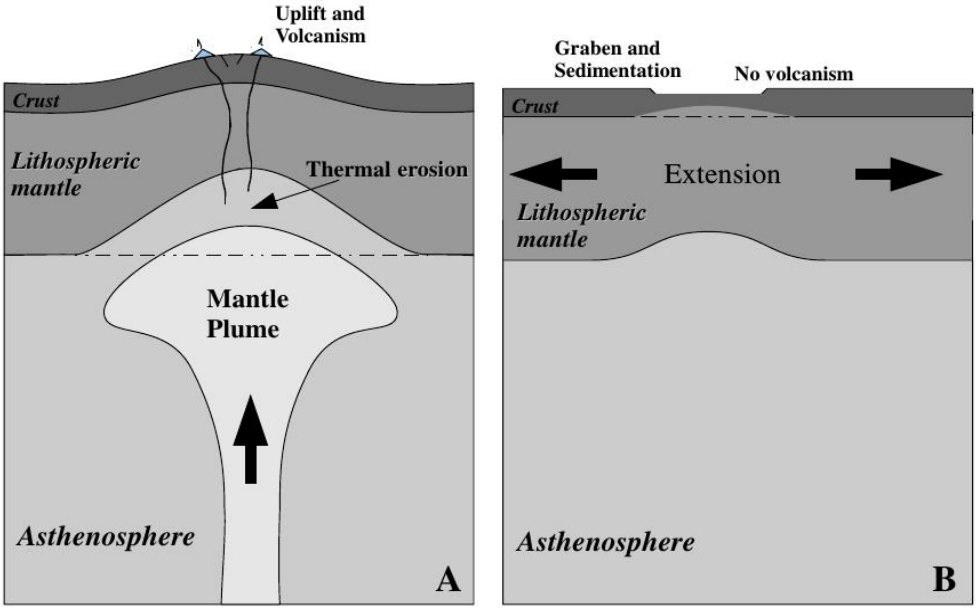

Figure 1.2 - The early stage of the tectonic evolution for "active" (A) and "passive" rifting (B). "Active" rifting displays lithospheric uplift and volcanism resulting from thermal erosion at the base of the lithosphere, whereas "passive" rifting displays graben formation and sedimentation without volcanism as a result of horizontal extension of the lithosphere (from Merle, 2011).

Thermal plumes in the Earth's mantle have been attributed to instabilities in the thermal boundary layers. One feeding region may be the D" layer, just above the core-mantle boundary, while another layer where plume formation is possible is the base of the transition zone (Schubert et al., 2004). The source region of plumes may vary in depth, but the upwelling mechanism does not show any remarkable difference (Burov et al., 2007). In its simplest formulation, the plume buoyancy mechanism may be approximated by a Rayleigh-Taylor instability, enhanced by the thickness of the layer where upwelling occurs, temperature and density differences between plumes and surrounding mantle, and hampered by thermal diffusivity and viscosity (Ito and van Keken, 2007). A further classification based on size has emerged in literature, where plumes have been distinguished in "baby-plumes", e.g. beneath western Europe (Ritter et al., 2001) to "superplumes", relative to past, large radius plumes (Condie, 2002), and present-day "mega-plumes", such as the case of Africa and Pacific plumes (Forte and Mitrovica, 2001; Romanowicz and Gung, 2002; Dziewonski et al., 2010).

Lithosphere impingement by the plumes can produce regional uplift driving to extensional stresses (e.g. Morgan, 1971; Sengor and Burke, 1978; Spohn and Schubert, 1982; Bott, 1991, Burov et al., 2007; Burov and Gerya, 2014). Furthermore, when plumes are characterized by a temperature excess of 100 to 200 K with respect to the surrounding mantle, small-scale

convective instability causes lithosphere erosion (Moore et al., 1999). However, the ridge push forces, associated with mantle upwelling and resulting topographic doming, are small or progressively decrease in intensity in comparison to plate-related far field forces (Schubert et al., 2004). In addition, in many rifting areas extension predates the main volcanic phases (Buiter and Torsvik, 2014, and ref. therein).Therefore, it appears that far field forces are a necessary component for the development of large scale rifting (e.g. Koptev et al., 2015a).

In addition, melts may result from both plumes or "plume head" upwelling (Richards et al. 1989; Griffiths and Campbell 1990; Hill 1991), and from passive upwelling related to the stretching and thinning of lithosphere (White and McKenzie 1989). The thermo-mechanical effects of magma intrusion and underplating at lithosphere-scale remain largely unquantified, although its important role in the evolution of the crust and lithosphere has long been acknowledged, especially in triggering the final phases of lithosphere breakup (e.g Furlong and Fountain, 1986). Plumes impinging a continental lithosphere already experiencing extension may constitute a fundamental factor for the deformation localization, thus contributing to plate breakup (Buiter, 2014).

1.4 Scope of the thesis

Physical models applied in geodynamics are extremely important to fully understand factors and processes involved in plate dynamics. However, they must assume simplified mechanisms and structures of the bodies involved. Furthermore, in natural cases multiple single factors act in the same area and often interact. The resulting feedback effects are difficult to predict and still poorly investigated. One of the areas where this is most evident is represented by the Afar Rift. This area has been commonly described as a classical extensional triple junction, but many recent studies suggest different dynamics leading to Afar breakup and block drifting (e.g. Bosworth, 2005, Buck, 2006, Bastow, 2011, Wright, 2012).

As described in more detail in Chapter 2, the presence of a plume impinging the Afar lithosphere is testified by many observations (such as the high thermal anomaly highlighted by seismic tomography, or the occurrence and the geochemical associations of the magmas), but its role in the Afar area evolution has been possibly overestimated. The plume may have played a major role in focusing the breakup of the lithosphere by causing the stress concentration and/or the local weakening of the lithosphere, but with regional plate tectonics providing the necessary stress field in order to generate rifting and following spreading. The highest contributions may have come from the slab pull generated by the subduction of the Arabian Plate along today's Bitlis-Zagros Main Thrust, subsequently to the closure of the Neotethys. In this setting, the role of pre-existing lithospheric heterogeneities may have influenced the geometry of breakup; most of these structures are Panafrican Orogeny-related and entail a framework of a locally thickened crust and thinned lithosphere.

The aim of this PhD thesis is the construction and numerical analysis of physical models where different mechanisms are taken into account and able to interact. The results from the numerical simulations might help to clarify some aspects relative to the initial and current phases of the Afar Rift evolution, and might also be applied to other rifting areas and contribute to give a better comprehension of breakup processes in the lithosphere, especially where rifting is accompanied by a marked volcanism.

The most important research question that this PhD thesis investigates in the Afar Rift is the relationship between mantle flow, plume presence and plate motion in the Afar area. As already mentioned, the interaction between lithosphere and mantle, in view of the validity of the distinction between active and passive riftings, is a controversial issue. Is it possible to describe

Afar Rift as a predominantly “active” rifting, or do far field stresses play a prominent role in the blocks breakup and drifting, as it happens in “passive” riftings? Are the stress fields acting on the Afar area determined by plume uprising or are they connected to the regional plate motion?

There are several issues of interest that are directly related to the main research question described above. Two of them are of particular relevance and can be summarized as follows:

1. What was the role of pre-existing lithosphere discontinuities in the rifting development? How might these be associated with the initial thinning of the crust?
2. How was the mantle plume upwelling influenced by the subduction-related stress field?

During this PhD project, a study of the Main Ethiopian Rift was included in the analysis of the more complex Afar region. This is because the Main Ethiopian Rift is the youngest rift branch converging in Afar area, and still in the continental rifting stage. Furthermore, intense plume-related activity is still occurring today, allowing the direct observation of plume-related processes. Another aspect to be taken into account is that its orientation in relation to the Bitlis-Zagros Main Thrust allows to deduce that subduction-related stress fields have had less importance here than in the Afar Rift, making the plume related processes the main ones acting on this rifting area. This allows us to study the effects of the plume and related melts directly on the Panafrican crust, and to apply the obtained results to the study of Afar.

This study of the Main Ethiopian Rift and Afar Rift is relevant to predict future evolution pattern of the Afar area, and is targeted to answer these two questions:

1. Is the East Africa rift a failed arm of the triple junction, or is a new ocean basin expected to occur?
2. What will be the evolution in the Danakil Depression, where the volcanism is no more directly plume-supported, but still occurring?

1.5 Outline of the thesis

In this PhD thesis several numerical modeling studies are presented, addressing different aspects of the tectonic and geodynamic evolution of the Main Ethiopian Rift and Afar Rift. The constructed models are based on different numerical codes and gradually enlarge the scale of observation and increase the complexity of the implemented characteristics.

In Chapter 2 a geological outline of the Afar Rift and Main Ethiopian Rift is given, including a brief reconstruction of the block kinematics in the area and a description of the rifting processes.

Chapter 3 presents results of thermomechanical models that are built to examine the rheology variations caused by dyke intrusion in the continental crust. Dyke intrusion can locally change the mineralogical composition of the crust in space and time as a result of temperature-induced metamorphism. In these models temperature-induced metamorphism was implemented, and a particular attention was paid to determine how different mineral assemblages and reaction kinetics during metamorphism impact on the thermo-mechanical behavior of the crust, in terms of differential stress values. Different lithologies were taken into account, to test the strength variations due to different initial crust compositions. Crustal anatexis was also introduced, due to mica-dehydration processes, and its effect on rock strength and rheology was implemented.

In Chapter 4, the aforementioned thermo-mechanical models were calibrated for the study of the Main Ethiopian Rift (MER), based on its extensional history and on the lithologies occurring in the area. Particular attention is given to reproduce the growing rates of the magmatic segments characterizing the axial area of the MER. In addition, crustal anatexis is also generated, due to mica dehydration and generation of granite melts.

In Chapter 5 we built a thermo-mechanical model where a layered lithosphere is subjected to both extensional stress and plume impingement. A lithospheric heterogeneity occurs in the lithosphere, at a predefined distance from the plume-lithosphere impact point. The aim of the model is to determine the conditions leading to either a lithospheric structure control or a plume control on the rifting location and features.

In Chapter 6 the main results of the models are summarized, with particular regard to application of these results to the Afar Rift area. In addition, several suggestions for future research in the MER and Afar Rift are presented.

2. Afar Rift, geological and tectonic setting

2.1 General overview

Continental rifting in the Afar region has been regarded a classical example of rift-rift-rift triple junction in literature (McKenzie and Morgan, 1969; Dewey and Bird, 1970) (Figure 2.1). More recent studies stated that the Afar area has been subjected to different processes, both extensional and compressional, which acted episodically since the Permian (Stampfli et al., 2001; Bosworth et al., 2005).

The Afar depression in Ethiopia is part of the East African Rift system, and represents the triple junction between the Main Ethiopian Rift, the Gulf of Aden and the Red Sea, separating the Nubia, Arabia and Somalia plates (Hoffman et al., 1997). At present day the region is characterized by the transition from continental rifting features to seafloor spreading westward in the Gulf of Aden and the Red Sea areas (Makris and Ginzburg, 1987; Bastow and Kleir, 2011). Rift branch terminations are represented onshore by the Asal Rift for the Gulf of Aden (Ruegg and Kasser, 1987, Stein et al., 1991; De Chabalier and Avouac, 1994), and the Dabbahu and Erta Ale Rift segments for the Red Sea, while the Main Ethiopian Rift terminates in central Afar at the Tendaho Goba'ad discontinuity (Bellhasen et al., 2003; Tesfaye et al., 2003; Wolfenden et al., 2005). Most of the area is capped by successions of volcanic rocks (Varet, 1978) and is characterized by a marked depression ranging from +800 to -100, surrounded by the Ethiopian and Somali Plateaus, whose elevation reaches ≈3000 m, and the Danakil Alps, reaching ≈2100 m (Bosworth et al., 2005). In this region, the presence of mantle plumes has long been identified as an important factor influencing volcanism and tectonic activity. In the south African area the plumes systems are identified as a part of a continental wide and more complex system named the African superplume (Camp and Roobol, 1992; Daradich et al., 2003; Ebinger and Sleep, 1998; Schilling, 1973; White and McKenzie, 1989).

2.2 Neoproterozoic to Eocene: before the African superplume

In the Afar region the crystalline basement is represented by Neoproterozoic rocks, exposed along the periphery of the Afar Depression and within the Danakil and Ali-Sabieh Blocks (Kazmin, 1971; Vail, 1976, 1985, Kazmin et al., 1978). These were assembled and metamorphosed between 800 and 650 Ma during the closure of the Mozambique Ocean along the East African Orogen (Stern, 1994; Kusky et al., 2003).

Basement structures eventually influenced rifting trends and volcanism during Tertiary times: significant examples are the N-S trending shear zones in the Danakil region (Ghebreab, 1998; Ghebreab et al., 2002) and in the western Afar (Collet et al., 2000). Other relevant features testifying the correlation between rifting and volcanism are the alignments among Marda fault, Red Sea and some Pleistocene volcanic centers (Black et al., 1974; Purcell, 1976). Some of these structures have been active since the Neoproterozoic, such as the Ethiopian high angle faults bounding western Afar (Kazmin and Garland, 1973).

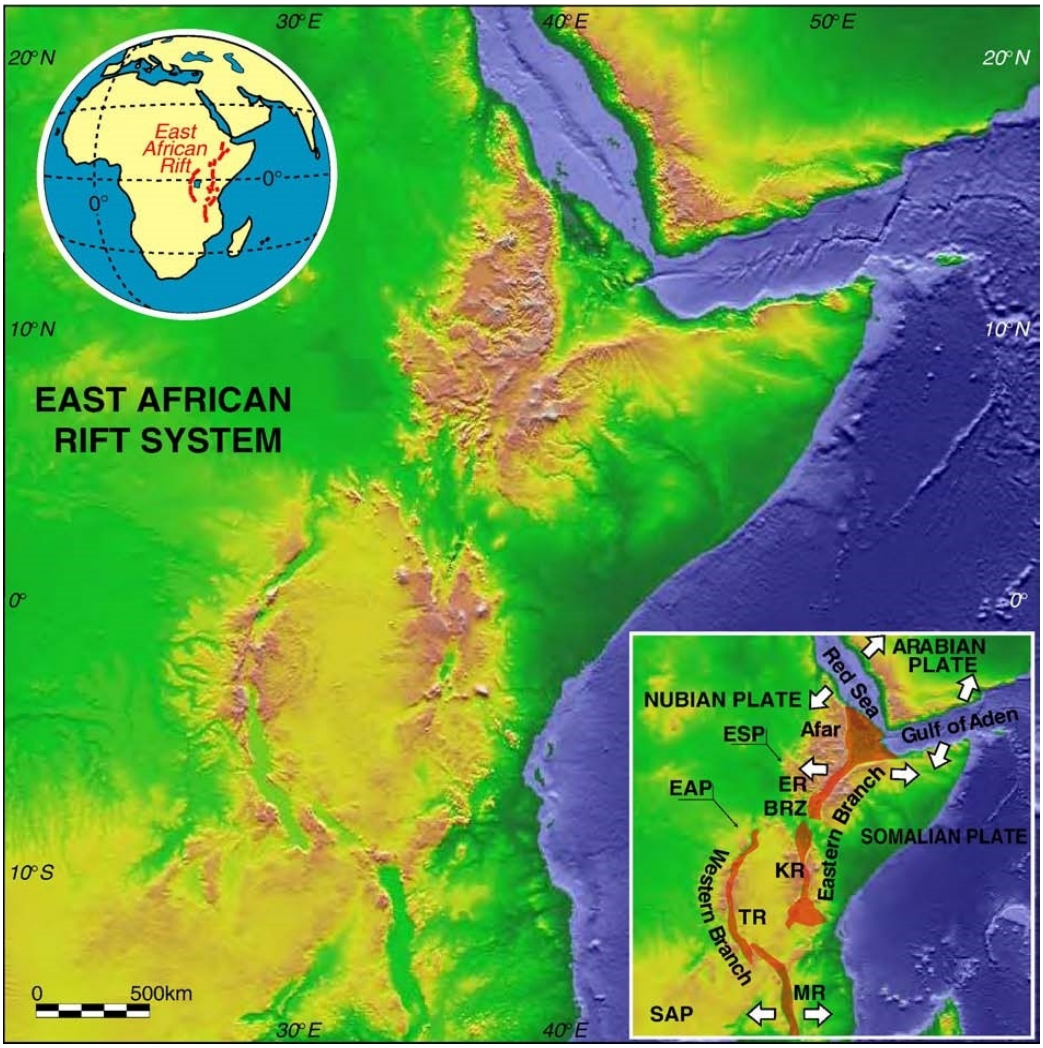

Figure 2.1 - Topography map of the East African Rift System. The inset shows the plate kinematic setting of the area. BRZ: Broadly Rifted Zone; EAP: East African Plateau; ER: Ethiopian Rift; ESP: Ethiopian–Somalian plateaus; KR: Kenya Rift; MR: Malawi Rift; SAP: Southern African Plateau; TR: Tanganyika Rift (from Corti, 2009).

The crystalline basement is overlain by the Adailo Series, a transgressive-regressive sedimentary sequence whose oldest strata are generally early Jurassic or possibly Triassic and with higher units of early Cretaceous age (Bunter et al., 1998; Bosworth et al., 2005). The Adailo Series is cut by numerous extensional faults, occurring after Oligocene basalts and leading to a thinning of the crust of ≈40% (Morton and Black, 1975). Furthermore, the Ethiopian Plateau is capped by the “trap series”, constituted by flood basalts whose thickness prior to erosion has been estimated at ≈4 km (Mohr, 1983; Zanettin, 1993). The age of these basalts is still controversial, but more acidic and lacustrine rocks interbedding indicate a late Eocene age. This age for these basalts would possibly represent the activity of an older plume that impinged beneath the southern Main Ethiopian Rift (Ebinger et al., 1993).

2.3 Oligocene to Pliocene: continental rifting and beginning of oceanic spreading

The first volcanic products directly related to the present-day Afar plume are represented by the Aiba basalts, undersaturated alkali basalts dated as Early Oligocene (Zanettin et al., 1978).

The presence of a laterite horizon at the base of the Aiba series in northern Eritrea suggests that this volcanism is not predated by an uplift of the area (Coleman, 1993), but rather that the tectonic context was characterized by simultaneous volcanism, doming and extension (Burke, 1996). More specifically, the eruption of these basalts occurred in a time span of 6 My, with the bulk of these bodies erupted between 30 and 29 Ma (Bosworth et al., 2005). This volcanic activity is accompanied by a modest extension during Oligocene, represented mainly by localized faulting (Barberi et al., 1972, 1975). Similar products are found in Saudi Arabia (Coleman et al., 1983; Brown et al., 1989; Coleman, 1993) and identified as Older Harrats. These products are mostly erupted from central vents (Bosworth et al., 2005) along N-S structured inherited from early Paleozoic and late Cretaceous deformation (Greenwood, 1972; Coleman, 1974).

During the early Miocene a marked decrease in volcanic activity is recorded in the Ethiopian Plateau, while volcanism proceeds along the western Afar margin and is represented by ignimbrite bodies dated as 19.76 ± 0.06 Ma (Ukstins et al., 2002). A series of alkaline and peralkaline granites also intruded the Precambrian basemen, Jurassic formations and the pre-plume traps along the Afar margins (Varet, 1978). Within the Afar depression, volcanic rocks are represented by the Adolei, Mabla and Dalha series (Barberi et al., 1975; Varet, 1978; Vellutini, 1990). The Adolei series is represented by basalt flow whose age is difficult to date due to the high degree of alteration. The few obtained samples demonstrate that these basalts range from 22 to 14.6 Ma (Chessex et al., 1975; Barberi et al., 1975; Black et al., 1975). This series represents a switch in the chemical overprint of the basaltic magmatism in Afar, since the Adolei basalts and, contemporary, more silicic terms mark the transition from plume-related products to syn-rift transitional basalts and associated peralkaline acid terms (Barberi et al., 1975). The Mabla series is mostly represented by fissural volcanic products and is represented by rhyolite, ignimbrite and subordinated basalts (Bosworth et al., 2005). They have been associated to the first phases of collision between Arabia and Eurasia (Şengör and Yilmaz, 1981; Hempton, 1987; Woodruff and Savin, 1989; Burke, 1996) with subsequent change in relative plate motions (Le Pichon and Gaulier, 1988) and the onset of rifting in the western branch of the East African Rift (Burke, 1996). The age of the Mabla products is still controversial: a few observations indicate an age spanning from 14 to 10 Ma (Barberi et al., 1975), but also rhyolite samples with age 20 and 17 Ma have been found (Audin et al., 2004). The last products of the Mabla series are coincident with the propagation of the spreading throughout the western-central Gulf of Aden (Bosworth et al., 2005). The Dalha series represent the return of the Afar volcanic activity to basaltic products and have an age from 8 to 3.5 Ma (Barberi et al., 1975). All these units were affected by extensional faulting during their extrusion, with the beginning of tectonic activity dated at ≈25 Ma (Barberi et al., 1972; 1975; Zanettin et al., 1978), coherent with dike emplacement and the syn-tectonic sedimentation in the Red Sea rift basin (Bosworth et al., 2005). The only undeformed bodies are represented by basaltic flows with ages ≈8 (Barberi et al., 1975) and ≈10 Ma, suggesting that the southern Red Sea has been stable since the late Miocene and extension foci were transferred within the Danakil Depression since this age (Bosworth et al., 2005).

Magmatic activity continues during Plio-Pleistocene and products are mostly attributed to the Afar Stratoid Series (Barberi et al., 1974, 1975; Varet, 1978; Berhe, 1986; Tefera et al., 1996), reaching a total thickness of ≈1500 m (Varet, 1978). Afar Stratoid Series overlies the Dalha series

unconformably and is mostly constituted by mafic products, but more silicic terms also occur. Age datings range from 3-2.7 Ma (Audin et al., 2004) to ≈0.4 Ma (Barberi et al., 1972, 1975; Civetta et al., 1974, 1975) for this series, although ages of ≈7.4 Ma also have been obtained (Berhe, 1986). These intervals are considered to represent the transition from continental rifting to oceanic spreading (Barberi et al., 1975). In this context, the break in the magmatic activity at 5 Ma (if occurring) could be related to the beginning of oceanic spreading in the Red Sea and the shifting of the spreading center in the Gulf of Aden (Bosworth et al., 2005).

2.4 Quaternary: last stages of the Afar evolution

During Quaternary, magmatic activity proceeded with extrusion of basalts, alkaline and peralkaline terms (Varet, 1978; Tefera et al., 1996), along both fissural and shield volcanoes (Bosworth et al., 2005), while rifting processes continued west of the Danakil horst and in the central Afar area (Tazieff et al., 1971; Barberi and Varet, 1977; Varet, 1978) with the connection between the Gulf of Tadjoura and Gulf of Asal, separating the Danakil block from the rest of Afar (Delibrias et al., 1975; Manighetti et al., 1998, 2001). These rifting areas have been interpreted as sub-aerial equivalents of oceanic spreading areas (Barberi and Varet, 1977), where ridges are separated by transform zones, as in the case of the Mak'arrasou region (Tapponier and Varet, 1974). The rifting has been accompanied by a 13° counterclockwise rotation of the Danakil block since 6-5 Ma (Tarling, 1970), reaching a total rotation of 23° since late Miocene (Sichler, 1980). Faulting in the Afar Rift shows predominant dip-slip movement. Nevertheless, strike-slip movements have been registered (Mohr, 1967; McKenzie et al., 1970; Gouin, 1979; Tapponier et al., 1990; Lépine and Hirn, 1992; De Chabalier and Avouac, 1994; Hofstetter and Beyth, 2003), with a predominant sinistral movement (Bosworth et al., 2005). These strike-slip faults are interpreted differently (Tapponier et al., 1990; Acton et al., 1991; Passerini et al., 1991; Abbate et al., 1995), but there is a general consensus about a complex interaction between different blocks (McKenzie et al., 1970; Chase, 1978; Acton et al., 1991; Collett et al., 2000).

2.5 A kinematic reconstruction of plate movement in the Afar area

According to recent plate motion reconstructions (Bosworth et al., 2005, and ref. therein), initial rifting stages occurred shortly after the onset of plume volcanism in Afar (≈31 Ma), at ≈29.9-28.7 Ma in the Gulf of Aden. Rifting started in the Indian Ocean and propagated towards the Afar area as an oblique rift, and subsequently at ≈27.5 – 23.8 Ma in the southernmost Red Sea. Movement of the blocks was modest during Oligocene, but became more marked during the Oligocene-Miocene transition, with a rapid development of the Red Sea at 24 Ma. More specifically, the Red Sea opened northward and its spreading direction, with exception of a few irregularities, was mostly dictated by stress fields generated at plate boundaries (Dixon et al., 1987). The extension affected the Afar region at ≈25 Ma (Barberi et al., 1972; 1975; Zanettin et al., 1978), but an earlier beginning of rift phase cannot be excluded, since older syn-rift sequences are covered by volcanics (Kenea et al., 2001). A feature of particular interest is the convergence of the three rift branches in the Afar province at different times: 31 – 27 Ma in the case of the Red Sea and the Gulf of Aden rifts and 14-10 Ma for the Main Ethiopian Rift. Today the spreading velocity in the Afar region ranges from 15 mm yr-1 to 20 mm yr-1, resulting in a conterclockwise rotation of the Danakil block and contributing to the typical triangular shape of the Afar Rift (McClusky et al., 2010).

2.6 Mechanics of Afar rifting and spreading: one or more plumes?

Complex interactions between active and passive rifting mechanisms can be recognized in the Afar area: the plume plays a major role in focusing the breakup of the lithosphere by causing stress concentrations and/or local weakening of the lithosphere (Malkin and Shemenda, 1991; Bellhasen et al., 2004). Moreover, regional plate tectonics provides the necessary stress field to generate rifting followed by spreading (Bosworth et al., 2005), with the largest contributions coming from the slab pull generated by subduction of the Arabian Plate along the today's Bitlis - Zagros Main Thrust (Wilson, 1993). In this framework, the role of the pre-existing lithospheric heterogeneities influenced the geometry of breakup. The overall obtained sequence was onset of both magmatism and extension with local uplift, followed by major uplift on rifting shoulders and major subsidence at the center, accompanied by ongoing extension (Bosworth et al., 2005).

At present day, the whole region is underlain by a ≈500 km wide low velocity zone, connected to the deeper African superplume in the lower mantle (Bastow et al., 2008; Debaye et al., 2001; Grand, 2002; Ritsema and Allen, 2003; Li et al., 2008). Furthermore, seismic tomography studies indicate that the mantle beneath Ethiopia is among the slowest worldwide (Poupinet, 1979; Bastow et al., 2005, 2008, 2011), with an abundant source of partial melt (Bastow et al., 2008; Hansen and Nyblade, 2013). Today the lowest velocity region is located in the western edge of the Main Ethiopian Rift, supporting the hypothesis of a control on the melt migration at the base of the lithosphere exerted by Miocene-to-Recent tectonics and previous structures (Bastow et al., 2008).

The thickness of the crust is extremely variable between the rift areas and the surrounding plateaus (Dugda et al., 2005). In the Main Ethiopian Rift, seismic studies indicate that the crustal thickness ranges from 27 to 38 km. This variability may be explained by local differences in either crustal stretching or underplating and intrusion. In addition, calculated Poisson's ratios in this area are equal or higher than 0.30, indicating the presence of both mafic crust and melt, in agreement with the historical magmatic activity within the Main Ethiopian Rift (Dugda et al., 2005). Similar results are obtained for the Afar area, where observations show a crustal thickness of 25 km (Dugda et al., 2005) (and interpolated data suggest a further thinning northward) and Poisson's ratio of 0.36. These data support the hypothesis of a predominant magma-assisted rift, where the whole thinning is primarily accommodated by magma intrusion (Ebinger and Casey, 2001). A similar interpretation is given for Afar (Ruegg, 1975; Searle, 1975; Makris and Ginzbourg, 1987), with an almost complete replacement of previous acid and intermediate crust by mafic products (Dugda et al., 2005). In view of this evidence, actual magmatic segments should be interpreted as the locations of extension, instead of borders of rifting (Dugda et al., 2005). Today the lithosphere thickness ranges from 70-80 km beneath the Ethiopian plateau to at most 50 km beneath the Main Ethiopian Rift. Thermal models suggest that these areas experienced a thermal thinning mostly due to the plume impingement (Dugda et al., 2007).

In contrast, the crust of the Ethiopian plateau shows a thickness ranging from 34 to 44 km, with an average value of 38 km. The thickness at the northern side reaches a 41 km mean value, while the thickness at the southern side reaches 35 km. The Poisson's ratios are 0.27 for the northern side and 0.28 for the southern side. It can be concluded that the Ethiopian plateau crustal thickness appears largely unmodified and with little evidence for crustal underplating (Dugda et al., 2005). However, a difference in magma impingement at depth may explain the small differences between southern and northern plateau crustal thickness (Dugda et al., 2005), reflecting the difference in basalt flood thickness already measured at surface (Pik et al., 2003).

Today the number of plumes occurring in the Afar area and its surroundings and the associated mantle flow features are still a matter of debate (Chang and Van der Lee, 2011). The most

supported hypothesis by geophysical data is the occurrence of a single large plume (Ebinger and Sleep, 1998), feeding multiple hotspots via channeled flow along a thinned lithosphere (Hansen et al., 2006; Park et al., 2007, 2008). In the Afar area seismic tomography studies highlight a ≈500 km wide, ≈3% S-wave low velocity anomaly, originating at the core-mantle boundary beneath southern Africa and rising toward the base of the lithosphere beneath the Red Sea – Gulf of Aden – Ethiopia areas (Grand, 2002; Ritsema and Allen, 2003; Simmons et al., 2007; Li et al., 2008), maintaining its continuity across the 660 and 410 discontinuities below the Kenia – Ethiopia region (Ritsema and Allen, 2003; Li et al., 2008; Montelli et al., 2004, 2006 and references therein, Sicilia et al., 2008). On the other hand, the presence of two mantle plumes (George et al., 1998; Nelson et al., 2007, 2008) would better fit the geochemical data, even though there are geochemical evidences for a common root localized in the deep lower mantle from which different smaller plumes could stem (Furman et al., 2006). Recently, other studies suggest the presence of several plumes beneath Afar and northern Kenia, keeping their independence from at least 1400 m of depth, and the presence of channeled flows propagating radially from the Afar zone (Chang and Van der Lee, 2011). It should be mentioned that at present day the highest thermal anomaly is registered beneath the Main Ethiopian Rift (Bastow et al., 2011), suggesting a possible migration of the spreading center in time.

3. Thermal perturbation, mineral assemblages,and rheology variations induced by dyke emplacement in the crust

3.1 Introduction

Intraplate deformation is a result of a complex interaction between mantle and lithosphere processes, with feedback effects which are often difficult to foresee (e.g., Burov et al., 2007, 2009). This is of a particular relevance for continental rifting, where the interplay of plate boundary forces, plate-asthenosphere friction, and mantle upwelling determine the rifting evolution throughout its history (Cloetingh et al., 2011). It has been long acknowledged that the characteristics of the lithosphere (with particular emphasis to thermal structure and thickness) may exert a profound effect on the tectonic evolution of an area (e.g., Sonder et al., 1987; Braun and Beaumont, 1989; Dunbar and Sawyer, 1989, Buck, 1991; Bassi, 1991). Although extensional models including only mechanical stretching conditions have proven successful at describing many typical features of rifting areas (e.g., McKenzie, 1978; Huismans et al., 2005), other common deformation characteristics occurring during extension can only be reproduced by taking into account more detailed lithospheric reconstructions.

It is well established that during initial rifting phases accommodation of deformation is mostly dominated by lithospheric stretching and characterized by the presence of large-scale border faults, whose presence defines a typical half-graben morphology (Hayward and Ebinger, 1996; Ebinger et al., 1999). A consensus is also growing on the important role of melt intrusion in favoring lithospheric breakup and extension. Analytical/numerical studies (e.g., Buck, 2004, 2006; Bialas et al., 2010), supported by field evidences (e.g., Björnnson et al., 1977; Hjartardóttir et al., 2012; Keir et al., 2006; Wright et al., 2006, 2012) have demonstrated the intimate relationship between rifting episodes and melt emplacement, resulting in an extension accommodated by magma filling.

The presence of melts has been recognized in a variety of geodynamic settings (e.g., Annen and Sparks, 2002; Annen et al., 2006; Michaut and Jaupart, 2006; Solano et al., 2012) and facilitates the breakup of continental lithosphere. Its effect on the rheological characteristics of the intruded plate, however, is still poorly investigated. Many recent studies point out the importance of lithospheric rheological structure in lithosphere extension, especially in the analysis of dynamic topography and the interaction between plumes and plates in general (e.g., Burov and Cloetingh, 2009; Cloetingh et al., 2013a, 2013b; Burov and Gerya, 2014). However, the rheological stratification currently adopted in many lithospheric models does not envisage the possibility that (1) the characteristics of the lithosphere are extremely variable both vertically and

This chapter is based on: Lavecchia A., Clark S., Beekman F., Cloetingh S., and Burov E. (2016a), Thermal perturbation, mineral assemblages and rheology variations induced by dyke emplacement in the crust. Tectonics, 35. doi:10.1002/2016TC004125.

laterally, even at a very short scale, and (2) discontinuities along the lithosphere are not only inherited but also developed during the rifting processes.

The aforementioned heterogeneities may be of various nature, but among these, lithological variation may play a primary role in determining the rheological behavior of the lithosphere, both horizontally and vertically. In geodynamically active settings, rocks are subjected to important temperature-pressure variations. As a consequence, their mineralogical assemblage and fabric may change considerably. This is particularly true in the case of the crust, due to inherited chemical and mineralogical heterogeneity.

Furthermore, thermal perturbation is a direct cause of partial melting, especially when crustal/lithospheric thinning is accompanied by magmatic activity (e.g., Annen and Sparks, 2002; Annen et al., 2006; Solano et al., 2012). The presence of magmas at crustal level is mainly due to asthenosphere decompression, partial crystallization of basaltic magmas and subsequent fractionation of more silica-rich melts, and/or partial melting of preexisting host rocks (e.g., Annen et al., 2006; Solano et al., 2012, and references therein). A melt-intruded crust is a polyphase mush, characterized by considerably lower strength values (e.g., Rosenberg and Handy, 2005). This, together with metamorphism, causes important deviations in the rheological behavior of rocks. Such deviations are focused most likely in the maximum deformation areas in the crust, where they may considerably influence the evolution of geodynamically active areas. This aspect, therefore, should be an integral part of future studies of crustal deformation in which intrusions and melts may occur.

In this paper we present the results of a 2-D thermomechanical model, designed to examine the changes in rheology of a continental crust which is subjected to a thermal perturbation representative of early magmatic phases of rifting. Our model takes into account different mineralogical assemblages and their variations with time, due to temperature-induced metamorphism. We adopted typical intracontinental lithologies, with a temperature- and melt-dependent rheology, and paid particular attention to determine how different mineral assemblage and metamorphism-related reaction kinetics may influence the mechanical behavior of the crust. The obtained results may contribute to reconstruct a more realistic response of the plates subjected to extension, especially in tectonic settings and/or rifting stages where the crust constitutes a significant percentage of the whole plate thickness.

Although the role of plumes as a direct cause of lithosphere extension and drifting has been the subject of intense debate (e.g., Ziegler and Cloetingh, 2004; Natarov and Conrad, 2012; Burov and Gerya, 2014), their role in triggering and focusing deformation has been acknowledged (e.g., Rychert et al., 2012). Thus, a crustal rheology, coherent with petrological observations, may contribute to a better understanding of the interaction between “active” and “passive” rifting, with a particular attention to aspects related to the propagation of plume-related topography perturbations (Burov and Cloetingh, 2009).

3.2 Characteristics of the crustal model

3.2.1 Geometrical and thermal features

We used a 2-D thermal model that numerically simulates the temperature variations in a two-layered crustal section, induced by the growth of an intruded basaltic body over a time span of 2 Myr (Figure 3.1).

Our model comprises a 35 km thick crust with a lateral extension of 30 km, divided into two crustal layers with same thickness (17.5 km) but different density and mineralogical composition. The thermal loading is implemented by a cyclic series of “injected” dykes that build up a basaltic

body with a thickness of 10 km. Each dyke has an individual thickness of 25 m and is added to the basaltic main body by outward lateral accretion to the left edge of the plate model.

The thermal evolution of the model is governed by the heat transfer equation (3.1):

$$\rho C_p \frac{\partial T}{\partial t} = k(T)\nabla^2 T + Q \quad (3.1)$$

where ρ is the density, C_p is the specific heat, T is the temperature, t is the time, k is the thermal conductivity, and Q is the internal heat production. The model does not take into account any advection of heat, because the dyke emplacement may be considered a quasi-instantaneous process, given a magma velocity in the order of meters per second (e.g., Wilson, 1981). The numerical solution is obtained by using FEniCS (Logg et al., 2012), a collection of free scientific computing codes for finite element based on the automated solution of partial differential equations.

The values assigned to the modeling parameters are given in Table 3.1. For the initial geotherm a fixed thermal conductivity (2.25 W m^{-1} K^{-1}), a surface temperature of 25 °C, and a basal temperature of 750 °C were used. These values were chosen in order to maintain the crust in thermal equilibrium with respect to the muscovite dehydration reaction and to avoid melt generation before the simulation starts. After dyke intrusion, the geotherm is updated by applying a temperature-dependent thermal conductivity, a fixed heat flux at the base of the crust of 27 mW m^{-2} , and a temperature-dependent heat flux calculated according to Newton's law of cooling (3.2) (see, e.g., Incropera et al., 2006):

$$q_S = h(T - T_S) \quad (3.2)$$

where q_S is the heat flux, h is the convection heat transfer coefficient, T is the temperature at the surface, and T_S it the atmosphere temperature. The values adopted for qS and h are chosen such that possible temperature fluctuations do not exceed ±6°C in the simulations.

The heat flux at the lateral boundaries has always been kept equal to 0, justified by the low thermal diffusivities that prevent fast heat transfer toward these edges.

The temperature-dependent thermal conductivity (Clauser and Huenges, 1995) varies according to the empirical equation by Zoth and Hänel (1988) (see Table 3.1). At T ≥ 200–300°C the resulting values for conductivity are ≤ 2.0 W m^{-1} $°C^{-1}$, in agreement with experimental determinations (Clauser, 2009).

At the start of each model run, stability iterations are carried out to ensure equilibrium of the metamorphic associations assigned to the crustal layers, constant values of the thermal conductivity values, and small adjustments in the geotherm with the new boundary conditions.

A novel aspect of our model is that the crustal heat production is not only due to radiogenic heat production but also to reaction enthalpy caused by intrusion-induced temperature variations and associated metamorphism. The radiogenic heat production rate has been conventionally assumed to be decreasing exponentially with depth (e.g., Ranalli, 1995). This is a common approximation since heat generation rates of different rock types generally decrease with decreased silica content (e.g., Vilà et al., 2010). The depth-dependent radioactive decay law is as follows (3.3):

$$A(z) = A_0 \exp\left(\frac{-z}{D}\right) \quad (3.3)$$

where $A(z)$ is the radiogenic heat production at depth z, $A0$ is the radiogenic heat production at surface, and D is the characteristic depth. In our model, the adopted value of D represents an average of the different values reported in literature (e.g., Lachenbruch, 1968; Jessop and Trevor, 1978). Values adopted are given in Table 3.1.

For the cooling of basaltic magma, the release of latent heat of crystallization has been taken into account by incorporating an effective specific heat instead of the true specific heat for the

interval of crystallization between 1300 and 1100°C (Paterson et al., 1998, and references therein). The effective specific heat has been calculated on the basis of the formula by Spear (1993) (3.4):

$$C_{eff} = C_P + \frac{LH}{\Delta T} \quad (3.4)$$

where C_{eff} is the effective specific heat, C_P is the specific heat, LH is the latent heat of crystallization, and ΔT is the crystallization temperature interval. The values adopted in the simulation lead to an effective heat valueof 2813 J kg^{-1} K^{-1} in the crystallization temperature interval (see Table 3.1).

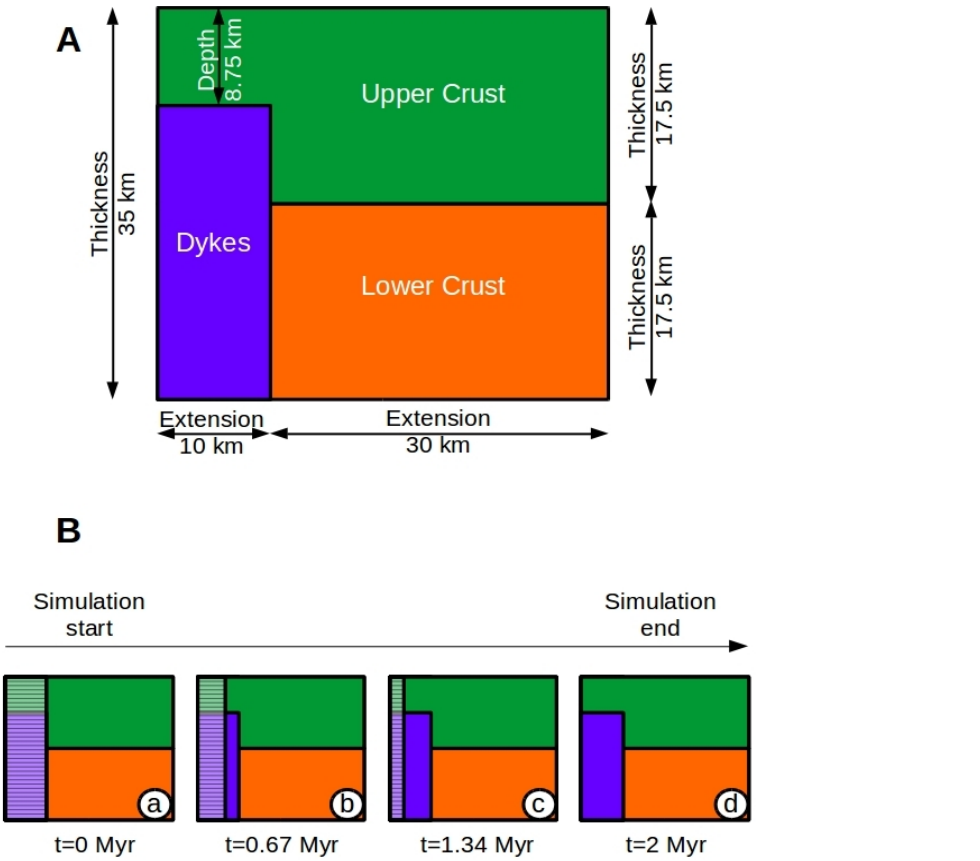

Figure 3.1 - (a) Schematic representation of the 2-D model geometry. (b) Illustration for four different time steps (1–4) of the magma body growth. During each time step dykes are added to the main body by outward lateral accretion to the left edge of the model. Hatched left rectangle indicates the portion of the model not computed at different time steps.

3.2.2 Metamorphic features

For a non quartz-feldspathic crust, any coherent model simulating the cooling of melts in the crust should take into account the possibility of metamorphic reactions due to the thermal perturbations. In our case, we have modeled prograde metamorphism in different mineralogical associations for the upper and lower crust (Table 3.2), adopting the following three combinations: (1) a crust composed of quartz (upper) and feldspars (lower) (model QF); (2) a crust with a

mineralogical association resembling the chemical composition for upper and lower crust given by Rudnick and Gao (2003) (model CC); and (3) a sedimentary protolith, metamorphic crust (model MS).

Parameter	**Symbol and equation**	**Value**
Surface temperature (preliminary geotherm)	T_S	25 °C
Crust base temperature (preliminary geotherm)	T_b	750 °C
Magma emplacement temperature	T_m	1300 °C (a)
Magma crystallization temperature	T_c	1100 °C (b)
Density	ρ	Upper crust: 2650 kg m^{-3} (b) Lower crust: 2850 kg m^{-3} (b) Dykes: 2900 kg m^{-3} (c)
Thermal conductivity	$k = A + \frac{B}{350+T}$	Upper and lower crust (d): A = 0.75 W m^{-1} °C^{-1}: B = 705 W m^{-1} Dykes: A = 1.18 W m^{-1} °C^{-1}; B=474 W m^{-1}
Surface heat flux	$q_s = h(T - T_s)$	h = 5 W m^{-2} K^{-1} (e)
Crust base heat flux	q_b	$2.7 \cdot 10^{-2}$ W m^{-2}
Lateral boundaries heat flux	q_l	0 W m^{-2}
Specific heat	C_P	Upper crust: 1370 J kg^{-1} K^{-1} (f) Lower crust: 1390 J kg^{-1} K^{-1} (f) Dykes: 1480 J kg^{-1} K^{-1} (f, g)
Latent heat of crystallization	LH	$4 \cdot 10^5$ J kg^{-1} (h)
Radiogenic heat generation	$A(z) = A_0 e^{\frac{-z}{D}}$	$A_0 = 2 \cdot \mu$W m^{-3} (i) $D = 1.2 \cdot 10^4$ m

Table 3.1 - Thermal parameters adopted in the model. When reference is not present, values have been chosen by the authors (see text for further explanation). a:Paterson et al. 1998; b: Holbrook et al., 1992; c: Carmichael, 1990; d:Zoth and Hanel, 1988; e:Incropera et al., 2006; f: Bohrson and Spera, 2001; g: Laube and Springer, 1998; h: Spear, 1993; i: Gerya, 2010.

For each of these three cases we analyzed both the initial and the postintrusion thermal evolution and the resulting variations in composition and rheology. More in detail, we have considered the most common mineral constituents in crustal rocks (quartz, plagioclase, K-feldspar, aluminosilicates, chlorite, muscovite, biotite, garnet, staurolite, and water), including the main metamorphic reactions leading to their appearance or consumption, and also the possibility to generate partial melting. Minerals belonging to aluminosilicates and chlorite, biotite, garnet,

staurolite, and feldspars groups are treated as pure mechanical mixtures among end-members. The metamorphic grid is illustrated in (Figure 3.2).

Crust case study	**Upper crust**	**Lower crust**
Quartz-Feldspathic (QF)	qz100	pl100
Crust average chemical composition (CC)	chl13, ms13, qz37, pl23, kfs14	ms13, qz13, pl20, ky4, grt15, bt20, st2, kfs13
Micaschists (MS)	chl30, ms25, qz25, pl10, kfs10	ms10, qz20, pl15, ky5, grt10, bt25, st5, kfs10

Table 3.2. - Mineral assemblages adopted in the model (values expressed as volume percentages).

The temperature-pressure curves have been extrapolated by Spear and Cheney (1989), taking into account the results obtained by Symmes and Ferry (1992) and incorporating the effect of Mn in decreasing the temperature values needed for garnet stability. The muscovite and biotite dehydration reactions are calibrated on the basis of studies by Vielzeuf and Holloway (1988) and Patiño Douce and Johnston (1991) by assuming an approximated melt composition of 40qz, 30kfs, and 30pl, based on studies by Luth et al. (1964) and an oligoclase composition of plagioclase.

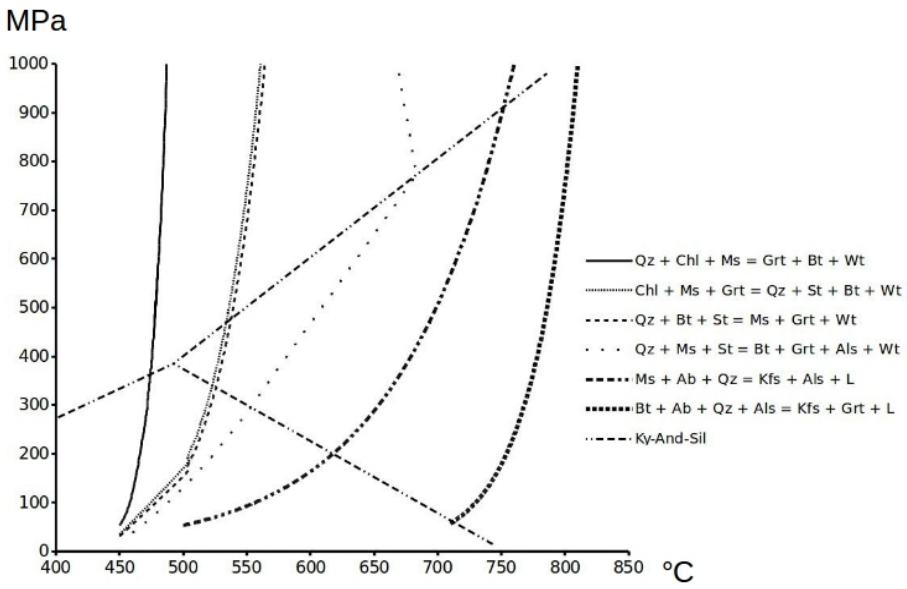

Figure 3.2 - Reaction grid used to simulate metamorphism in the crust. Reactions in the legend occur with increasing temperature.

To account for eventual variations in the simulation thermal balance due to metamorphic reactions, their reaction enthalpy has been determined, according to the formula (3.5):

$$H = E + PV \quad (3.5)$$

where H is the enthalpy of the system, E is the internal energy, P is the pressure, and V is the volume. In our model we treat the influence of the enthalpy variations in the temperature equation

as energy variations where appropriate temperature-pressure conditions are reached. This simplification has been adopted, since rock volume variations due to metamorphism seldom exceed 10%. Thus, as a first approximation, the *PV* term of the equation can be considered negligible in the enthalpy calculation.

For every mineral, we calculate the enthalpy of formation, according to Philpotts and Ague (2009) (3.6):

$$\Delta H = a(T-298) + \frac{b}{2}(T^2-298^2) - c(T^{-1}-298^{'1}) + 2d(T^{0.5}-298^{0.5}) \quad (3.6)$$

where *a*, *b*, *c*, and *d* are thermodynamic parameters, with values given by Holland and Powell (1998). Afterward, we calculate the reaction enthalpy (3.7):

$$\Delta H_{reaction} = \sum_{i=1}^{n} \Delta H_i - \sum_{j=1}^{m} \Delta H_j \quad (3.7)$$

where n and m are, respectively, the number of the products and the reactants in the metamorphic reaction. The muscovite- and biotite-dehydration melts are similarly treated, by transforming their latent heat of fusion ($4 \cdot 10^5$ J kg^{-1}) (Spear, 1993) in formation enthalpy.

The metamorphism in our model is not instantaneous but develops over a certain time span, ruled by imposed values of reaction kinetics and in response to cyclic dyke intrusion. To implement a realistic reaction kinetics scenario, we took garnet growth velocities as estimated by Cashman and Ferry (1988) and Christensen et al. (1989, 1994) and related these to garnet population density and crystal dimensions estimated by Cashman and Ferry (1988), Pattison and Tinkham (2009) and Gaidies et al. (2011). Garnet growth characteristics are among the best studied and therefore adopted for our simulations. By crossing data, we obtained values for garnet growth velocities ranging from 50 mol m^{-3} yr^{-1} to 500 mol m^{-3} yr^{-1} and even up to 5000 mol m^{-3} yr^{-1}. These values have been used to calibrate the other minerals' growth velocities, depending on their stoichiometric index in the studied reactions. Where garnet was not involved, the reaction kinetics of the other minerals has been determined by the weighted mean of values in the garnet-occurring reactions kinetics.

3.2.3 Rheological features

Two-dimensional strength profiles have been obtained using the frictional criterion for the brittle field and the power law creep equation for the ductile field. For every deformation mechanism the differential stress σ (i.e., $\sigma = \sigma_1 - \sigma_3$) has been calculated. We assumed as dominant deformation the mechanism that requires the least differential stress.

For the frictional criterion we have used the equation (3.8) (Sibson, 1974):

$$\sigma_B = \sigma_1 - \sigma_3 = \beta \rho g z (1-\lambda) \quad (3.8)$$

where $\sigma_B = \sigma_1 - \sigma_3$ is the friction-related differential stress (compression is positive). β is a dimensionless parameter depending on the frictional coefficient and deformational regime, ρ is the rock density at depth *z*, and *g* is gravity acceleration. The pore fluid factor λ (ratio of pore fluid pressure to lithostatic pressure) is set to 0.4, which is representative for hydrostatic pore fluid pressures. For an extensional tectonic regime and a uniform friction coefficient $\mu = 0.75$ for all rocks, $\beta = 0.75$ for our crustal model (Ranalli, 1995). The values of density adopted in the model are given in Table 3.1.

The creep flow law implemented in the model is (3.9) (e.g., Gerya, 2010; Karato, 2008; Ranalli, 1995)

$$\dot{\varepsilon} = A h^m (\sigma_D)^n \exp\left(\frac{-E + V_A P}{RT}\right) \quad (3.9)$$

where $\dot{\epsilon}$ is strain rate, h is the grain size raised to the power of the parameter m, σ_D is the differential stress (similarly to σ_B), P is the pressure, R is the gas constant, T is the temperature, and A, n, E, and V_A are the mineral's rheological parameters. Ductile deformation in the crust mainly occurs by dislocation creep (e.g., Kirby, 1985), for which $m = 0$ and V_AP is negligible (since $V_AP \ll E$).

The rheological parameters adopted in the model for each mineral are listed in Table 3.3. The parameters adopted for staurolite and aluminosilicates are a mean between "weak" minerals (quartz and feldspars) and "strong" minerals (garnet) (Kruhl and Vernon, 2005; Kruhl et al., 2007). The rheological parameters for the single minerals were used to calculate the parameters of the multiphase rock for each time step, following the average procedure suggested by Ji and Zhao (1993) and Ji et al. (2003).

The implementation of partial melting, due to muscovite- and biotite-dehydration reactions, requires a separate approach for partially molten rocks. In our simulation we have identified two rheological thresholds when melting is occurring. A first rheological threshold occurs with melt fraction Φ = 6–8%, corresponding to the melt connectivity transition (MCT) (Rosenberg and Handy, 2005). In this melt fraction interval, the brittle strength of the rock diminishes, according to the relationship (3.10)

$$\log_{10}(\sigma_B^{MCT}) = \log_{10}(\sigma_B) - 0.5\left(1 - \cos\left(\pi\left(\frac{\phi}{2} - 3\right)\right)\right) \quad (3.10)$$

where Φ is the melt fraction, σ_B^{MCT} is the brittle strength when Φ = 6–8%, and σB is the brittle strength of the melt-free rock. The decrease in the crustal brittle strength between the indicated melt percentages is 1 order of magnitude for $\Phi \geq 8\%$.

Model mineral	**Adopted mineral**	**A ($MPa^{-n}\ s^{-1}$)**	**n**	**E ($kJ\ mol^{-1}$)**
Chlorite	Mica (a)	$1.10 \cdot 10^{-15}$	18	51
Muscovite	Mica (a)	$1.10 \cdot 10^{-15}$	18	51
Biotite	Mica (a)	$1.10 \cdot 10^{-15}$	18	51
Quartz (dry)	Quartz (b)	$1.10 \cdot 10^{-4}$	4	223
Plagioclase	Albite (c)	$2.34 \cdot 10^{-6}$	3.9	234
K-feldspar	Albite (c)	$2.34 \cdot 10^{-6}$	3.9	234
Allumosilicates	(d)	23.4	4	410
Staurolite	(d)	23.4	4	410
Garnet	Pyralspite (e)	276	3	444

Table 3.3 - Rheological parameters for minerals in the model. a: Kronenberg et al., 1990; b: Gleason and Tullis, 1995; c: Shelton and Tullis, 1981; d: chosen by authors, see sect. 3.2.3; e: Wang and Ji, 1999.

The second rheological threshold is reached when Φ = 30–40% and corresponds to the solid to liquid transition (SLT) (Rosenberg and Handy, 2005), equivalent to the rheologically critical melt percentage (Arzi, 1978). For these melt fraction values the strength of the whole rock resembles the strength of a melt-crystal mush with features in between two extreme terms: a rock with a rheology influenced by the presence of melt batches and a melt with a viscosity affected by the presence of crystals. Thus, in calculating the mush strength, we take into account (1) the viscosity (and consequently, the strength) of a pure, crystal-free melt and its variations with temperature;

(2) The viscosity variation of the produced melt, as a function of different crystals percentage; and (3) The mush strength when a melt percentages is Φ = 30–40%.

The viscosity of the crystal-free melts has been calculated by using the Arrhenius equation (3.11) (Dingwell, 1995):

$$\log_{10}(\eta_T) = \log_{10}(\eta_0) 2.303 \frac{E}{RT} \quad (3.11)$$

where η_T is the melt viscosity at temperature T, η_0 is a preexponential factor, E is the activation energy, and R is the gas constant. In order to calibrate the viscosity curve, data have been excerpted from Shaw (1965) for magmas with 4 vol% H_2O, leading to values η_0 = -3.0 and E = 36,500. The obtained values for crystal-free melts have been inserted in the Einstein-Roscoe equation (3.12) (Roscoe, 1952), to calculate the crystal-melt system viscosity:

$$\eta(\phi, T) = \eta_T \left(1 - \frac{\phi}{\phi_C}\right)^{-2.5} \quad (3.12)$$

where $\eta(\Phi,T)$ is the mush viscosity at a certain melt fraction Φ and temperature T, and Φ_C is the critical melt fraction when the crystals-melt system assumes features of a solid. Subsequently, the magma strength has been calculated by characterizing the system as a Newtonian fluid (3.13):

$$\sigma_M = \eta(\phi, T)\dot{\varepsilon} \quad (3.13)$$

where σ_M is the mush strength. The simulation takes into account the transition rock strength/mush strength, in a similar manner to the MCT transition, according to the relationships (14) and (15):

$$W_M = 0.5\left(1 + \cos\left(\pi\left(\frac{\phi}{10} - 3\right)\right)\right) \quad (3.14)$$

$$\sigma = \sigma_R W_M + \sigma_m (1 - W_M) \quad (3.15)$$

where W_M is a weight factor, dependent on the melt fraction (taking the value 1 when Φ = 30 vol% and 0 when Φ = 40 vol%) and σ_R is the solid rock strength.

3.3 Modelling results and sensitivity

3.3.1 Modelling results

Our modeling results are presented as contoured sections for selected time steps (Figures 3.3, 3.5, and 3.7). A more detailed view in the dyke aureole is presented as temperature-time paths (Figure 3.4) in three selected points located at a distance of 250 m from the first intruded dyke and at depths of 10, 20, and 30 km. Moreover, Figure 3.6 shows a stress-time projection of a Y transect, located in the crust at a distance of 250 m from the dyke-crust boundary.

The temperature contours (Figure 3.3) show that thermal perturbation related to dyke intrusion persists after 2 Myr, and it is still intense after the emplacement of the last dyke. The periodical emplacement of dykes produces a quick but smooth temperature increase with time, followed by a slow, constant decrease. The smoothness of the temperature profile is due to the progressive emplacement of thin dykes equally distributed during simulation time and is in agreement with results obtained by Annen and Sparks (2002).

In a crust with quartz-feldspathic composition (QF case study), the T-t path relative to the upper crust (Figure 3.4) shows a temperature increase up to a temperature peak of approximately 495°C, reached after 400 kyr of simulated time. In the lower crust, at a depth of 20 km, the temperature peak is 820°C reached after 1.57 Myr, while the peak temperature has not been reached in the lower crust at a depth of 30 km, and the maximum registered temperature is 935°C.

The T-t path geometry predicted for polymineralic mineralogical assemblages (Figure 3.4) resembles the trend of a quartz-feldspathic crust, albeit with slightly lower temperatures. These

differences, which are described in more detail later on, are maximum between the T-t paths relative to a quartz-feldspathic and a micaschists mineral assemblage and for slow reaction kinetics. Temperature variations are negligible in the lower crust at depths greater than 30 km but tend to increase at shallower depths, with lower peak temperature and subsequent slightly faster cooling. Temperature differences become negligible at greater distances from the dykes-crust boundary.

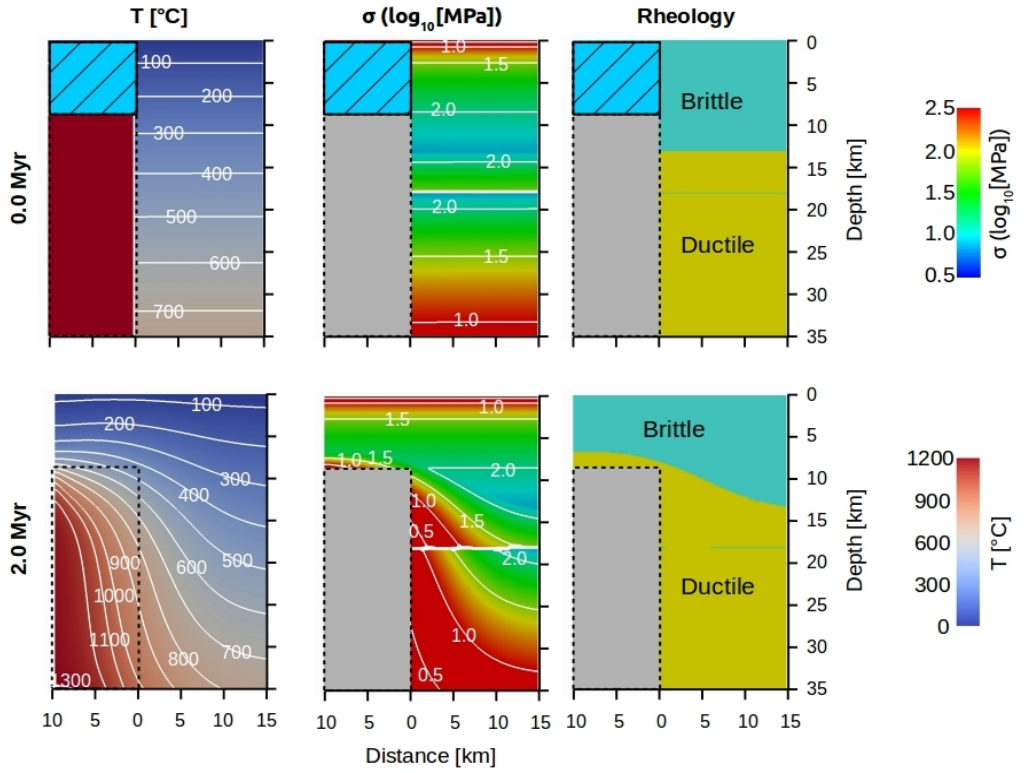

Figure 3.3 - (left column) Temperature, (middle column) differential stress, and (right column) brittle-ductile transition contour sections for a quartz-feldspathic (QF) crustal composition, at initial and final simulation time steps. (top row) The initial crustal configuration. (bottom row) The crustal configuration at the end of simulation. Temperatures are expressed in °C, while differential stress values are expressed as log10 of the value in megapascals. Dimensional values are expressed in kilometers. The light blue field in the brittle-ductile transition contour sections represents the brittle behavior, while the yellow field represents the ductile behavior. The blue hatched squares at the top of the dyke body represent the portion of the crust which is initially not included in the computation. The orange rectangles indicate the model portions simulating the dykes, not included in the strength and rheological calculations.

The different mineralogical assemblages adopted during the simulations determine strong variations in the crust differential stress (σ) values and its rheological behavior (Figure 3.5). In the QF model, the chosen geotherm determines a crustal rheological transition at an approximated depth of 13 km, corresponding to a temperature of 350°C. Brittle behavior is restricted to a thin layer located in the uppermost lower crust and corresponding to a temperature of 450°C. The thermal perturbation due to melt emplacement results in a notable uprise of the brittle-ductile transition and in a strong decrease in crustal strength.

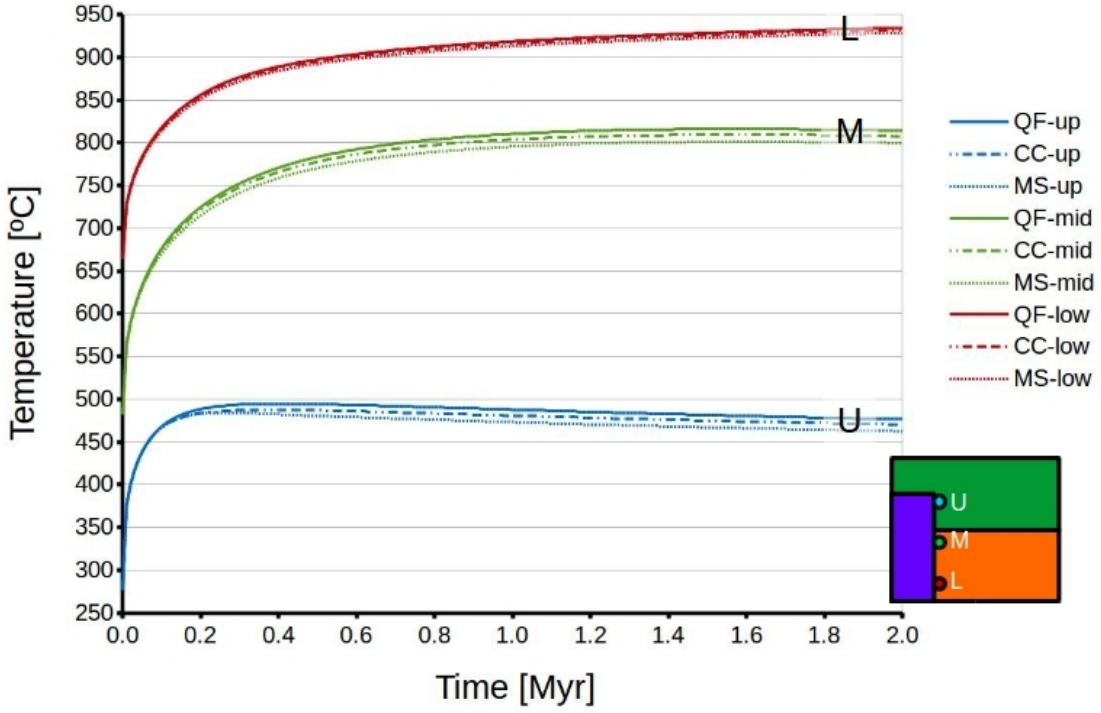

Figure 3.4 - T-t paths in different locations within the dyke aureole. Paths are for slow kinetics. Circles indicate locations of points selected for T-t plots (see transect); every point is located at 250 m away from the dykes-crust boundary at depths of, respectively, 10 km (U), 20 km (M), and 30 km (L).

If a mineralogical assemblage approximating an average crust chemical composition (CC model) is adopted (Figure 3.5), the upper crust is characterized by a marked decrease in differential strength values and a shallowing of the brittle-ductile transition (depth around 8 km, T around 260°C). In contrast, the lower crust shows higher differential strength values (approximately 320 MPa) and is partially brittle (depth of rheological transition around 24 km, T around 570°C). The low σ values in the upper crust are due to a high mica content, whereas in the lower crust the different composition and metamorphism determine an enrichment in minerals characterized by high strength values (mostly garnet) and with a subsequent deepening of the brittle-ductile transition. Subsequent to dyke intrusion, the thermal perturbation causes an overall decrease in strength, except in a thin lateral aureole in the upper crust and at the top of the dyke body, where we predict an abrupt increase (and later decrease) in σ values. This σ trend is due to the enrichment in strong minerals (mostly garnet) at the expenses of micas (mostly chlorite) in the first stages of simulation, followed by a further temperature increase and subsequent decrease in σ values. This increase-decrease in rock strength is accompanied by a transition from brittle to ductile behavior of the aureole, evidencing the alternation between metamorphic and thermal control on rock rheology.

After 800 kyr the innermost part of the upper aureole is characterized by brittle behavior, albeit with low strength values. This low-strength nucleus is the result of the generation of melts

(up to a quantity of 8 vol %) and capable to break up the rock's solid framework (i.e., the structure, constituted by crystals, representing the rock's continuous phase and determining its rheological characteristics). When compared to fast kinetics, a slow reaction kinetics results in a smoother transition in the upper crust from weak rocks to a strong aureole; also, the melt nucleus is slightly more extended. Furthermore, partial melting also occurs in the lower crust, up to a distance of 10 km, but melting percentages do not exceed 5 vol%. The SLT threshold is thus not reached, and the lower crust still keeps a solid framework.

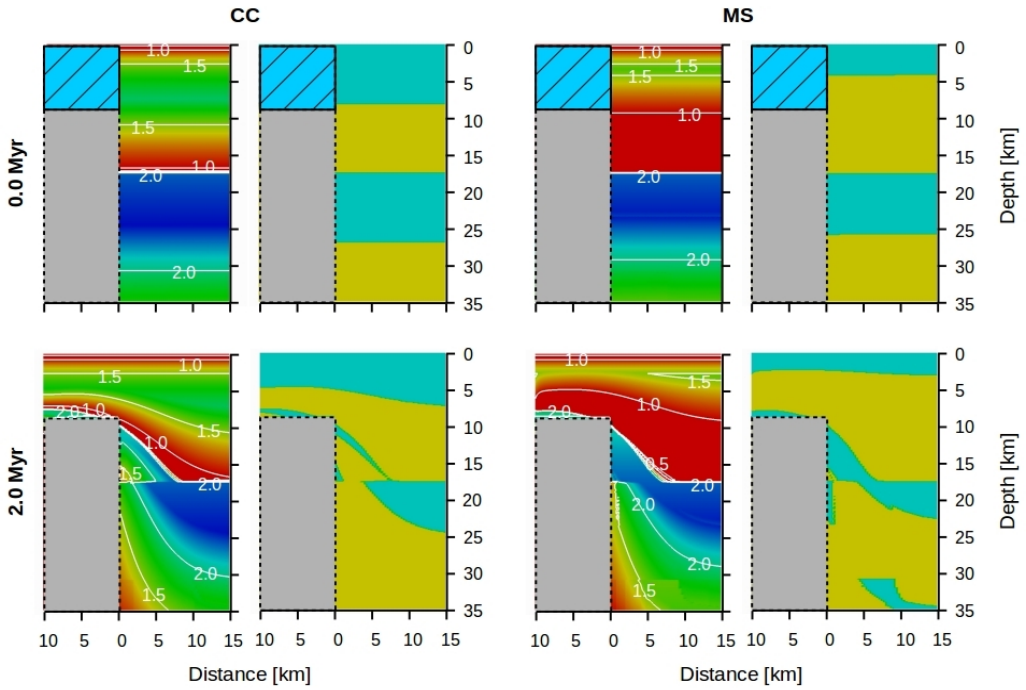

Figure 3.5 - Differential and brittle-ductile transition contour sections for a mineralogical assemblage approximating average crustal composition (CC) and micaschist crust (MS), taking into account a slow reaction kinetics. For color scale, see Figure 3.3. (top row) The initial crustal configuration. (bottom row) The crustal configuration at the end of simulation. (first and second columns) Relative to CC case study. (third and fourth columns) Relative to MS case study. Temperatures are expressed in °C, while differential stress values are expressed as log10 of the value in megapascals. Dimensional values are expressed in kilometers. The light blue field in the brittle-ductile transition contour sections represents the brittle behavior, while the yellow field represents the ductile behavior. The blue hatched squares at the top of the dyke body represent the portion of the crust which is initially not included in the computation. The orange rectangles indicate the model portions simulating the dykes, not included in the strength and rheological calculations.

In the micaschist crust (MS) model, where a micaschists mineralogical assemblage is implemented, the chosen geotherm determines a very weak upper crust with a brittle-ductile transition less than 4 km deep, at a temperature of 130°C (Figure 3.5). Compared to the CC model, the lower crust is also weaker, with a brittle-ductile transition depth of 22 km (T 530°C), but not as weak as in the QF model.

Dyke-induced thermal metamorphism in the upper crust determines strong mineralogical associations, resulting in a consistent brittle domain in the upper lateral aureole. The lower crust also is deeply affected by reaction kinetics variations: when a slow kinetics is adopted, the melt

percentage may reach values >15%, with subsequent breakup of the rock solid framework. Consequently, contoured sections in Figure 3.5 show a brittle interval at the base of the lower crust, appearing immediately after the emplacement of the first dykes (i.e., the first represented time steps). This brittle interval slowly migrates toward more peripheral parts of the base of the crust, suggesting that crustal deformation is controlled initially by melt. The metamorphism also affects the top of the lower crust, where a 1 km thick brittle domain develops at the dykes-host rocks boundary.

Variations in crustal differential stress values are largest in the proximity of the intruding dykes (Figure 3.6). In the QF model, the σ trend is in general agreement with temperature variations, which is not the case for the CC and MS models. When a polymineralic crust is taken into account, we observe in the first 200 kyr a sharp increase in differential stress values, caused by dyke-induced metamorphism. This is particularly evident in the upper crust of the MS model. In the CC model the strength increase is followed by a rapid decrease due to the subsequent thermal perturbation and generation of melts during the last time steps. In the MS model, the top of the lower crust is characterized by a brittle interval (related to the presence of partially molten rocks close to the intrusion-crust boundary), which, however, is too thin to be detectable in the stress contour sections.

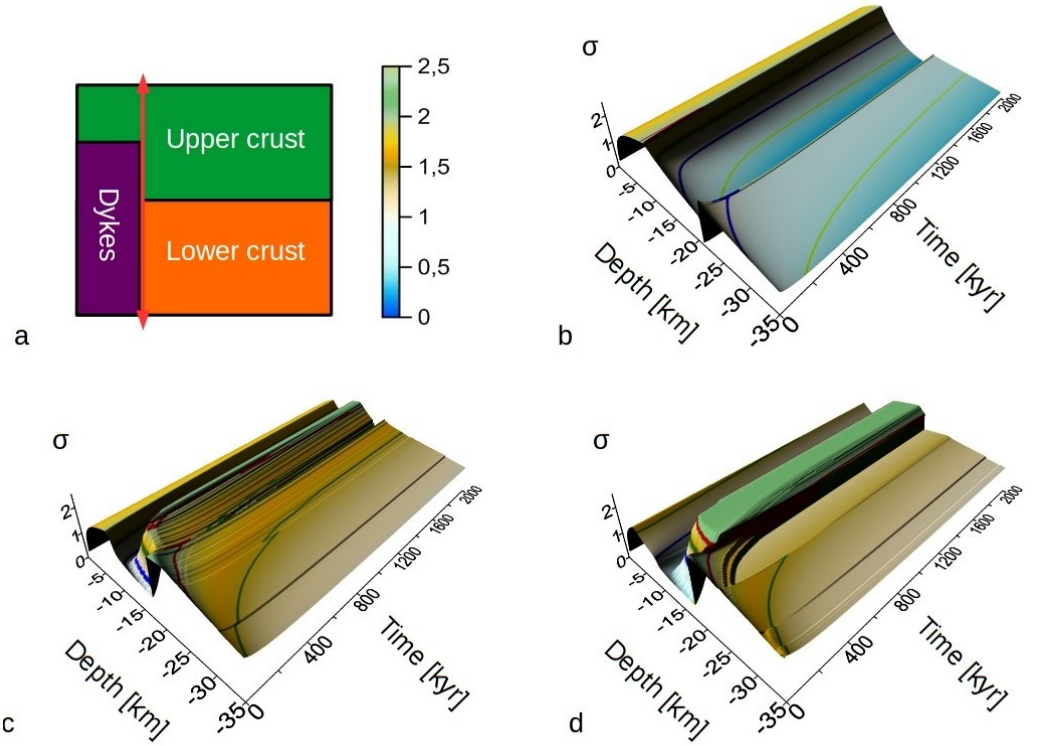

Figure 3.6 - Differential stress-time projections along a transect located in the crust, at a distance of 250 m from the dykes-crust boundary; (a) location of the measurement profile and color scale, and σ-t trend in the (b) QF, (c) CC, and (d) MS case studies. σ is expressed as log10 of the value in megapascals. The isolines in Figures 3.6b–3.6d indicate the reference values of 1.0 (blue), 1.5 (green), and 2.0 (red).

3.3.2 Parameter sensitivity

We have tested the sensitivity of our models by varying several parameters of the MS model with low reaction kinetics, as this model proved to be the most sensitive to metamorphism and melt generation (Figure 3.7).

First, to assess if the intrusion rate exerts a major control on the rheology, we tested our model (1) by considering a set of 10 dykes, each with a thickness of 1 km, intruding the crust over a period of 2 Myr, thus simulating instantaneous injections of huge quantities of melts followed by long periods of zero melt emplacement and (2) by expanding the overall intrusion time to 10 Myr, assuming a constant growth of the dyke body, with a resultant melt intrusion rate of 1 mm/yr.

Results show that when dyke thickness increases while the growth time of the whole magmatic segment remains constant, the geometry of the brittle-ductile transitions does not show major variations. Metamorphic aureoles are somewhat larger, and the basal brittle interval caused by partial melting shifts toward more peripheral parts of the model. These differences do not exceed a few hundreds of meters and therefore can be neglected, except for the top of the lower crust where the brittle domain reaches an average thickness of 3 km. Moreover, the tests show that variations in melt production also are negligible and that final differential stress values are reduced, with minimum values at the base of the upper crust.

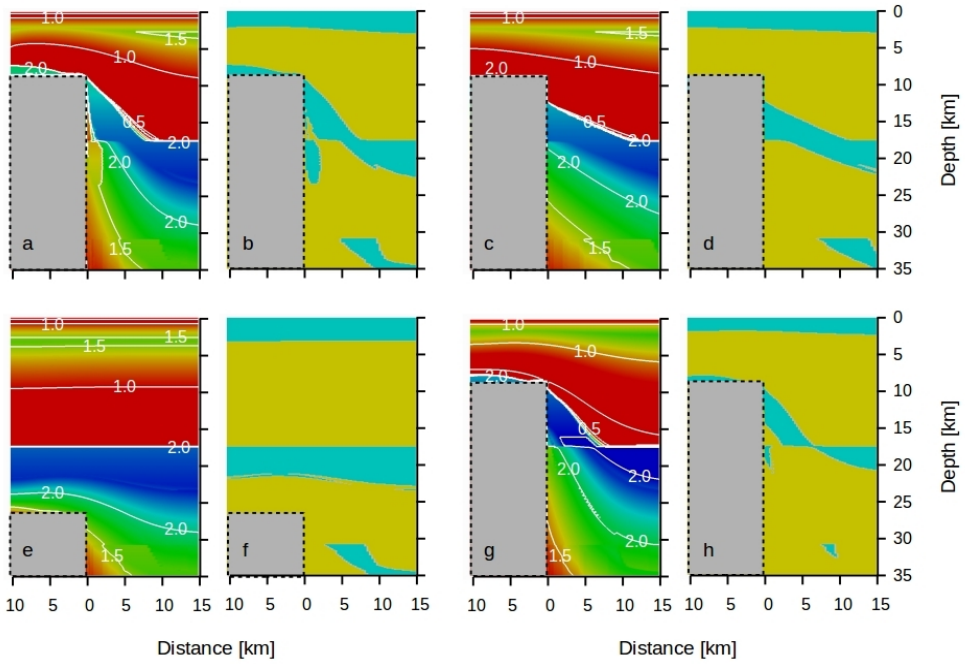

Figure 3.7 - (a, c, e, g) Differential and (b, d, f, h) brittle-ductile transition contour sections for a micaschist crust (MS), when different parameters are tested. All panels refer to the end of simulation. Ten dykes with thickness of 1 km, intruded in a time span of 2 Myr (Figures 3.7a and 3.7b); a 10 km dyke body intruded in a time span of 10 Myr (Figures 3.7c and 3.7d); dyke body top at a depth of 26,250 m (Figures 3.7e and 3.7f); λ value = 0 (Figures 3.7g and 3.7h). For color scale see Figure 3.3.

Rheological variations become more pronounced when we adopt a longer simulation time for the growth of the intrusive magma body, allowing the thermal perturbation to reach more

peripheral parts of the crust. This observation is in line with results by Daniels et al. (2014). An opposite effect of the slower intrusion rate is the reduction in temperature peaks, especially in the upper crust. The combined effect results in a larger upper metamorphic aureole but does not affect the uppermost intruded rocks.

Although partial melting at the base of the crust affects brittle behavior of the rocks at a farther distance from the dykes-crust boundary, it shows no substantial first-order variations. This confirms the thermal control already observed in the dyke lower aureole in the previous simulations. Differences in differential stress values follow the earlier observed trend in the brittle-ductile transition, with higher values in the proximity of the intruded dykes.

Other tests involved the intrusion depth, with default values of 17.5 km (corresponding to the upper-lower crust boundary) and 26.25 km (half thickness of the lower crust). The temperatures computed in the tests are considerably less than those of the previous runs, and variations in differential stress values and rheology are consequently also smaller. An exception occurs at the top of the dyke body where temperatures reach 800°C for an emplacement depth of 26.25 km. However, as the reduced volume of emplaced magmas does not allow melt percentages higher than 4 vol%, the solid crust framework is maintained and no brittle intervals develop in the thermally perturbed lower crust.

The final test involves setting $\lambda = 0$, which results in an uplift of the brittle-ductile transition by 1 km in the upper crust and by 2 km in the lower crust. Moreover, the intracrustal brittle domains located at the contact with the dyke body are considerably reduced in size, and the crustal strength increases, with maximum σ values of 420 Mpa.

3.4 Discussion

The results of our simulations show that different lithologies may exert a first-order control on both the strength and the rheological behavior of the crust. Another outcome is that the fertility of the crust (i.e., its capacity to generate melts at a given temperature) cannot be established a priori by assuming a direct correlation between anatexis and reached temperature peaks. In contrast, the composition of the crust exerts a primary role and must be taken into account.

The pristine QF case study (Figure 3.3) demonstrates the dominant control of temperature on the rheology of the crust. Here we observe that the isodifferential stress contour lines follow the isotherms, with the only exception at the upper-lower crust boundary. This observation is supported also by the geometry of the brittle-ductile transition, which lies at a temperature between 350°C and 390°C (assuming $\lambda = 0.4$). The thermal perturbation propagating from the intruding magma body causes a pronounced decrease in crustal strength, in agreement with the findings by, e.g., Buck (2004; 2006). When more complex lithologies are considered, the crustal rheology exhibits a pronounced dependence on mineral assemblages, which therefore may result in important deviations in tectonic deformation of a crust subjected to heating and extension. Heat absorption by metamorphism and melt generation reduces the thermal perturbation in our model (Figure 3.4), although temperature differences are negligible at a first order of approximation. At the same time, metamorphism and melt generation do exert a main control on the rheological features of the crust, especially within a distance of a few kilometers from the dykes-crust boundary (Figure 3.5). Differently from previous studies (e.g., Buck, 2004, 2006; Daniels et al., 2014), the thermal perturbation in the upper crust causes an increase in the rock strength and a change in the rheology of the host rocks. Furthermore, the depth of the brittle-ductile transition in the lower crust significantly increases to 23 to 25 km, roughly corresponding with the 600°C isotherm. This result is in agreement with findings by Daniels et al. (2014).

The extension of the aureole 2 Myr after intrusion is much smaller when the intrusion rates are 1 mm/yr, compared to a fast value of 5 mm/yr (Figure 3.7). In addition, the brittle aureole developed in 10 Myr is more extended than the one developed in 2 Myr. It, however, does not develop in proximity to the uppermost part of the magma body (Figure 3.7), which is consistent with the temperatures controlled by the intrusion rates. Thus, the geometry and extension of a brittle aureole depend on the adopted intrusion rates: low intrusion rates will lead to laterally more extended and vertically less extended metamorphic aureoles.

Another important parameter appears to be the reaction kinetics: we predict in both the CC and MS case studies a less extended brittle aureole for faster kinetics. This is not due to temperature but to a more effective mica consumption, resulting in relatively higher volume of strong minerals (such as garnet). The strong aureole located at the base of the upper crust may hamper magma ascent in proximity of older dykes and instead promote the emplacement of sills along the upper-lower crust boundary (already favored by the density jump). Consequently, in a sedimentary host rock setting, this may constitute an alternative explanation to other dyke spacing mechanisms (e.g., Bunger et al., 2013; Maccaferri et al., 2014).

An increase in rock strength may also occur in the lower crust and may be coupled with an extended partial melting at its base. Here melt production does not exceed the Rheological Critical Melt Percentage (RCMP) due to both reduced temperatures and crust fertility, in agreement with Solano et al. (2012). The quantity of melts retained by the crust in partially molten intervals is uncertain, depending intrinsically on the quantity of melt and its viscosity. Melt migration is generally hampered by the high viscosity of the fluid (Laporte and Watsons, 1995). However, results by Brown (2007, 2010a, 2010b, 2013) show that when a differential stress is applied melt can segregate at fluid fractions $\leq$ 7 vol%, leaving approximately 1 vol% melt, retained on grain boundaries (Holness and Sawyer, 2008; Marchildon and Brown, 2002; Sawyer, 2001). According to our results, the presence of migmatites is mainly foreseen at the base of the crust and for depths larger than 30 km, producing a migmatitic layer of approximately 5 km thickness. This is in agreement with migmatitic paragneisses exposed in other deep crustal intervals, e.g., in Calabria (Caggianelli and Prosser, 2001, 2002; Del Moro et al., 2000). Furthermore, these are also the most favorable layers where crustal melt migration may occur. If conditions for melt movement are reached, generated melts may reach shallower levels, generating and/or contributing to a coeval acidic volcanism, as observed in rift areas, such as the Afar Rift and surroundings (e.g., Mohr, 1991, and references therein; Wolfenden et al., 2004; Ayalew and Gibson, 2009; Bastow et al., 2011; Natali et al., 2011). However, our model shows that a slow reaction kinetics favors anatexis and determines a higher melt production, since micas are not only reactants for melt production but also for other reactions occurring at lower temperatures not involving melt generation.

When a different thickness of the intruded dykes is adopted (Figure 3.7), while keeping the intrusion rate constant, we do not observe marked variations in the crust fertility, which is in agreement with results by Annen and Sparks (2002) and Annen et al. (2006). Variations in produced melt volumes are also negligible, even for higher intrusion rates. This is in contrast with findings by the aforementioned authors but can be explained by the fact that in our simulations melt production is foreseen if minerals are still available and not consumed by previous metamorphic reactions. Thus, our results show that when temperatures are appropriate for melting, lithology exerts a primary control on crustal fertility.

In such cases, where lithology indeed exerts a main control on the quantity of melt generated in the crust, temperatures and thermal diffusivity also influence the volume of rocks affected by anatexis. At the end of a model run, melt is generated up to a distance of 20 km from the dykes-crust boundary. However, in our simulations the intruded body maintains a temperature higher

than the established crystallization temperature (1100°C) in a substantial part of its volume. In addition, the T-t paths in the aureole, relative to a point located at a depth of 30 km, show that the temperature is constantly increasing up to the end of the model simulation. This suggests that the crust might be subjected to further heating over a longer time span, especially in the lower crust, and that therefore a larger part of the crust may be affected by anatexis. As a result, the base of the crust can be marked by a migmatite layer, where the relative weakness and the preexisting melt veins (Rosenberg and Handy, 2005) may favor the magma ascent from underplated bodies.

3.5 Conclusions

We have investigated the thermorheological behavior of a two-layered, polymineralic crust affected by a thermal perturbation caused by lateral intrusion of melts during extension phases. The obtained model predictions were compared with results of a simpler two-layered monomineralic crust.

During an intrusion-induced temperature increase, a quartz-feldspathic crust shows a significant decrease in strength values, coherently with the temperature propagation in time. The crustal response becomes even more complex when metamorphism is taken into account. In the investigated models the lithology variations exert a main control as metamorphism may cause a transition from ductile to brittle behavior in the crust for increasing temperatures. These model predictions differ from results from previous studies (e.g., Buck, 2004; 2006). This is particularly evident in the upper crust, where the presence of a wedge-shaped brittle body is predicted in all our simulations.

Another main factor controlling the rheology of the crust is the presence of melts. We have tested during our simulations that the amount of melt produced is sufficient to exceed the MCT and to cause breakup of the solid framework of rocks. Melts, therefore, promote brittle behavior in the crust and a reduction of strength values.

Differently from previous studies (e.g., Annen and Sparks, 2002; Annen et al., 2006), we observe that the crust fertility is mainly influenced by (1) lithology and (2) reaction kinetics. For fast reaction kinetics, the obtained melt fraction was considerably less, whereas slow reaction kinetics enhances the melt productivity by preservation of reactants for muscovite and biotite dehydration melting. This, therefore, plays a key role in changing the rheological behavior of the lower crust, with, for instance, brittle behavior in the case of a slow kinetics and ductile behavior when fast kinetics is adopted. The importance of lithology and reaction kinetics over temperature for melt production is also tested when melt intrusion rate variations are introduced: in all tested cases, obtained melt fractions show no significant differences.

The more complex rheological stratification resulting from dyke intrusion might lead to important deviations from expected rheological behavior of the crust during extension. This, for instance, could contribute to an explanation for the observed spacing of dykes during melt intrusion in extensional settings. Our findings suggest that the distance between dykes may be influenced by the increase in strength caused by previous melt intrusions.

4. Thermo-rheological aspects of crustal evolution during continental breakup and melt intrusion: The Main Ethiopian Rift, East Africa

4.1 Introduction

Continental break-up is an important geodynamic process occurring during plate evolution, and may mark the response of the lithosphere when it is subject to tensional stresses of a sufficient intensity and duration. Plate rupture is the final result of the thinning and heating of the lithosphere, and is associated with upwelling of mantle material, whose decompression may lead to partial melting and subsequent magmatic activity (e.g. Ebinger and Sleep, 1998; Burov et al., 2007). This process is further enhanced when the mantle is subjected to thermal anomalies, such as in hot spot areas, where the presence of mantle plumes may also lead to lithosphere doming and extension (e.g. Burov et al., 2007; Burov and Gerya, 2014). The nature of the interaction between lithosphere- and plume-related tensile stress fields is subject to extensive debate, and their effective role in causing continental thinning and rupture (e.g. Burov et al., 2007, and references therein; Cloetingh et al., 2013). However, it is well established that mantle upwelling-related magmatic activity strongly favors plate extension and breakup (e.g. Buck, 2004, 2006). This is testified to by the collocation of extension and strong magmatic activity in many different areas, including a large number of passive continental margins worldwide. In such magmatic margins, thick sequences of igneous rocks may extrude, intrude and underplate the crust (e.g. Menzies et al., 2002). In many extensional models (e.g. Buck, 1991; Davis and Kusznir, 2004), magmatism is either absent or mainly considered as a consequence of rifting. This is in contrast with observations in extensional areas, where time relationships between igneous rocks emplacement ages and extension evolution demonstrate that magmatic activity occurs prior to, or simultaneously with, extension (e.g. Buck, 2006, and references therein). In addition, magmatic activity and rifting associated deformation may focus along inherited lithospheric heterogeneities (such as former suture zones), where the plume had the function of further triggering the rupture, more than being the direct cause of rifting (e.g. Cloetingh et al., 2013; Buiter and Torsvik, 2014).

The presence of lithospheric heterogeneities may influence the extensional history of rifting areas. However, the evolution of plate strength and rheology, due to melt intrusion, is still poorly understood (e.g. Lavecchia et al., 2016). One of the least investigated aspects is the lithological evolution of rifting areas and their fertility (i.e. their capacity to produce melts when subjected to temperature and pressure variation). Although most magmatic products associated with rift areas are represented by mantle-derived melts, the presence of magmas characterized by a mixed (e.g. Thompson et al., 2001) or crustal origin (e.g. Kirstein et al., 2000) has been widely recognized.

This chapter is base on: Lavecchia A., Beekman F., Clark S.R., and Cloetingh S. (2016), Thermo-rheological aspects of crustal evolution during continental breakup and melt intrusion: The Main Ethiopian Rift, East Africa. Tectonophysics, 686, 51–62, doi: 10.1016/j.tecto.2016.07.018.

This testifies the profound effect that pressure and temperature conditions may exert on the same nature of the lithosphere, and, especially, on the crust.

One of the best studied rifting areas is the Main Ethiopian Rift (MER) (Figure 4.1), a slowly extending continental rift constituting the northernmost section of the East African Rift System (e.g. Ebinger and Casey, 2001). Indeed, the relationship between magmatic activity, anomalous topographic swells and the presence of mantle plumes has long been recognized in the MER region (e.g. Ebinger and Sleep, 1998). However, both the evolution of the intruded crust and its response to the thermal perturbation are still poorly understood. These two elements are of a particular importance as the mantle lithosphere in this region is characterized by a marked thinning beneath the whole area (e.g. Ebinger and Sleep, 1998; Dugda et al., 2007), suggesting a major role of crust rheology in determining the strength of the whole plate.

In this paper, we present a thermo-mechanical model with the aim to examine the rheology variations of a continental crust subjected to a melt intrusion-related thermal perturbation. Our model includes temperature-induced metamorphic variations in crustal mineralogical association. The model characteristics have been calibrated adopting MER lithological and geometrical constraints, with the aim to better understand the evolution of the Ethiopian continental crust during the development of magma segments characterizing the axial rifting area.

4.2 Tectonic setting

The Main Ethiopian Rift (MER) (Figure 4.1) constitutes the northern part of the East African Rift System (e.g. Ebinger and Casey, 2001) and converges, together with the Red Sea and Gulf of Aden rifts, in the Afar area. Among the three branches, it is the youngest and least evolved (e.g. Bastow et al., 2011, and references therein). The onset of extension in the MER is dated at ≈11–10 Ma (e.g. Ukstins et al., 2002; Wolfenden et al., 2004) within the Precambrian metamorphic crustal basement of the Pan-African Mozambique belt (Kazmin et al., 1978) and was mostly accommodated along mid-Miocene border faults delineating half-grabens (Morley, 1988; Wolfenden et al., 2004). The last phases of extension are characterized by an intense magmatic activity, leading to the construction of approximately 20 km thick, right-stepping, en echelon magmatic segments during the Pliocene-Pleistocene time (Ebinger and Casey, 2001; Beutel et al., 2010, and references therein; Bastow et al., 2011).

The strain pattern highlighted by geodetic and seismic studies shows that at present day the border faults are relatively inactive, with earthquakes concentrated within magmatic segments (e.g. Keir et al., 2006). The Main Ethiopian Rift is characterized by a seismic moment release in the MER that is b 50% than what is expected from the estimated extension velocity (Hofstetter and Beyth, 2003), which suggests that most extension is accommodated aseismically. These observations are supported by gravity (Cornwell et al., 2006) and geodetic data (e.g. Ebinger and Casey, 2001), showing that N 80% strain is accommodated along magmatic segments and without a marked crustal thinning. P- and S-wave tomography models indicate that the lithosphere–asthenosphere boundary lies at a depth of approximately 70 km, associated with the presence of a broad mantle upwelling beneath the MER and the Ethiopian plateau. The asthenosphere is characterized by some of the lowest-velocity worldwide (Bastow et al., 2011, and references therein) and constitutes the main source zone for melts emplaced in the MER and magma-assisted extension (e.g. Bastow et al., 2011). Deeper in the mantle, the low-velocity anomaly continues down to the transition zone, and likely connects to the African Superplume (Bastow et al., 2011). SKS analysis and crustal splitting observations point out that melt accumulates in vertically oriented dykes cross-cutting the lithosphere (e.g. Keir et al., 2005). Furthermore, magnetotelluric

surveys highlight the presence of intruded and partially molten material; these melt zones occur at various depth in the crust and are associated with seismicity (Bastow et al., 2011).

Geophysical and geochemical data show that the crust has been extensively modified by magmatic modification and that the presence of melt is strictly related to extension by faulting. Crustal thickness is greatest (40–50 km) beneath the uplifted plateau flanking the rift valley, where thickness registered is approximately 45 km and associated with evidences of magmatic underplating (Dugda et al., 2005). Beneath the MER, crustal thickness decreases to values ranging from 38 km to 27 km, and are associated to Poisson's ratio values of 0.27 to 0.35, indicating a marked crustal thinning associated with massive presence of intruded mafic material and a presence of partial melting (Dugda et al., 2005) (Figure 4.3).

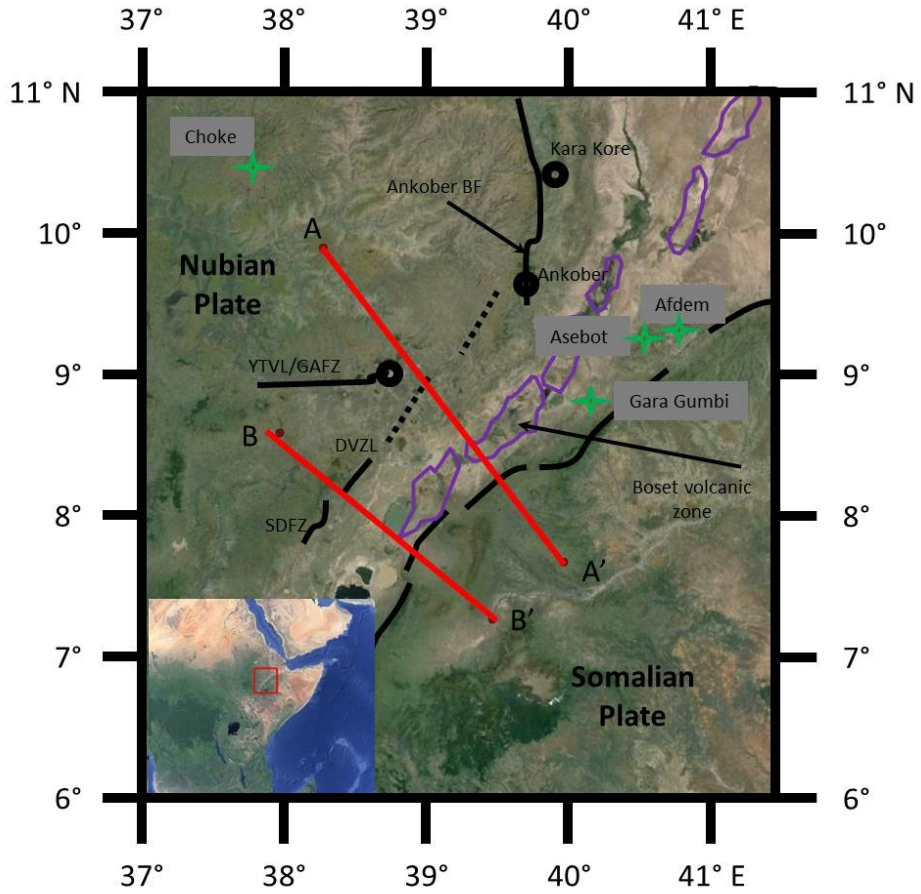

Figure 4.1. - Sketch map of Afar Rift and northern Main Ethiopian Rift (after Bastow et al., 2011, modified). Violet closed lines represent magmatic segments and solid black lines depict major mid-Miocene border faults. Dashed lines are faulted monoclines. Green stars are selected Cenozoic volcanoes. Red lines are the traces of gravimetric cross sections adopted for simulations (AA'': Cornwell et al., 2006; BB': Mahatsente et al., 1999; see Figure 4.2). SDFZ—Silti Debre Zeyit fault zone; GAFZ—Guder Ambo fault zone; YTVL—Yerer-Tullu Wellel volcanotectonic lineament; BF—Border Fault; DZVL—Debre Zeit Volcanic Lineament.

4.3 Model description

4.3.1 Geometrical features

We used a 2D thermal model that numerically simulates the temperature variations in a multilayered crustal section, induced by the emplacement of a sequence of basaltic dykes, over a time span ranging from 1.6 Myr (Ebinger and Casey, 2001) to 3.0 Myr (Beutel et al., 2010, and references therein). The geometries and densities adopted in the model are based on previous reconstructions, based on works by Mahatsente et al. (1999) and Cornwell et al. (2006) (Figure 4.2); they comprise a 35 km thick crust with a lateral extension of 40 km, divided in intervals with different density and mineralogical composition. The lateral crustal extension in the model ensures that the thermal perturbation does not propagate sufficiently fast to reach the crust boundary and create undesired overheating effects. The thermal loading is implemented by "injecting" a sequence of 400 dykes (conform Lavecchia et al., 2016), each being 25 m thick, forming a basaltic body growing by outward lateral accretion (from the right leftward). The magmatic segment growth rate corresponds to an intrusion rate ranging from ≈3.5 to ≈6 mm yr^{-1}.

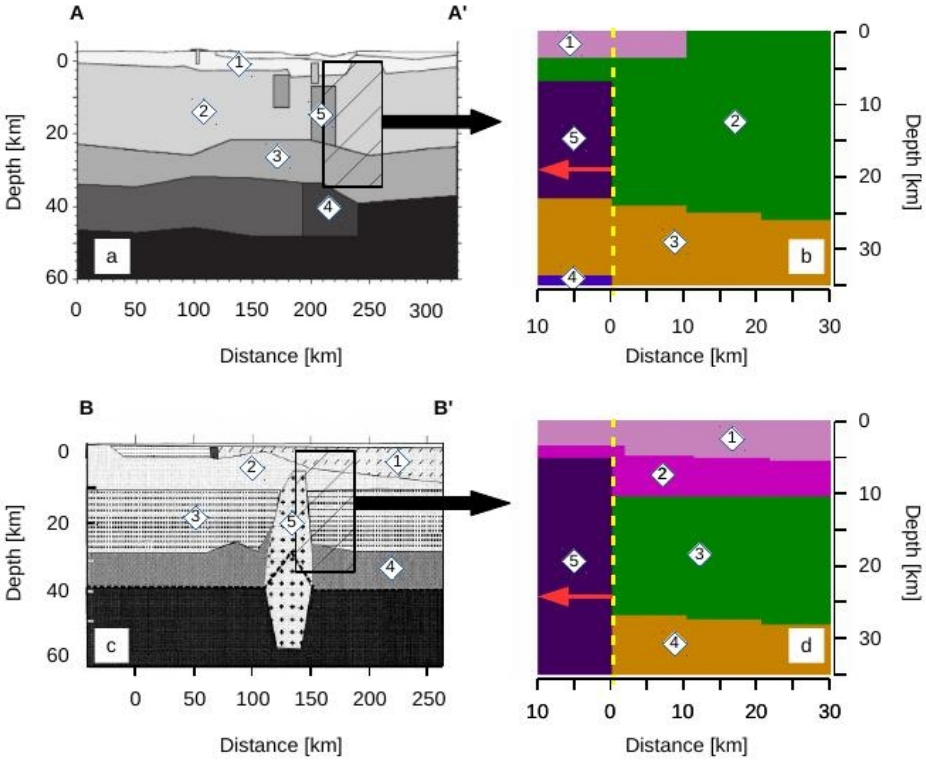

Figure 4.2 - Two vertical cross-sections of the northern MER, based on studies by Cornwell et al., 2006 (a, section AA') and Mahatsente et al., 1999 (c, section BB'), and their geometrical representations adopted in the model (b, d). For location of the sections, see Figure 4.1. The numbering refers to different layers inferred from constrains by geophysical studies (see text for explanation); red arrows point out the direction of the magmatic segment growth, indicating that each dyke is added to the previous segment by leftward lateral accretion. The red and blue dashed lines are the traces for differential stress-depth profiles (see Figures 4.7, 4.8).

The geometry implemented in the first case study (CR case study, Figure 4.2a, b) incorporates the 2D density model obtained by Cornwell et al. (2006), where 5 main different bodies are detected at a depth b =35 km:

1. A supra-basement interval, with density = 2570 kg m −3 , interpreted as pre-rift Jurassic to Palaeogene sedimentary rocks, interbedded with Oligocene flood basalts. The model takes into account the buried horst, constituting a rift flank related to the Arboye border fault (Cornwell et al., 2006, and reference therein).
2. An upper crust whose age ranges from lower to middle Proterozoic, composed of clastic metasediments.
3. A high density lower crust layer, interpreted as an Archean cratonic basement (age ≥ 2.5 Ga), composed of high grade gneisses (granulite to amphibolite facies) (Kazmin et al., 1978, and references therein), underplated by Oligocene and more recent material (Mackenzieet al., 2005).
4. A mafic wedge, interpreted as low density mantle (rather than high density underplate) and consistent with the presence of 3–5% partial melt (Cornwell et al., 2006, and reference therein).
5. A gabbroic body, intruded in correspondence of the rift axis, whose high conductivity suggests the presence of melts at present day (Cornwell et al., 2006, and references therein).

The second case study (MR case study, Figures 4.2c, d) implements the geometry obtained by Mahatsente et al. (1999), where the following intervals are detected in the northern MER:

1. A cover interval, mainly constituted by siliceous domes and flows, whose composition ranges from pantellerites to obsidians to volcanoes characterized by andesite to rhyolite activity (Mahatsente et al., 1999).
2. An upper layer, interpreted as the upper part of the crystalline basement and correspondent to the Miocene Magdala group (Molly, 1959, and references therein); it is mainly constituted by rhyolites, trachytes, ignimbrites and basalts (Mahatsente et al., 1999).
3. An intermediate interval, whose density roughly corresponds with the clastic layer occurring in Bastow et al. (2011), and thus interpreted as such in our simulation.
4. A lower crust, with a lower density than the one adopted in the model by Bastow et al. (2011). We assume in our simulation that the difference in density is due to a lower volume of underplated material.
5. An intruded gabbroic body, whose density variation has been interpreted as due to difference in crust contamination in the upper portion by Mahatsente et al. (1999) (in our model we assign the same density for the whole body).

4.3.2 Thermal and petrogenetic features

The thermal evolution of the model is governed by the heat transfer (4.1):

$$\rho C_p \frac{\partial T}{\partial t} = k(T)\nabla^2 T + Q \quad (4.1)$$

where ρ is the density, C_p is the specific heat, T is the temperature, t is the time, k is the thermal conductivity and Q the internal heat production. The dyke emplacement has been assumed a quasi-instantaneous process, and hence the model does not take into account any advection of heat. The numerical solution is obtained by using FEniCS (Logg et al., 2012), a collection of free scientific computing codes for finite element based automated solution of partial differential equations.

Parameter	**Symbol and equation**	**Value**
Surface temperature	T_S	25 °C
Crust base temperature	T_b	600 °C, 750 °C
Melt emplacement temperature	T_m	1300 °C
Melt solidus temperature	T_S	1100 °C
Model base heat flux	q_b	27 mW m^{-2}
Latent heat of crystallization	LH	400 kJ kg^{-1}
Radiogenic heat generation	$A(z) = A_0 e^{\frac{-z}{D}}$	A_0 = 2 μW m^{-3} D = 12 km

Case study and layer	**Mineral assemblage (%vol.)**	**Density (kg m^{-3})**	**A (W m^{-1} °C^{-1}); B (W m^{-1})**
CR			
1	qz40, pl25, kfs35	2570	0.64; 807
2	chl30, ms25, qz25, pl10, kfs10	2790	0.75; 705
3	ms10, qz20, pl15, ky5, grt10, bt25, st5, kfs10	2940	0.75; 705
4	ol100	3230	0.73; 1293
5	ol100	3000	1.18; 474
MR			
1	qz40, pl25, kfs35	2500	0.64; 807
2	qz25, pl15, kfs45,	2700	0.64; 807
3	chl30, ms25, qz25, pl10, kfs10	2780	0.75; 705
4	ms10, qz20, pl15, ky5, grt10, bt25, st5, kfs10	2900	0.75; 705
5	ol100	3050	1.18; 474

Table 4.1 - Thermal and compositional parameters adopted in the model. LH value comes from Spear (1993); densities for different layers have been taken from Cornwell et al. (2006) and Mahatsente et al. (1999) (see text for further explanation). A and B parameters are used to calculate the temperature-dependent thermal conductivity, according to the formula: k(T) = A + B / (350 + T (°C)) (Clauser and Huenges, 1995, and references therein). Mineral abbreviations are as follows: bt = biotite, chl = chlorite, grt = garnet, kfs = K-feldspars, ky = kyanite, ms = muscovite, ol = olivine, pl = plagioclase, qz = quartz, st = staurolite.

The values adopted for different parameters are given in Table 4.1. We consider two different geotherms, both constituted by a temperature-dependent thermal conductivity, a fixed surface temperature of 25 °C, a heat flux at the base of the crust of 27 mW m^{-2} and a heat flux at the lateral boundaries equal to 0. The different geotherms are distinguished in a “cold” geotherm, characterized by a transient temperature of 600 °C at the crust base, a “warm” geotherm,

characterized by a temperature of 750 °C at the crust base. These different temperature values were chosen in order to compare different preliminary situations, where in the "cold" simulations we isolate the effect of thermal perturbation in an initially unperturbed continental crust, and in a "warm" case we take into account the possibility of a thermal perturbation (e.g. due to magmatic underplating) prior to dyke intrusion.

The release of heat during melt crystallization in the dyke body has been taken into account for the cooling magma by implementing an effective specific heat instead of the true specific heat, in a temperature interval between 1300 and 1100 °C (Paterson et al., 1998, and references therein). The effective specific heat has been calculated on the basis of the formula by Spear (1993) (4.2)(Ayalew and Gibson, 2009):

$$C_{EFF} = C_p + \frac{LH}{\Delta T} \quad (4.2)$$

where C_{EFF} is the effective specific heat, C_p is the specific heat, LH is the latent heat of crystallization and ΔT is the crystallization temperature interval.

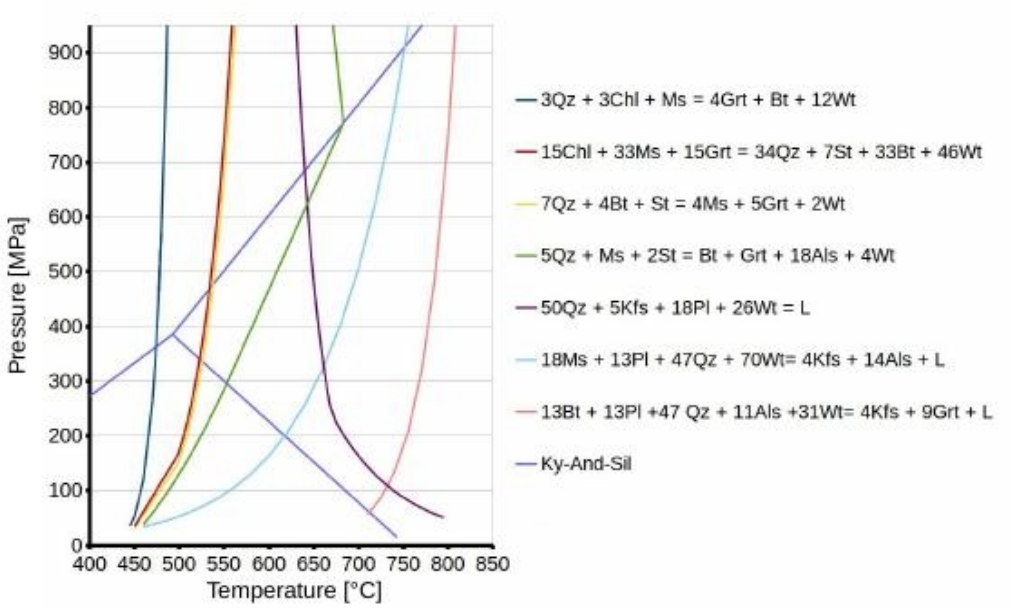

Figure 4.3 - Reaction grid used to simulate metamorphism in the crust. Reactions in the legend occur with increasing temperature. For mineral abbreviations see caption of Table 4.2. Additional abbreviations: als = allumosilicates; ky-and-sil = kyanite-andalusite-sillimanite; L = melt; wt = water.

Our model takes into account prograde metamorphism occurring in a polymineralic crust, including the most common minerals in crustal rocks (i.e. quartz, plagioclase, K-feldspars, allumosilicates, chlorite, muscovite, biotite, garnet, staurolite, olivine and water) (Table 4.1).

The metamorphic grid is illustrated in Figure 4.3; the reaction stoichiometry has been calculated on the basis of oxides balance and kept fixed at different T-P conditions; it is as follows:

1. Ky-And-Sil
2. 3Chl + Ms. + 3Qz = Bt + 4Grt + 12Wt

3. 15Chl + 15Grt + 33Ms = 33Bt + 34Qz + 7St + 46Wt
4. 4Bt + 7Qz + St = 5Grt + 4Ms + 2Wt
5. Ms. + 5Qz + 2St = 18Als + Bt + Grt + 4Wt
6. 18Ab + 5Kfs + 50Qz + 26Wt = L
7. 13Ab + 18Ms + 47Qz + 70Wt = 14Als + 4Kfs + L
8. 13Ab + 11Als + 13Bt + 47Qz + 31Wt = 9Grt + 4Kfs + L.

The temperature-pressure curves have been extrapolated by Spear and Cheney (1989), while the curve for rhyolite melt generation (reaction 6) takes into account results by Luth et al. (1964) and the muscovite- and biotite-dehydration reactions (7 and 8) are calibrated on the basis of studies by Vielzeuf and Holloway (1988) and Patiño Douce and Johnston (1991).

In order to estimate the release/adsorption of heat during metamorphism, we have included the metamorphism-related reaction enthalpy in the thermal balance; this term has been quantified basing on the procedure described in Philpotts and Ague (2009). In order to estimate the release/adsorption of heat during metamorphism, the enthalpy variation relative to each metamorphic reaction has been calculated, according to formula (4.3):

$$H = E + PV \quad (4.3)$$

where H is the enthalpy of the system, E is the internal energy, P is the pressure and V is the volume. For each mineral, the enthalpy of formation has been calculated according to Philpotts and Ague (2009) (4.4):

$$\Delta H = a(T - 298) + \frac{b}{2}(T^2 - 298^2) - c(T^{-1} - 298^{'1}) + 2d(T^{0.5} - 298^{0.5}) \quad (4.4)$$

where a, b, c and d are thermodynamic parameters with values given by Holland and Powell (1998). Therefore, the reaction enthalpy is given by (Beutel et al., 2010) (4.5):

$$\Delta H_{reaction} = \sum_{i=1}^{n} \Delta H_i - \sum_{j=1}^{m} \Delta H_j \quad (4.5)$$

where n and m are respectively the number of the products and the reactants in the metamorphic reaction.

4.3.3 Rheological features

Temperature estimations and calculated lithologies were used to calculate differential stress values σ (i.e. $\sigma = \sigma_1 - \sigma_3$) and to estimate the rheological behavior in the modeled crust by adopting the frictional criterion for the brittle field and the power-law creep equation for the ductile field (as described hereafter). We assume that the stress distribution in the crust is locally dominated by the rheological behavior requiring the lowest differential stress to activate, which for a multilayered crust results in a typical "Christmas tree" depth-dependent variation of differential stress with depth (e.g. Cloetingh et al., 2013). The adopted parameters are given in Table 4.2.

For the frictional criterion we have used the equation (Sibson, 1974) (4.6):

$$\sigma_B = \sigma_1 - \sigma_3 = \beta \rho g z (1 - \lambda) \quad (4.6)$$

where $\sigma_B = \sigma_1 - \sigma_3$ is the friction-related differential stress (compression is positive), β is a dimensionless parameter depending on the frictional coefficient and deformational regime, ρ is the rock density at depth z, g is gravity acceleration and λ is the pore fluid factor.

The flow law implemented in the model is (e.g. Ranalli, 1995; Gerya, 2010) (4.7):

$$\dot{\varepsilon} = A h^m (\sigma_D)^n \exp\left(\frac{-E + V_A P}{RT}\right) \quad (4.7)$$

where $\dot{\varepsilon}$ is the strain rate, h is the grain size, raised to the power of the parameter m, σ_D is the differential stress (similarly to σ_B), P is the pressure, R is the gas constant, T is the temperature

and A, n, E and V_A are minerals rheological parameters. Ductile deformation in the crust mainly occurs by dislocation creep, thus the term h^m assumes value 1 (m = 0), while the term V_AP has been neglected, being $V_AP \ll E$ (e.g. Ranalli, 1995).

The rheological parameters for the single minerals were used to calculate the parameters of the multiphase rock for each time-step, following the average procedure suggested by Ji et al. (2003, and references therein).

When rocks are partially molten, variations in both strength and rheology occur, according to the melt fraction generated during melt intrusion. Two thresholds have been considered in our model:

1. A first rheological threshold occurs with melt fraction $\Phi \approx 0.06–0.08$, corresponding to the Melt Connectivity Transition (MCT), and determines a breakup of the rock solid framework, with subsequent decrease in crust brittle strength, quantified as ≈ 1 magnitude order (e.g. Vanderhaeghe, 2001; Rosenberg and Handy, 2005).
2. A second rheological threshold occurs with melt fraction $\Phi \approx 0.3$ and corresponds to the Rheologically Critical Melt Percentage (RCMP) (Arzi, 1978). In a crystals-melt mush, this threshold marks the transition from a solid to a liquid system.

When melt fraction exceeds the RCMP, we have adopted the rheology of rocks involved as purely Newtonian, with a viscosity calculated by using the Arrhenius equation (4.8) (Dingwell, 1995):

$$\log_{10}(\eta_T) = \log_{10}(\eta_0) 2.303 \frac{E}{RT} \quad (4.8)$$

where η_T is the melt viscosity at temperature T, η_0 is a pre-exponential factor, E is the activation energy and R is the gas constant. Data for viscosity curve calibration are taken from Shaw (1965), relative to magmas with 4 vol.% H_2O, leading to values $\eta 0 = -3.0$ and E = 36,500.

Model mineral	**A ($MPa^{-n} s^{-1}$)**	**n**	**E ($kJ\ mol^{-1}$)**
Chlorite (a)	$1.1 \cdot 10^{-15}$	18	51
Muscovite (a)	$1.1 \cdot 10^{-15}$	18	51
Biotite (a)	$1.1 \cdot 10^{-15}$	18	51
Quartz (b)	$1.1 \cdot 10^{-4}$	4	223
Plagioclase (c)	$2.34 \cdot 10^{-6}$	3.9	234
K-fledspar (c)	$2.34 \cdot 10^{-6}$	3.9	234
Allumosilicates	23.4	4	410
Staurolite	23.4	4	410
Garnet (d)	276	3	444

Table 4.2 - Parameters for staurolite and allumosilicates are the result of a mean between "weak" minerals (phyllosilicates, quartz and feldspars) and "strong" minerals (garnet) parameters, obtaining a fitting rheological behavior with a less deformable mineral than micas, quartz and feldspars, but still deformable and subject to recrystallization. a Kronenberg et al. (1990). b Gleason and Tullis (1995).c Shelton and Tullis (1981). d Wang and Ji (1999).

4.4 Results

Two-dimensional model calculations have been carried out for simulation times of 1.6 Myr and 3.0 Myr, testing two different isotherms, characterized by a bottom temperature of, respectively, 600 °C and 750 °C. The monitored temperature variations are here shown as 2D isotherms contours (Figures 4.4, 4.5), as partial melting sections (Figure 4.6) and (σ_D, z) paths (Figure 4.7, 4.8).

As shown by the isotherm trend in both the crustal geometries adopted (Figures 4.4, 4.5), when the simulation time span Δt is 1.6 Myr the thermal perturbation due to melt emplacement affects the crust laterally for a distance of ≈15 km from the dyke intrusion. If the value of Δt is increased to 3 Myr, then the propagation distance of thermal perturbation slightly exceeds 20 km; at a depth N 20 km the crust undergoes significantly more heating in the MR case study than in the CR reconstruction, due to the different estimated sizes of the intruded body. At the same time at the top of the intruded body we observe smaller temperature differences and a slightly farther propagation of the thermal perturbation in the CR compared to the MR case study. These small variations at shallow depths are due both to the cooling effect at the surface and the temperature-dependent thermal conductivity; the latter is characterized by higher values in the CR model setting.

In the MR case study (Figure 4.5), the temperature registered in the lateral dyke aureole shows negligible differences when we adopt different geotherms and keep the model geometry unvaried. However, the temperature shows a marked increase when shorter simulation times (and thus higher intrusion rates) are taken into account, denoting a primary control exerted by magma intrusion rates on the temperature field. In the CR reconstruction (Figure 4.4), the effect of different adopted geotherms on the registered thermal perturbation is also marked laterally and at the bottom of the intruded dyke body, due to the smaller size of the magmatic segment. In our case, the different geotherms lead to temperature differences of up to 100 °C.

In the innermost part of the intruded body, we observe that registered temperatures exceed 1100 °C in all our simulations. This latter value has been chosen as our solidus temperature for basaltic melts (e.g. Paterson et al., 1998, and references therein), assuming in our simulations that fractioned crystallization does not determine appreciable variations in the melt solidus temperature. As already observed in the temperature field at the top of the dyke body, temperature variations are mostly influenced by the intrusion rates: in both the CR and MR case study, by considering a growth time of 1.6 Myr, we observe that the innermost interval of the intruded body is still molten at depth varying from 7.5 km to 9 km, whereas with a growth time of 3.0 Myr, temperatures are ≈200 °C lower in the same location.

By varying both the geometry and the geotherm in our model, we observe that the melt production affects extended intervals of the crust, with produced volumes ≈ 20–27 vol.% (Figure 4.6). At shallow to mid depths, melt production closely follows the heat diffusion. As a consequence, a growth time of 3.0 Myr favors extended partial melting, compared with an intrusion duration of 1.6 Myr, due to the longer time available for heat propagation. Melt productivity drastically reduces in proximity of the boundary between upper and lower crust due to a decrease crust fertility. In addition, the lower crust comprises a deep basal layer where the volume of produced melt depends on the chosen geotherm. When the imposed temperature at the base of the crust is 600 °C, melt does not exceed 6 vol.% and is strictly coupled with propagating thermal perturbation from the dykes. On the other hand, a crust base temperature of 750 °C determines values ≈13 vol.%, affecting extensively the crustal base.

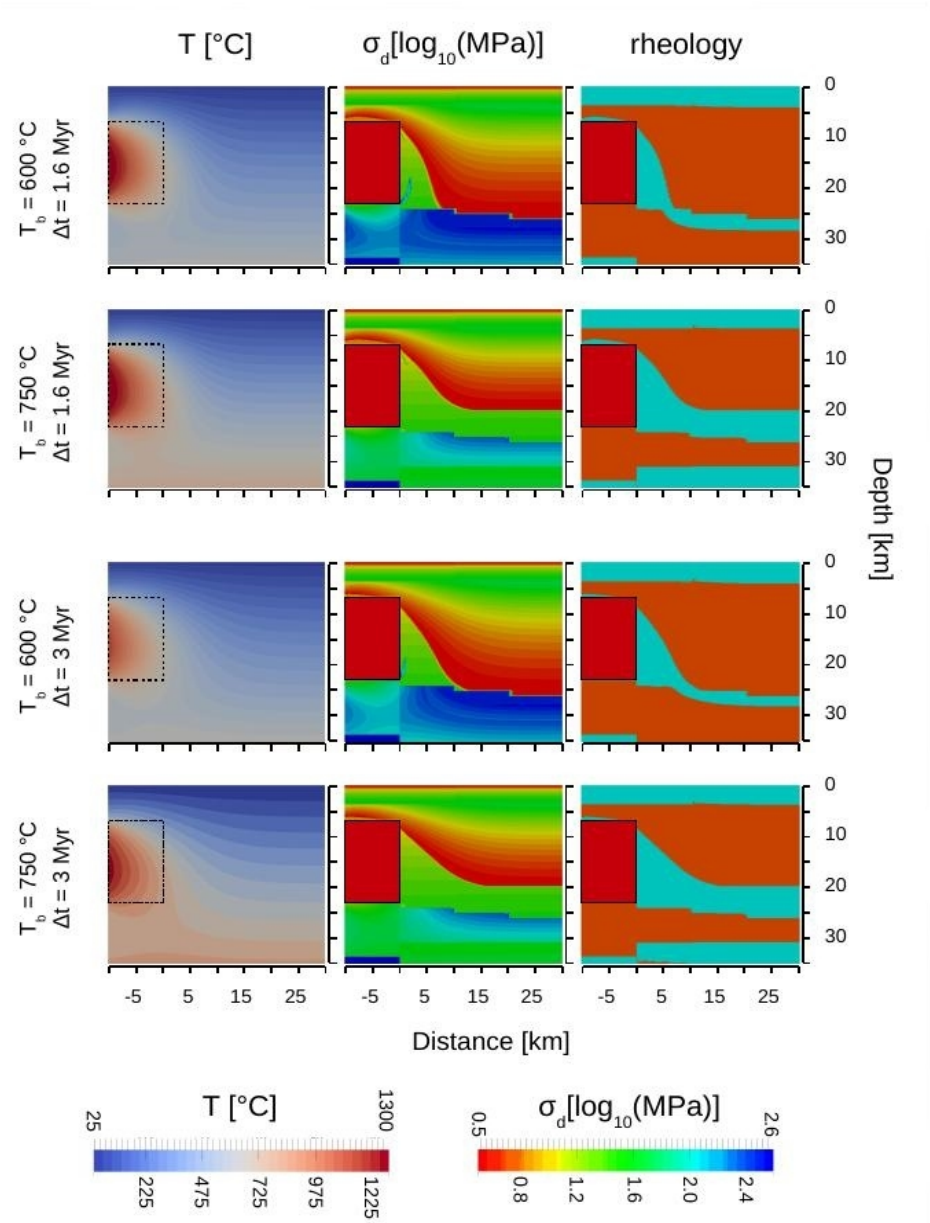

Figure 4.4 - Temperature (T, left column), differential stress (σ_d, center) and rheology contour sections (right) in the CR case study (see Figures 4.1, 4.2, section AA'), at the end of the simulation. T_b indicates the temperature adopted at the base of the model. Δt indicates the time step represented in the figure, coincident with the end of the simulation and the complete growth of the magmatic segment (top panels, Δt = 1.6 Myr; bottom panels, Δt = 3 Myr). The light blue field in the brittle-ductile transition contour sections represents the brittle behavior, while the orange field represents the ductile behavior. The areas bounded by the black dashed lines in the left panels and the red boxes in the middle and right panels represent the geometry of the intruded dyke body.

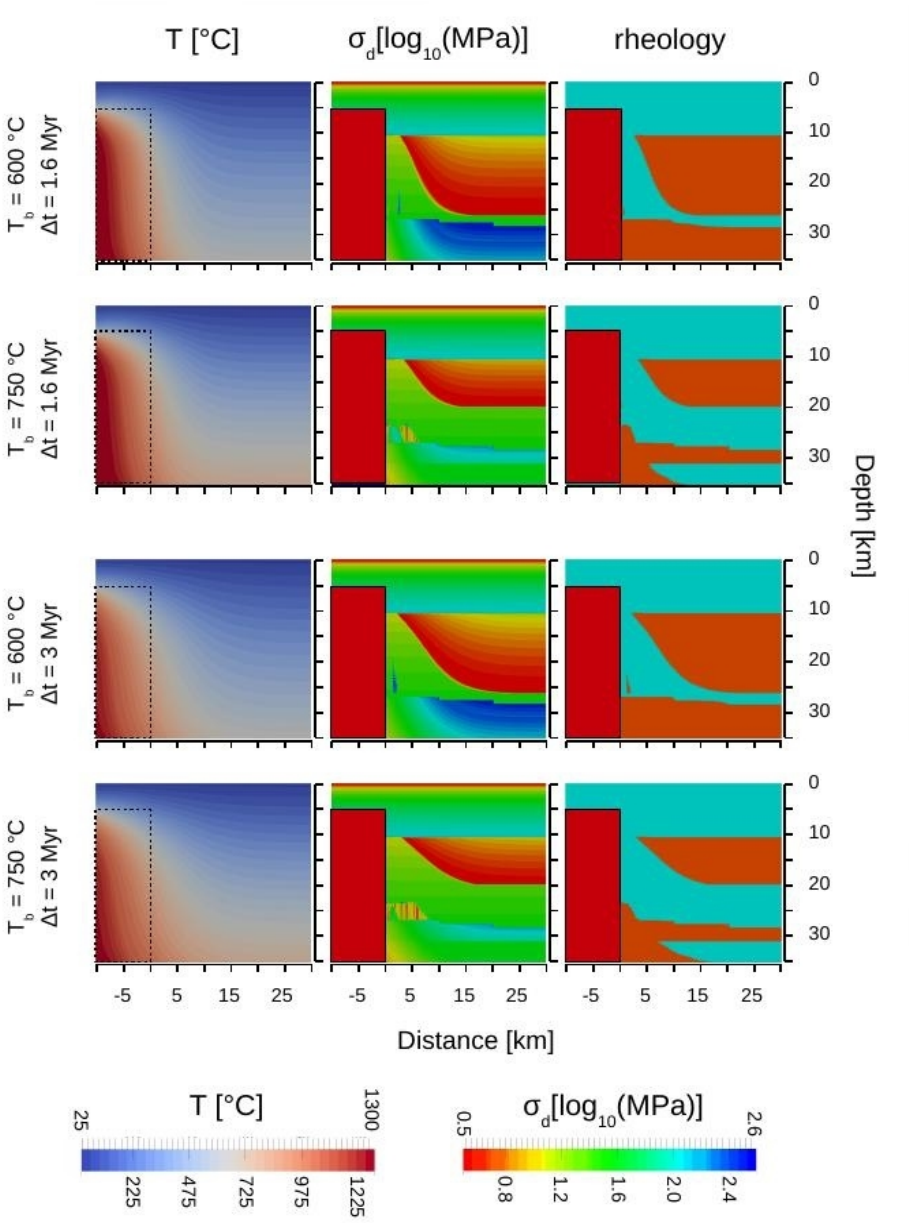

Figure 4.5 - Temperature (T, left column), differential stress (σ_d, center) and rheology contour sections (right) in the MR case study (see Figures 4.1, 4.2, section BB'), at the end of the simulation. T_b indicates the temperature adopted at the base of the model. Δt indicates the time step represented in the figure, coincident with the end of the simulation and the complete growth of the magmatic segment (top panels, Δt = 1.6 Myr; bottom panels, Δt = 3 Myr). The light blue field in the brittle-ductile transition contour sections represents the brittle behavior, while the orange field represents the ductile behavior. The areas bounded by the black dashed lines in the left panels and the red boxes in the middle and right panels represent the geometry of the intruded dyke body.

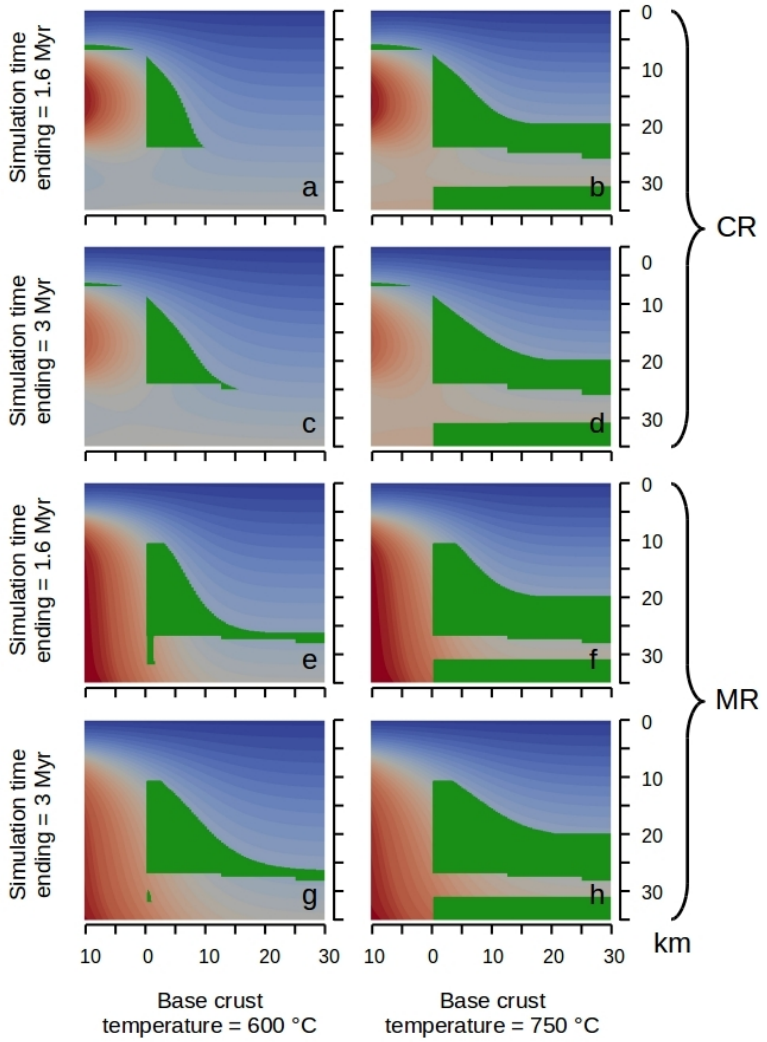

Figure 4.6 - Temperature sections for both the CR and the MR case studies. Green areas indicate where generated melt fraction leads to significant strength reduction and rheological variation. Left panels are for a geotherm where the temperature at the base of the crust is 600 °C, while right panels are for a geotherm where the temperature at the base of the crust is 750 °C. The areas bounded by the black dashed lines represent the geometry of the intruded dyke body.

The variations in mineralogical assemblages due to temperature increase and subsequent metamorphism cause pronounced variations in crustal strength values and rheological behavior in space and time (Figures 4.7, 4.8). In all the simulations carried out (Figures 4.4, 4.5), we observe an increase in strength in the upper crust, which is coupled with the propagation of the thermal perturbation at temperatures between 500 °C and 600 °C. The metamorphic reactions included in our models determine an increase in volume percentage of minerals characterized by marked strength (mainly feldspars and garnet). This occurs at the expense of minerals characterized by low strength values, namely quartz and micas. The most notable strength increase is observed

during the first 200 kyr after the intrusion onset, i.e. during early stages of crustal heating. This has been interpreted as an effect of the low temperature metamorphic reactions and, more specifically, as related to garnet appearance at relatively low temperatures, due to Mn presence. In addition, temperature increase is accompanied by crustal anatexis, which has a profound effect on both crust strength and rheology, especially when a "hot" geotherm is considered. The two combined effects cause a transition from ductile to brittle behavior in the most proximal areas to the sides, and partially above, the intruded body (Figure 4.7).

In our models, the adopted geotherm determines important variations in the calculated differential stress values (σ) (Figure 4.7). In all our simulations we observe the presence of a brittle layer characterized by relatively high σ values, and marking the upper-lower crust boundary. When a "cold" geotherm is adopted, this interval is located at a depth ≈ 27 km. In contrast, the adoption of a "hot" geotherm causes this layer to move up at a depth of b20. This causes an unexpected strength increase up to an order of magnitude, accompanied by a transition from a ductile to a brittle rheology at a depth between 20 km and 25 km, because the equilibrium of mineralogical associations is characterized by higher strength. The effect of melts on the rheological behavior is also predicted at the base of the crust where a ≈5 km thick brittle interval, coupled with a drop in σ values, has formed due to partial melting.

The magmatic segment aureole is the location where the interaction between melt production and rheology appears more evident (Figure 4.8); in all our simulations the crust shows high strength values only in the uppermost layer (≈ 4 km in the CR case study, to 10 km in the MR case study), and subsequently it is subjected to a marked drop in σ values. This decrease, however, is not accompanied by a switch from a brittle to a ductile rheological behavior. In contrast, brittle behavior is maintained up to depths of ≈ 25 km in both case studies. In the CR reconstruction, the lower layers in the model are subjected to partial melting only when the temperature adopted at the base is 750 °C. Together with the relatively small dimension of the magmatic segment, this determines higher value of crustal strength and a brittle behavior of the aureole only when anatexis occurs. However, in the MR case study the base of the dyke aureole exhibits ductile behavior, although melt is still produced, leading to larger sizes of the magmatic segments and the high temperatures reached.

4.5 Discussion

Most previous studies relate the presence of axial mafic bodies in areas of crustal extension and breakup with an overall weakening of the intruded crust (e.g. Buck, 2004; Bialas et al., 2010). In this paper we propose that a thermal perturbation related to melt emplacement in a crust with a polymineralic lithology causes crustal strengthening. This behavior occurs only at a limited distance from the intruded body, causing an increase in strength of the rocks (Figures 4.4, 4.5) where there is direct contact with generated melts.

At present day, the Main Ethiopian Rift is characterized by >80% strain accommodated along magmatic segments, without evidences of a marked crustal thinning. Thermo-rheological models where mineral assemblage is kept constant throughout the simulation shows that the emplacement of dykes is accompanied by crustal heating and, subsequently, progressive weakening. Under such conditions, magma-assisted crustal rifting by repeated dyke injection should also be accompanied by distributed strain across the weakened crust, thus hampering the marked localization of the extension in the MER along-axis magmatic segments. In addition, our model shows that dyke intrusion is accompanied also by a progressive, albeit moderate increase in crustal strength. This also may contribute to localization of the extension in the rift axial region by dyke filling, conform previous results (e.g. Buck, 2004, 2006).

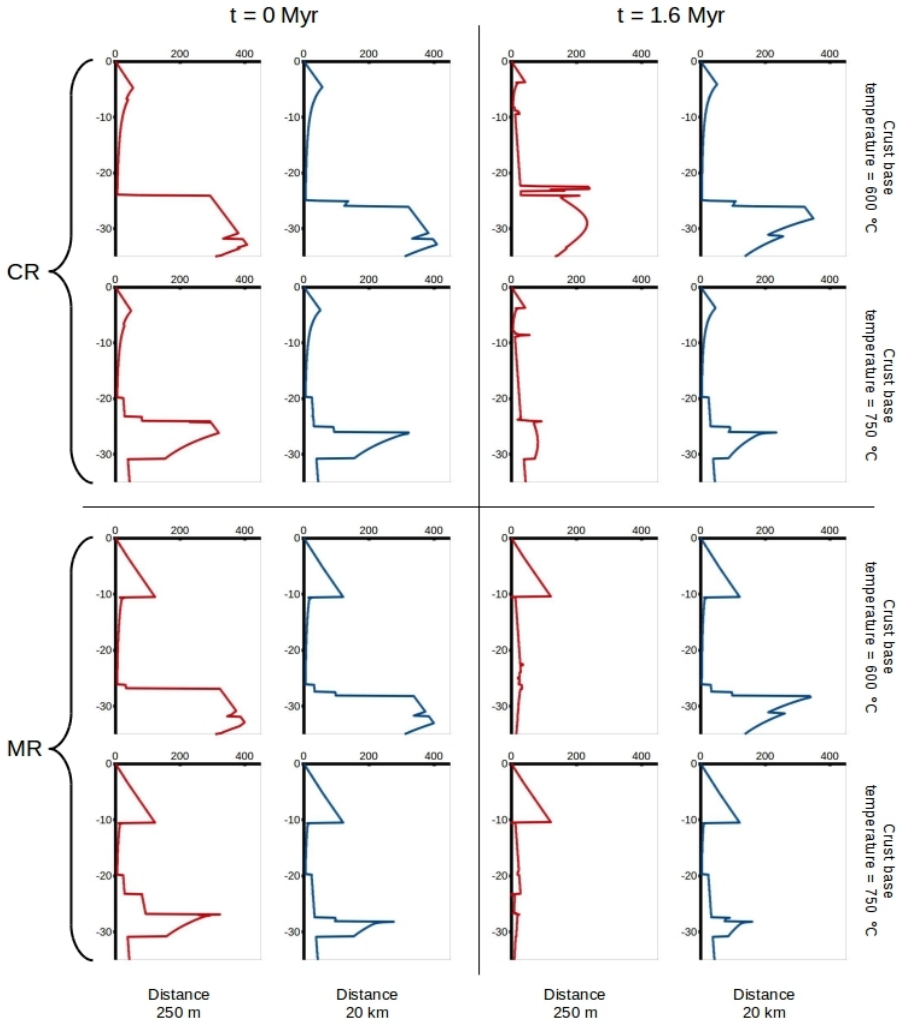

Figure 4.7 - Differential stress-depth diagrams for the CR and MR case studies, relative to a simulated time of 1.6 Myr. Left panels illustrate strength profiles in the crust prior to dyke intrusion, whereas values in the right panels correspond to the end of simulation. See Figure 4.2 for locations of the profiles. Red profiles are located at a lateral distance of 250 m away from the intruded dykes (red lines, Figure 4.2b, d), whereas the blue profiles are located at a distance of 20 km (blue lines, Figure 4.2b, d). Horizontal axis scale is expressed in MPa; vertical axis scale is expressed in km. All the profiles relative to the thermally perturbed aureole show a moderate increase in differential stress values at a depth between 10 km and 25 km, despite the presence of a melt exceeding the MCT threshold.

At high intrusion rates, the internal part of the dyke body remains partially molten, and therefore it constitutes a weak crustal zone. Consequently, this interval is a favorable area for melt intrusion, contributing in localization of deformation in the axial rift zone, in line with results obtained by Beutel et al. (2010).

The increase of the differential stress values in the upper and middle aureole, following the emplacement of magmatic segments, is accompanied by a switch from ductile to brittle

rheological behaviors (Figure 4.8). This variation is mostly due to the formation of new mineral associations, but is also promoted by crustal anatexis. Consequently, stress may be initially localized in this interval and accompanied by the formation of cracks and vein networks. The presence of melts in the MER crust, intruded at various depth (Beutel et al., 2010), is widely observed by tomographic (e.g. Guidarelli et al., 2011), seismic (Keir et al., 2005) and magnetotelluric (Whaler and Hautot, 2006) studies, and is mainly characterized by both mafic sills and dykes (e.g. Bastow et al., 2011) and felsic products (e.g. Boccaletti et al., 1999).

At present day, seismic activity in the MER is mostly distributed along the rift axis at a depth of 15 km within a 20 km wide zone of Quaternary eruptive centers (Keir et al., 2006). In our reconstruction, the estimated depth of the brittle-ductile transition in the upper crust ranges from a depth of ≈5 km to ≈10 km, in agreement with previous studies (see Daniels et al., 2014, and references therein). However, our observations suggest that melt production may exceed the MCT threshold even at shallow depths. Since the rock framework controls magma mobility (e.g. Vanderhaeghe, 2001) it appears that this depth, where melt migrates and where brittle behavior is enhanced by melts intrusion, may be locally underestimated. Consequently, we propose that the dyke aureole and the lower crust are favorable locations for anatexis, and that melt percentages are sufficiently high to cause break-up of the solid structure of the rocks, thus promoting further seismic activity.

According to Rooney et al. (2007) and Ayalew and Gibson (2009), volcanic activity in the MER does not show clear evidence of interaction between deep, plume-related melts and continental crust, but should be ascribed to fractionation of melts at various depths. At the same time, other studies show that Quaternary basalts are 10–13% contaminated by the lower crust (e.g. Boccaletti et al., 1995). Our results show that a “hot” geotherm, related to episodes of melt ponding and pre-dating the dyking event, may determine partial melting in the lower crust. On the other hand, when the base of the crust is characterized by cooler temperatures, melt injection is needed for crustal anatexis. The MER crust is characterized by crustal thicknesses ranging from 27 km to 38 km, and Poisson's ratio values ranging from 0.27 to 0.35. This indicates that MER crust has been extensively intruded by mafic rocks (Dugda et al., 2005), and consequently higher temperatures may be expected at its base. As a result, the presence of partial melts may be expected at the base of the lower crust. However, volcanic activity related to the presence of crust-derived magmas is expected only when the melt fraction reaches a threshold of 30% to 50% (Bergantz, 1989, and references therein). Such high melt fractions were not predicted in any of our simulations, and we, therefore, tend to exclude the possibility of a widespread volcanic activity of crustal origin.

Unlike findings by Corti (2008, 2009), who argued that the rift evolution and segmentation are independent of magmatic processes and controlled only by rift obliquity, our modeling results show that magmatic processes do play a key role in the Main Ethiopian Rift development. These two mechanisms, including mutual feedbacks, may significantly affect the thermo-mechanical structure of the Main Ethiopian Rift, resulting in the localization of deformation and magmatic activity along the rift axis.

Gravimetric studies by Cornwell et al. (2006) highlight the presence of a dense body at the top of the main dyke body located at the rift axis, situated beneath the Boset volcano at a depth between 2 km and 7.5 km. This body is characterized by a density of 2850 kg m^{-3} and is composed of ≈25% gabbroic material. Two hypotheses have been formulated for the origin of this intruded body: 1) fractionation of pre-emplaced melts, or 2) partial melting of crust and sediments due to previous intruded material. According to our model, temperatures at the roof of the dyke body may lead to partial melting of crustal material in a very thin layer above the magmatic segment. Furthermore, the recorded melt fraction is lower than the MCT threshold. As a

consequence, the produced melt is devoid of mobility and not sufficient to justify the dimension of this felsic body. We therefore propose that the presence of the melt body is mostly due to fractionation of pre-intruded magmas at various depths in the crust, with a minimal contribution of crustal material.

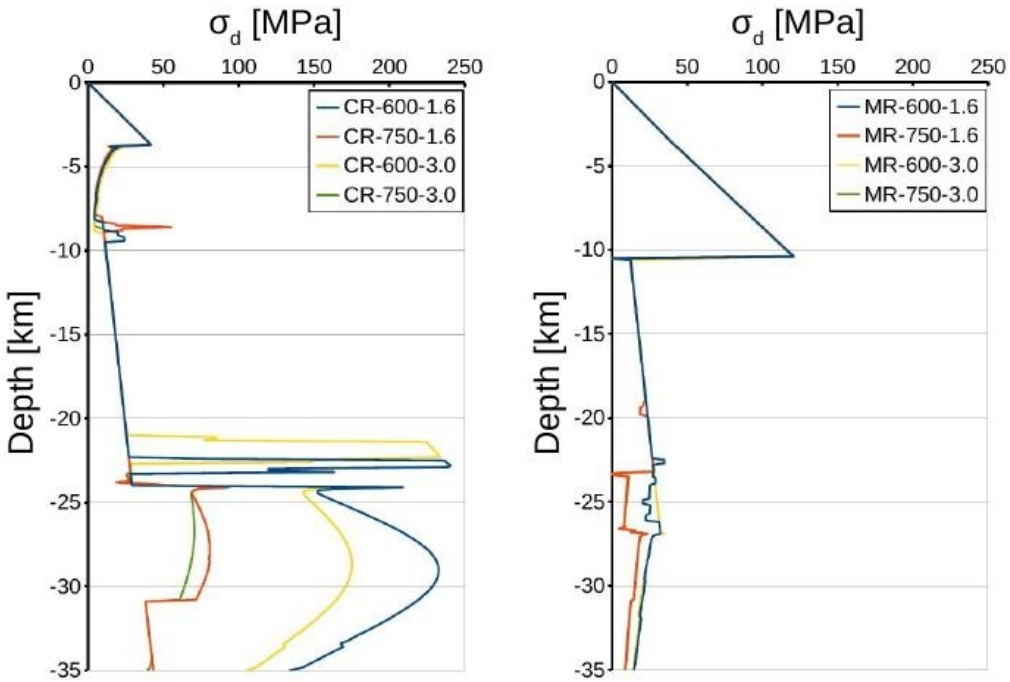

Figure 4.8 - Differential stress-depth profiles for the crust in the CR (left panels) and MR (right panels) case studies. Legend gives adopted temperature at the base of the model (°C) and total simulated time (Myr) for each case study. For the measurement location, see the red (panels a and b) and blue (c and d) dashed lines in Figure 4.2. The CR case study is associated with an overall weakness of the upper crust, down to a depth of 20 km, followed by a pronounced differential stress increase. In the MR case study, strength is focused in the top 10 km.

4.6 Conclusions

We have investigated the effect of metamorphism and melt production on the crust of the Main Ethiopian Rift, resulting from the development of magmatic segments characterizing the axial zone of the rifting area. Our aim was to provide a more realistic description of the evolution of the MER crustal rheology and to better understand the interaction occurring between melts and intruded rocks in view of their effect on crustal strength.

For a polymineralic and metamorphism-sensitive crust an important predicted effect is the moderate increase in crustal strength in proximity of the magmatic segments, which increasingly affects larger volumes of crust when the thermal perturbation propagates into the crust. This behavior could explain the observed transition in the MER from initial rift phases, when strain is mostly accommodated by crust extension, to more recent Plio-Quaternary phases, when strain accommodation is mostly due to magmatic processes and is concentrated along axial intruded bodies in an estimated percentage >80%.

The thermal perturbation due to the magma presence is accompanied by the production of crustal anatexis derived melts, which locally may migrate. The produced amount of melt is sufficient to induce variations in the depth of the brittle-ductile transition, and thus promote seismicity. At the same time, crustal anatexis can probably not feed widespread volcanic activity due to the relatively low melt production in the investigated area.

This study represents a first step in tracing the evolution of crustal scale features during continental rifting phases, especially when lithosphere breakup is accompanied by extended magmatic activity. Further research may focus on the effect of rheological stratifications in the MER, to better understand the influence of strain partitioning on the evolution of MER especially during initial rift phases.

5 Lithosphere erosion and continental breakup: interaction of extension, plume upwelling and melting

5.1 Introduction

Extension and rifting of lithosphere are fundamental processes in geodynamics, resulting from the interaction between mantle flow and plate movements. These processes involve different mechanisms acting simultaneously. Among them, heat transfer, plate-related far field stresses, mantle flow and possibly magmatism are acknowledged as playing a major role in determining the evolution pattern of rifting areas (e.g. Koptev et al., 2015, and ref. therein). These mechanisms are capable to interact, with significant feedback effects as a result, which are often difficult to predict. Mantle drag is one of the key factors influencing the distribution and thickness of the lithosphere, together with plate boundary forces and gravitational potential, but at the same time the lithosphere exerts a profound effect on mantle flow: previous studies have demonstrated that convection cells, temperature and flow regime in the mantle are affected by the thickness and distribution of continents (e.g Guillou-Frottier et al., 2012). Consequently, lithosphere thinning and breakup should be considered as integrated processes involving a coupled lithosphere-mantle system, where different mechanisms act simultaneously and influence one another.

Rifting processes have long been classified in two main categories: active and passive rifting (e.g. Ziegler and Cloetingh, 2004). In active rifting, thinning and extension are driven by force fields generated by mantle plumes impacting against the base of the lithosphere (e.g. Bott and Kusznir, 1979), whereas in passive riftings tensional stresses are subsequent to movement and interaction of plates (e.g. Cloetingh and Wortel, 1986). Although this distinction has been long kept, not all evidences may fit into these two end-member models (e.g. Huismans et al., 2001). Rather, active and passive components may act coupled and be dominant one another at different extension and breakup stages. This is particularly true in the case of extensional far field forces associated with slab pull, which become progressively intense with subduction proceeding (Schubert et al., 2001). Thus, the meaning of “active” and “passive” components must be reviewed in light of recent studies, although they can be still envisaged (Ziegler and Cloetingh, 2004).

Among the mechanisms controlling the plate dynamics, slab pull and roll-back, ridge push and frictional resistance are acknowledged as giving a major contribution in the force balance (Bott and Kusznir, 1979). However, the role of other factors in influencing rifting style and evolution is still a matter of debate. Among these, the presence of mantle plumes has long been recognized as capable of playing an important role during lithosphere extension (e.g. Buck, 2004). Plumes are focused upwellings of plate-scale mantle material (e.g. Burov et al., 2007, and ref. therein), driven by temperature- and composition-related density differences. The source region of plumes may vary in depth, but the upwelling mechanism does not show any remarkable difference (Burov et

This chapter is based on: Lavecchia A., Thieulot C., Beekman F., Cloetingh S., and Clark S., (2017), Lithosphere erosion and continental breakup: interaction of extension, plume upwelling and melting. Earth Planet. Sci. Lett., 467, 89–98, doi: 10.1016/j.epsl.2017.03.028.

al., 2007). A further classification basing on size has emerged in literature, where plumes have been distinguished in “baby-plumes”, e.g. beneath western Europe (Ritter et al., 2001) to “superplumes”, relative to past, large radius plumes (Condie, 2002), and present-day “mega-plumes”, such as the case of Africa and Pacific plumes (Dziewonski et al., 2010).

Lithosphere impingement by the plumes may produce regional uplift driving to extensional stresses (e.g. Burov et al., 2007; Burov and Gerya, 2014). Furthermore, plumes are often associated with small-scale convective instability and thermos-mechanical lithosphere erosion (e.g. Fischer and Gerya, 2016). However, the ridge push forces, associated with mantle upwelling and resulting topographic doming, are small, or progressively decrease in comparison with plate-related far field forces (Schubert et al., 2001). Therefore, previous studies show that far field forces are a necessary component for the development of large scale rifting (Koptev et al., 2015).

An aspect characterizing most hot spots is the presence of significant volumes of melts intruding and extruding the lithosphere at various depths (e.g. Menzies et al., 2002). As suggested by analytical/numerical studies (e.g. Buck, 2004) and field evidences (e.g. Wright et al., 2012), an intimate relationship exists between rifting episodes and melts emplacement, resulting in an extension accommodated by magma filling. However, melts may result from both plumes or “plume head” upwelling (Hill 1991), and from passive upwelling related to the stretching and thinning of lithosphere (White and McKenzie 1989). In addition, the thermo-mechanical effects of magma intrusion and underplating at lithosphere-scale remain largely unquantified, although its important role in the evolution of the crust and lithosphere has long been acknowledged (e.g Ziegler and Cloetingh, 2004, and ref. therein).

In this paper we present a thermo-mechanical model with the aim to examine the evolution pattern of a continental lithosphere subject to extension. In our model the lithosphere is characterized by the presence of heterogeneities and impinged by a mantle plume. The novel aspect of this model is the incorporation of partial melting for mantle materials, as a response to pressure-temperature variations. Our model allows to assess the importance of melts during the evolution of rifting areas, including the most favorable conditions that maximize their effects.

5.2 Model setting

5.2.1 Model geometry and governing equations

We constructed a 2D visco-plastic model, simulating a continental lithosphere subjected to a constant, extensional velocity, where an upper mantle layer and a plume at the base of the model are incorporated (Figure 5.1). The model has a width of 1000 km and a thickness of 400 km; it is constituted by 1) a two-layered crust with thickness 40 km, where both the upper and lower crust have the same thickness (20 km), 2) a mantle lithosphere with thickness 80 km, and 3) an upper mantle, 280 km thick. The shape of the plume at the beginning of the simulation is a semicircle with radius 100 km. In addition, a lithosphere weakness is introduced in correspondence of the boundary between lower crust and lithospheric mantle, as a square of dimension 10 km constituted by a different material from the lithosphere (see Table 5.1). The centers of the plume and the lithospheric weakness are equidistant from the central vertical axis of the model, and their mutual distance Δ is a parameter investigated in different simulation sets (Figure 5.1). The lithosphere is subjected to an extensional velocity of 5 mm yr^{-1} at both sides of the model, compatible with slow spreading ridges and breakup areas (e.g. Wolfenden et al., 2004; McClusky et al., 2010) The applied velocity on the lithosphere results in a mass outflow at both lateral boundaries of the model, and is counterbalanced by a mass inflow that keeps the simulation

volume constant. The bottom boundary condition is free slip, while a free surface is incorporated at the top boundary. Other parameters are given in Table 5.1.

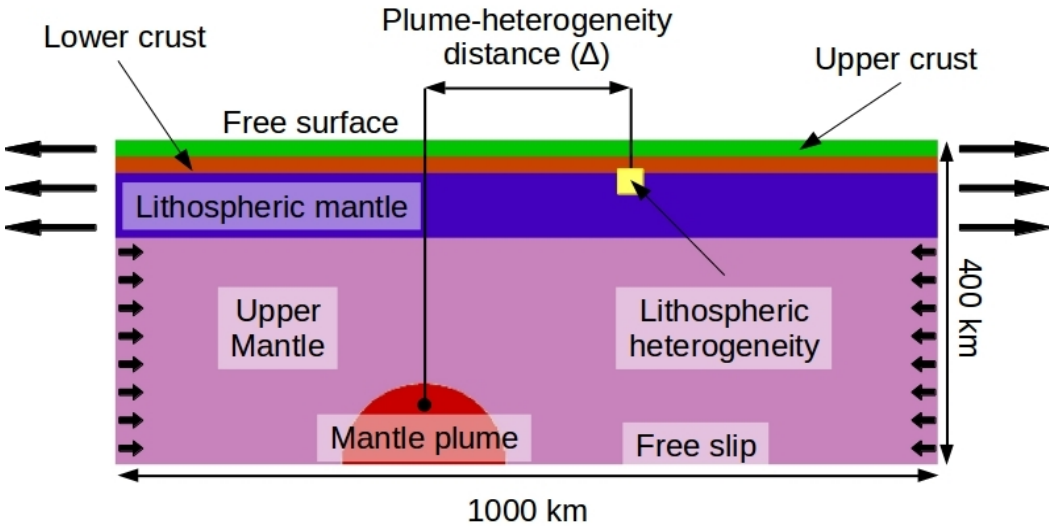

Figure 5.1 – Schematic representation of the model. The black arrows indicate the direction of applied velocity and relative mass outflow/inflow (see Table 5.1 for the adopted value).

The code used for our simulation sets is ELEFANT, a nonlinear fluid Arbitrary Lagrangian-Eulerian (ALE) code, specifically designed for the solution of visco-plastic flow at lithospheric scale. The code is based on the algorithm already implemented in FANTOM (e.g. Thieulot, 2011), and assumes that, at a regional scale of observation and at geologic time scale, earth materials may be treated within the realm of continuum mechanics and inertial forces may be neglected (i.e. the flow Reynold number is ≈0) (e.g. Gerya, 2010). It derives that the momentum equation may be expressed as (5.1):

$$\nabla \cdot \sigma + \rho g = 0 \quad (5.1)$$

where σ is the stress tensor, ρ is the density and g is the gravity acceleration vector. Materials are assumed to be incompressible, implying zero divergence of the velocity v tensor (5.2):

$$\nabla \cdot v = 0 \quad (5.2)$$

The stress tensor σ can be separated into a spherical part $p1$ and a deviatoric part s, as follows (5.3):

$$\sigma = -p1 + s \quad (5.3)$$

The deviatoric part s of the stress tensor σ is related to the strain rate tensor , according to the relationship (5.4):

$$s = 2\mu\dot{\varepsilon} \quad (5.4)$$

where μ is the dynamic viscosity and is given by (5.5):

$$\dot{\varepsilon} = \frac{(\nabla v + (\nabla v)^T)}{2} \quad (5.5)$$

Basing on the equations (5.1)-(5.5), it is possible to obtain the following form of the Stokes equation (5.6):

$$\nabla \cdot (\mu(\nabla v + (\nabla v)^T)) - \nabla p + \rho g = 0 \quad (5.6)$$

Equation (5.6) expresses that changes in buoyancy and constitutive relationship in any point of the domain determine an effect on the whole domain.

Parameter	**Value**
Surface temperature	20 °C
Lithosphere base temperature	1200 °C – 1300 °C
Model base temperature	1400 °C – 1475 °C
Δ temperature plume	200 °C
Extensional velocity	5 mm yr^{-1}
Thermal conductivity	2.5 W m^{-1} K^{-1} (crust) 3.5 W m^{-1} K^{-1} (lithosphere and mantle)
Heat capacity melt	771 J kg^{-1} K^{-1}
Radiogenic heat production at surface	2 μW m^{-3}
D for radiogenic heat production	14 km
Depleted mantle density	3325 kg m^{-3}
Melt density	2950 kg m^{-3}
Cohesion	20 MPa
Angle of friction	15 º

Material parameters						
	Upper crust (a)	Lower crust (b)	Lith. mantle (c)	Upper mantle (c)	Plume (c)	Lith. weakness (c)
A (MPa^{-n} s^{-1})	$1.1 \cdot 10^{-28}$	$3.98 \cdot 10^{-16}$	$2.41 \cdot 10^{-16}$	$2.41 \cdot 10^{-16}$	$2.41 \cdot 10^{-16}$	$1.1 \cdot 10^{-28}$
n	4	3 8	3.5	3.5	3.5	4
E (kJ mol^{-1})	223	356	540	540	540	223
V_a (kJ Pa^{-1})	0	0	0	$5 \cdot 10^{-9}$ (df) $2 \cdot 10^{-8}$ (dl)	$5 \cdot 10^{-9}$ (df) $2 \cdot 10^{-8}$ (dl)	0
d (m)	10^{-3}	10^{-3}	10^{-3}	10^{-3}	10^{-3}	10^{-3}
n	0	0	2.5	2.5	2.5	0
ρ0 (kg m^{-3})	2800	2900	3325	3300	3275	3325

Table 5.1 – Thermo-mechanical parameters adopted in the model. A=pre-exponential parameter; n=exponent; E=activation energy; Va=activation volume; d=grain size; m=grain size exponent (a=wet quartz, Gleason and Tullis, 1995; b=wet plagioclase, Rybacki and Dresden, 2000; c=dry olivine, Karato and Wu, 1993; activation volumes: df=diffusion creep; dl=dislocation creep).

Earth material properties (e.g. density, viscosity, thermal conductivity…) depend on temperature. Consequently, temperature field must be taken into account during the computation. The energy transport equation is then solved (5.7):

$$\rho C_P\left(\frac{\partial T}{\partial t}+v\cdot\nabla T\right)=\nabla\cdot(k\nabla T)+H_r+H_m \quad (5.7)$$

where C_P is the heat capacity (J kg^{-1} K^{-1}), T is the temperature (K), k is the thermal conductivity (W m^{-1} K^{-1}), H_r is the internal heat production due to radioactive decay (J m^{-3} s^{-1}) and H_m is the heat released by melts at emplacement levels. This term will be further described in the following sections.

5.2.2 Rheology

The code used for our simulations adopts a visco-plastic rheology for earth materials. A more detailed description of the adopted methodology is described in Thieulot (2011, Appendix B). The plastic behavior is here modeled for rocks at a relative low temperature condition, and it is approximated by a viscous deformation following the Drucker-Prager criterion (see e.g. Kachanov, 2004, Thieulot, 2011). Obtained viscosity values are given by the following equation (5.8):

$$\mu_{PL}=\frac{C\sin\phi+P\cos\phi}{2\dot{\varepsilon}_{II}} \quad (5.8)$$

where μ_{PL} is the plastic viscosity, C in the cohesion term, P is the pressure, Φ is the friction angle and $\dot{\varepsilon}_{II}$ is the second invariant of the strain rate tensor (cfr. Burov and Gerya, 2014). Viscosity values are locally adapted to limit the stress generated during the deformation. For further details, see Thieulot (2011, Appendix B).

Strain weakening has been incorporated by following a linear relationship between the accumulated strain in the deforming rocks and values of cohesion C and angle of friction Φ: when the accumulated strain is less that a given threshold value $\varepsilon 1$, then C and Φ are maintained as constant. For accumulated strain values between $\varepsilon 1$ and $\varepsilon 2$, then both C and Φ decrease down to values C_{SW} and Φ_{SW}, and these values are kept for accumulated strain values higher than $\varepsilon 2$. For further details, see Thieulot (2011, and references therein).

At higher temperature, rocks experience nonlinear viscous deformation, expressed by a temperature and stress/strain rate dependent viscosity. The relationships between stress and strain rate are described by the following equations for dislocation (5.9) and diffusion creep (5.10) (e.g. Gerya, 2010):

$$\dot{\varepsilon}_{II,DISL}=A\sigma_{II}^{\,n}\exp\left(\frac{-E+pV}{RT}\right) \quad (5.9)$$

$$\dot{\varepsilon}_{II,DIFF}=A\,h^m\exp\left(\frac{-E+pV}{RT}\right) \quad (5.10)$$

where $\dot{\varepsilon}_{II,DIFF}$ and $\dot{\varepsilon}_{II,DISL}$ are the strain rate second invariant for diffusion and dislocation creep, A, n, m, V and E are material parameters, h is the grain size, σ_{II} is the stress second invariant, R in the gas constant and T is the temperature. The adopted values of parameters are given in Table 5.1.

Basing on the equations (5.9, 5.10), the viscosity values are calculated for dislocation and diffusion creep:

$$\mu_{DISL}=A^{\frac{-1}{n}}\dot{\varepsilon}^{\frac{1-n}{n}}\exp\left(\frac{E+pV}{nRT}\right) \quad (5.11)$$

$$\mu_{DIFF} = A^{-1} h^{-m} \exp\left(\frac{E + pV}{RT}\right) \quad (5.12)$$

and averaged to calculate the effective viscosity μ_{EFF} (5.13):

$$\mu_{EFF} = \left(\frac{1}{\mu_{PL}} + \frac{1}{\mu_{DISL}} + \frac{1}{\mu_{DIFF}}\right)^{-1} \quad (5.13)$$

5.2.3 Density model

The model implements a temperature dependent density, according to the equation (5.14):

$$\rho_S(T) = \rho_0(1 - \alpha(T - T_0)) \quad (5.14)$$

where $\rho_S(T)$ is the rock density at the modeled temperature T, ρ_0 and T_0 are the reference density and temperature and α is the thermal expansion coefficient. The materials subjected to partial melting also experience an increase in density, depending on the melt fraction that is extracted during the whole simulation history. The density increase follows the equation (5.15):

$$\rho(T) = \rho_S(T)(1 - \varphi_{P,T}) + \rho_{DM}\varphi_{P,T}(1 - \alpha(T - T_0)) \quad (5.15)$$

where $\rho(T)$ is density of the rock subjected to partial melting, ρ_{DM} is the density value of depleted mantle (see Table 5.1) and $\varphi_{P,T}$ is the melt fraction obtained at different values of temperature and pressure. The details of the procedure for calculating $\varphi_{P,T}$ are illustrated in Section 5.2.4.

A density correction is also applied for materials subjected to melt intrusion, which experience a density decrease according to the equation (5.16):

$$\rho(T) = \rho_S(T)(1 - \varphi_{P,T}) + \rho_M \varphi_{P,T} \quad (5.16)$$

where ρ_M corresponds to the density of intruded melts (see Table 5.1).

5.2.4 Partial melting

Our model includes partial melting for mantle rocks, due to temperature and pressure variations during the simulations. We have constructed curves for solidus temperature (T_S) for lithospheric mantle, upper mantle and plume materials, based on data by Takahashi (1986), Takahashi et al. (1993) and Ueki and Iwamori (2013, 2014) and relative to fertile anhydrous peridotite (Figure 5.2). A solidus temperature variation of +25 °C has been introduced for the melting curve of lithospheric mantle, in order to assess the higher melting temperature of depleted mantle material, in agreement with findings by Wasylenki et al. (2003). Likewise, a solidus temperature variation of -25 °C is considered for mantle plume, assuming a lower T_S for more primitive material. Differently, in our model the liquidus temperature (T_L) curve is not subjected to variations depending on different materials. The liquidus temperature at pressure P_0=0.1 MPa is T_L=1860 °C, relative to a Fo92 olivine composition in anhydrous conditions, while we assume that the Clapeyron slope for the Fo92 curve does not show significant variations from the Fo100 curve (Deer et al., 2013, and ref. therein). Basing on the constructed curves, pressure-dependent solidus and liquidus temperatures are calculated at every time step to estimate the melt fraction φ occurring in mantle materials at different conditions of temperature and pressure.

When mantle rocks temperature is in the range between solidus and liquidus temperature, they are subjected to partial melting. The produced melt fraction is computed basing on a linear interpolation between the solidus and liquidus temperature (5.17-5.19):

$$T < T^S_{P,T} \rightarrow \varphi_{P,T} = 0 \quad (5.17)$$

$$T^S_{P,T} < T < T^L_{P,T} \rightarrow \varphi_{P,T} = \frac{T - T^S_{P,T}}{T^L_{P,T} - T^S_{P,T}} \quad (5.18)$$

$$T > T^L_{P,T} \rightarrow \varphi_{P,T} = 1 \quad (5.19)$$

where $\varphi_{P,T}$, $T_{P,T}^{S}$ and $T_{P,T}^{L}$ are the pressure- and temperature-dependent melt fraction, solidus and liquidus temperatures, and T are temperature values registered in the mantle domain during each time step.

The melt produced is collected and redistributed by markers at the level of melt neutral buoyancy (i.e. where the density of melts is equal to the host rock density), where the receiving markers store melt up to their total filling. When a receiving marker is full, the remaining melt is stored in the underlying marker, following a model of underplating by downward accretion (e.g. Annen et al., 2011). The melt movement occurs on a much shorter timescale than the velocity of rocks deformation (e.g. Hawkesworth et al., 1997), due to its composition and its relative low viscosity (e.g. Dingwell, 1995). Consequently, magma transfer is assumed to be instantaneous.

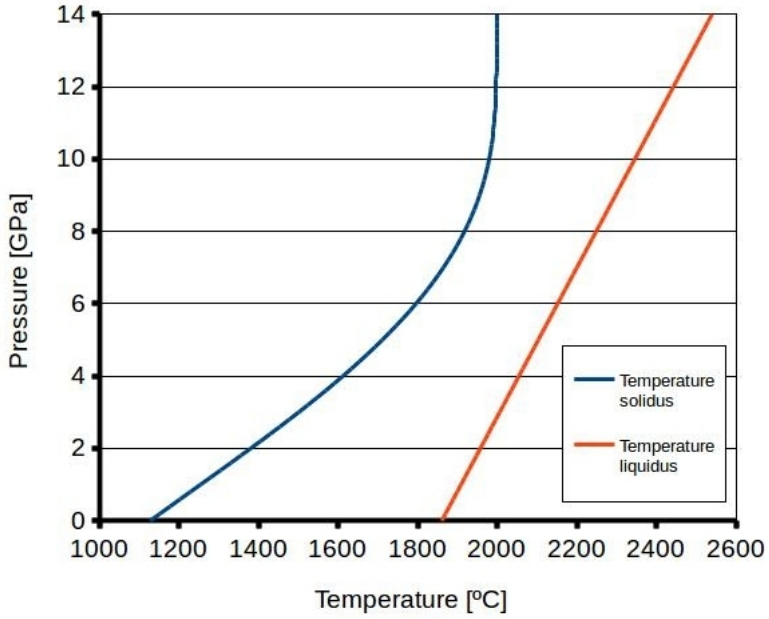

Figure 5.2 – Solidus and liquidus curves adopted in the model.

At the emplacement level, the effect of melts affects both the plastic and the viscous behavior. In our model the effect of fluids on plastic strength follows the results by Rosenberg and Handy (2005), taking into account that a rock where melt presence exceeds φ=0.07 is subjected to a decrease in strength. This effect has been introduced by predicting a drop in the plastic yield strength, equal to one order of magnitude. Furthermore, the loss of cohesion caused by melt percolation in the intruded bodies has been incorporated, by introducing a viscosity drop down to μ=1018 in the rock intervals where the quantity of melt exceeds the threshold RCMP=35% vol. (Rheological Critical Melt Percentage, Arzi, 1971) and a temperature T_T=1100 ºC. In addition, the heat released during melt solidification also exerts a profound effect on the viscous strength of intruded rocks. We insert the term H_m in equation (5.7), quantifying the heat transported and released by moving melts:

$$H_m = \frac{\rho_M C_P \left(T_M - T_{HR}\right) \varphi}{\Delta t} \quad (5.20)$$

where ρ_M, C_P, T_M and φ are respectively the density, heat capacity, emplacement temperature and melt fraction of the intruded melt, T_{HR} is the temperature of the host rocks at the moment of intrusion and Δt is the duration of the time step at the moment of H_M calculation (see Table 5.1 for a resume of the adopted values).

5.3 Results

The tested parameters are useful to highlight the different features that characterize the lithosphere-plume interaction, and specifically they are 1) relative plume-lithospheric discontinuities distance, and 2) different mantle temperature field. These parameters exert a key role in the final rifting configuration and activity, including the location of melt underplating. Our model results are presented for models with and without melt generation, as plot sections for selected time steps (Figure 5.3-5.7, 5.9), and topography plots (Figure 5.8). The time period shown for each simulation set depends on the time needed for the rifting to develop. According to the adopted configuration, it varies from 12 Myr to 24 Myr.

In all the simulations two phases of rifting development can be distinguished. The first phase is characterized by the uprising of plume material throughout the upper mantle, and the beginning of the continental extension where the lithospheric weak zone is located. In this phase, although the lithospheric thinning and extension assumes “passive” rifting characteristics, the horizontal distance Δ between plume and lithospheric weakness reflects over a) the velocity of the plume material uprising, and b) the amount of lithospheric thinning in the rifting area.

For a Δ value of 125 km (Figure 5.3, 5.4), the proximity of hot and weak mantle material to the rift axis determines a strain concentration along an interval connecting the rift and the plume tail. Consequently, the rising mantle material experiences an acceleration after 7 Myr, leading to a plume impact against the lithosphere between 8 Myr and 9 Myr. This is the case study when we have registered the fastest velocities of plume uprising and interaction with the lithosphere. At the same time, high temperatures and strain rates experienced in the mantle wedge beneath the rifting area determine a stronger decrease in viscosity than in other simulations. This results in a very effective thinning of the lithospheric mantle, by a factor of more than 2 at the location of the rift. To give a comparison, in the simulation sets where the value of Δ has been increased, the impact age of plume material against the lithosphere is delayed and occurs after 11 Myr (Figure 5.5). This is due to lower temperatures and strain rates registered in the mantle interval between the plume and the lithosphere discontinuity. In addition, with increasing Δ values, the amount of lithospheric thinning drastically reduces, becoming modest when Δ = 500 km (Figure 5.6, 5.7).

The second phase of rift development is subsequent to the impact of plume material below the lithosphere, sometime between 8 Myr and 11 Myr from the simulations start, depending on the adopted Δ value. In this phase, different Δ values determine more profound variations of the rift style than in the first phase. When Δ = 125 km (Figure 5.3), we observe, in time span of about 1 Myr, a channeling of plume material in the area previously occupied by the upper mantle wedge, with subsequent very high temperatures and stain rates. In this model, the mantle wedge beneath the rifting area experiences a temperature peak in proximity of the rift side opposite to the one directly impinged by the plume. On the other hand, in the same mantle wedge the highest values of strain rate are localized around the area of plume impingement. This leads to viscosity values in the mantle that are almost symmetric with respect to the rift axis, and to a roughly symmetric thinning of the lithosphere, only slightly more pronounced in the rift side directly above the plume impact point.

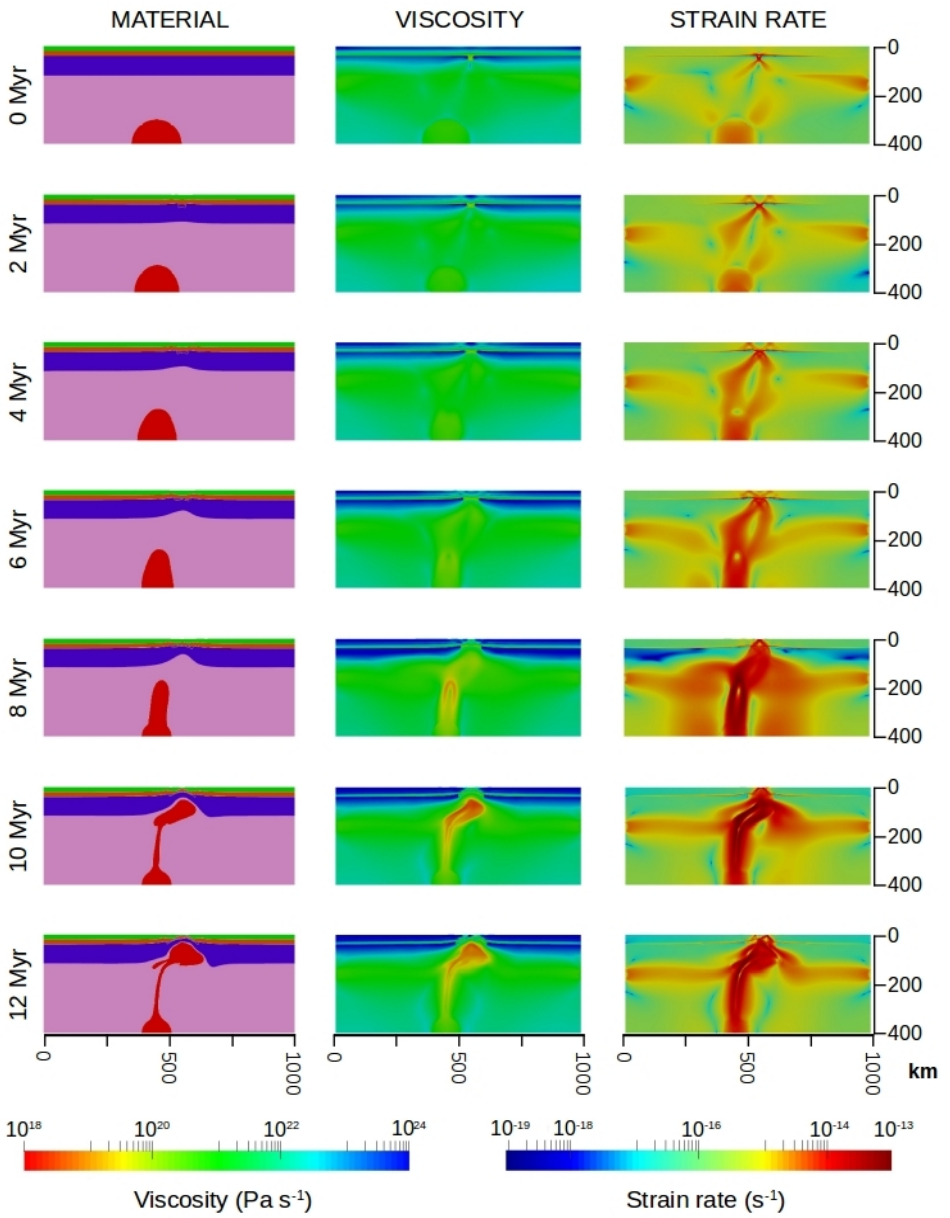

Figure 5.3 – Model plots resulting from the simulation set where 1) the lithospheric mantle base temperature is 1300 °C and the model base temperature is 1475 °C, 2) melt is not included in the model and 3) the plume-lithospheric weak seed distance (Δ) is 125 km. Dimensional values are expressed in km. Left column: material deformation (green: upper crust; orange: lower crust; violet: lithospheric mantle; pink: upper mantle; red: plume). Central column: viscosity values. Right column: strain rate values. Color scale in the central and right column is expressed as log10 of the obtained values.

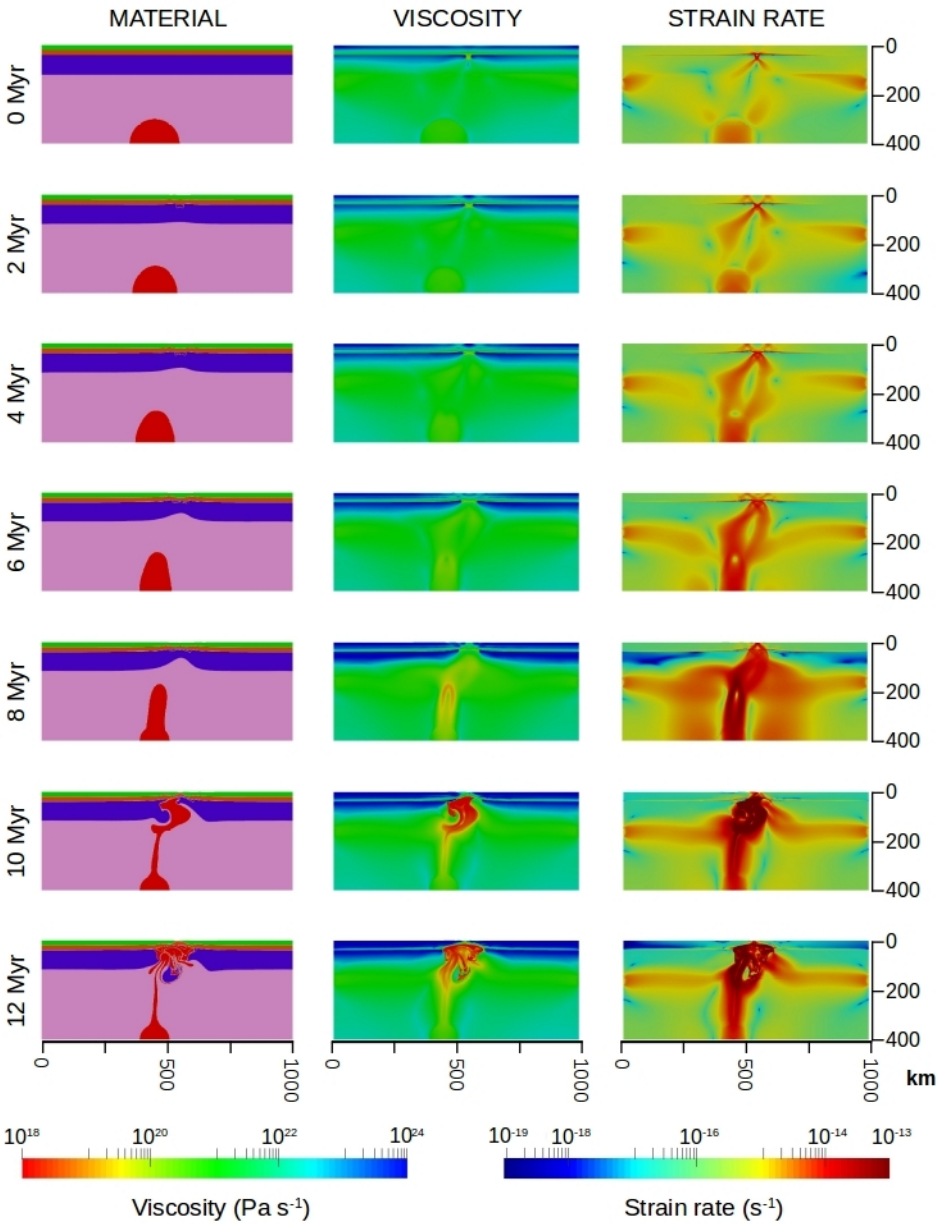

Figure 5.4 – Model plots resulting from the simulation set where 1) the lithospheric mantle base temperature is 1300 °C and the model base temperature is 1475 °C, 2) melt is included in the model and 3) the plume-lithospheric weak seed distance (Δ) is 125. Dimensional values are expressed in km. Left column: material deformation (green: upper crust; orange: lower crust; violet: lithospheric mantle; pink: upper mantle; red: plume). Central column: viscosity values. Right column: strain rate values. Color scale in the central and right column is expressed as log_{10} of the obtained values.

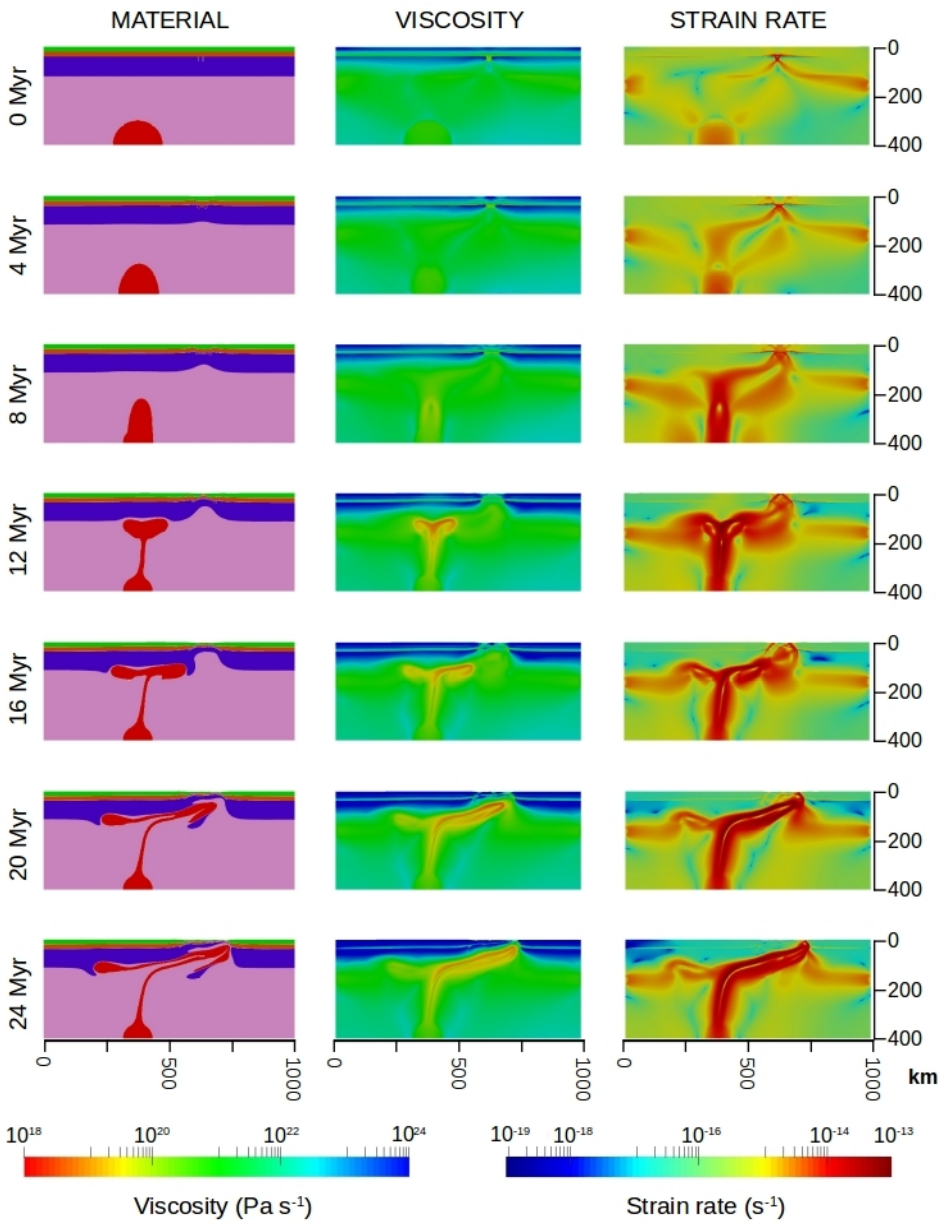

Figure 5.5 – Model plots resulting from the simulation set where 1) the lithospheric mantle base temperature is 1300 °C and the model base temperature is 1475 °C, 2) melt is included in the model and 3) the plume-lithospheric weak seed distance (Δ) is 250 km. The same model configuration shows negligible variations when melting is incorporated. Dimensional values are expressed in km. Left column: material deformation (green: upper crust; orange: lower crust; violet: lithospheric mantle; pink: upper mantle; red: plume). Central column: viscosity values. Right column: strain rate values. Color scale in the central and right column is expressed as log_{10} of the obtained values.

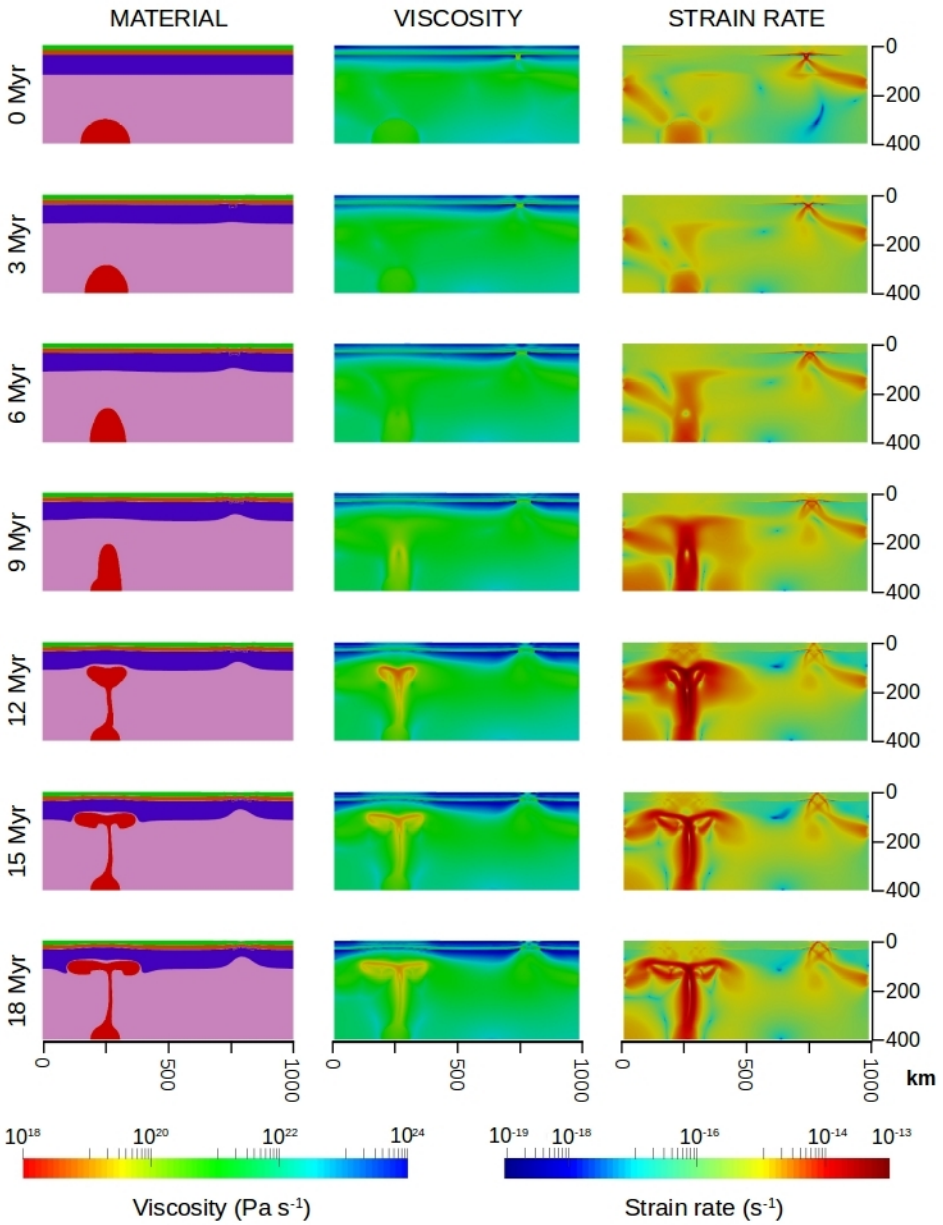

Figure 5.6 – Model plots resulting from the simulation set where 1) the lithospheric mantle base temperature is 1300 °C and the model base temperature is 1475 °C, 2) melt is not included in the model and 3) the plume-lithospheric weak seed distance (Δ) is 500 km. Dimensional values are expressed in km. Left column: material deformation (green: upper crust; orange: lower crust; violet: lithospheric mantle; pink: upper mantle; red: plume). Central column: viscosity values. Right column: strain rate values. Color scale in the central and right column is expressed as log_{10} of the obtained values.

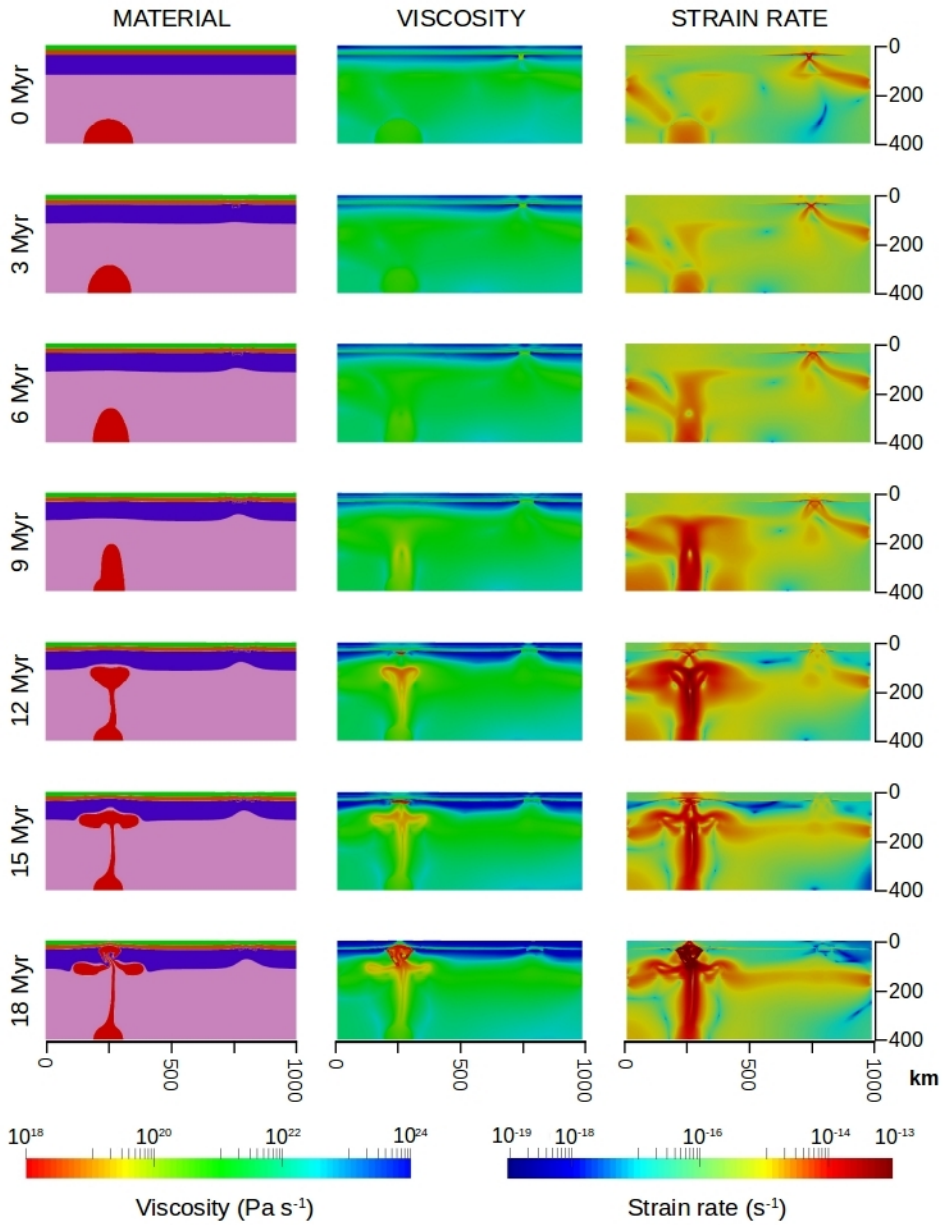

Figure 5.7 – Model plots resulting from the simulation set where 1) the lithospheric mantle base temperature is 1300 °C and the model base temperature is 1475 °C, 2) melt is included in the model and 3) the plume-lithospheric weak seed distance (Δ) is 500 km. Dimensional values are expressed in km. Left column: material deformation (green: upper crust; orange: lower crust; violet: lithospheric mantle; pink: upper mantle; red: plume). Central column: viscosity values. Right column: strain rate values. Color scale in the central and right column is expressed as log_{10} of the obtained values.

When Δ = 250 km (Figure 5.5), the plume exerts a pronounced erosion on the lithospheric mantle on both the developed plate margins, which show a marked asymmetry in plate thickness. Between 19 Myr and 20 Myr after the onset of simulation, part of plume material is channeled through the lithosphere into the asthenospheric wedge beneath the rifting area, with associated delamination of the lithospheric mantle. As a consequence, the plate half-space previously unaffected by the plume presence is now subjected to erosion, with subsequent migration of the rifting area away from the plume. For Δ = 500 km, the lithosphere discontinuity and the plume does not interact (Figure 5.6): the former gives rise to a moderate lithospheric thinning and incipient rift system, while the latter proceeds with lithospheric mantle erosion, accompanied by a slight topographic swelling and crustal thinning. Differently from the previous simulation sets, the plate segment in between the plume and the lithospheric discontinuity is relatively undeformed (with registered strain rate values one magnitude order lower than in the rifting areas), and not subjected to any relevant strain rate for the whole simulation history.

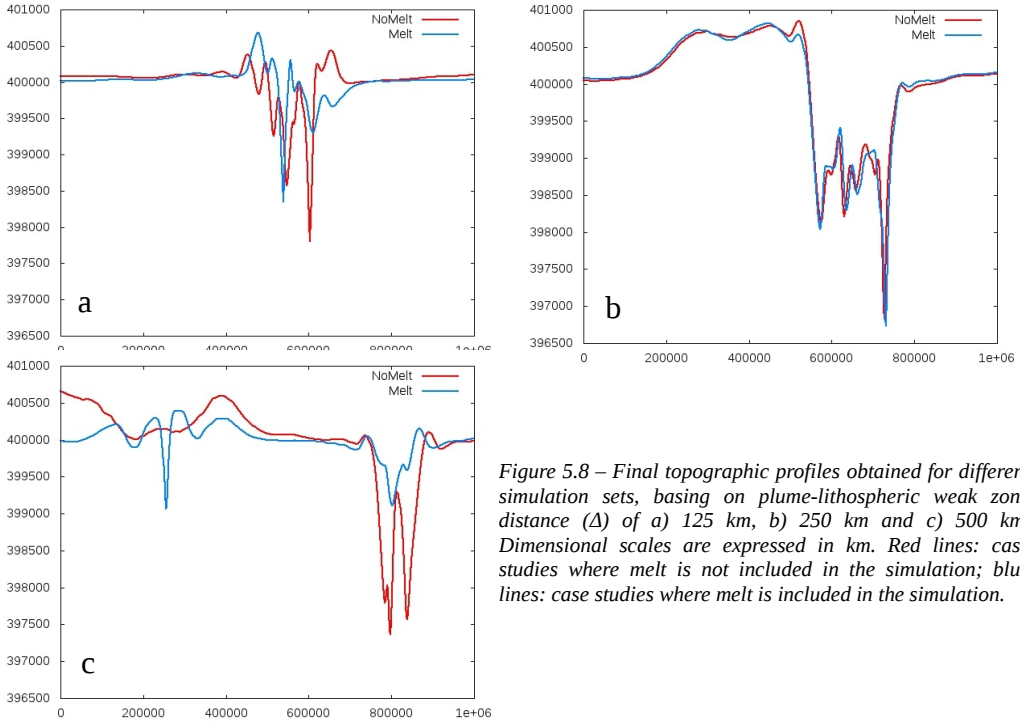

Figure 5.8 – Final topographic profiles obtained for different simulation sets, basing on plume-lithospheric weak zone distance (Δ) of a) 125 km, b) 250 km and c) 500 km. Dimensional scales are expressed in km. Red lines: case studies where melt is not included in the simulation; blue lines: case studies where melt is included in the simulation.

The aforementioned results may show important variations when the melt effect is introduced in the simulations, based on the value of the parameter Δ. In all simulations (Figure 5.4, 5.5, 5.7), the plume is the material subjected to melting, occurring at a depth not greater than 150 km. The start of melt generation slightly post-dates the beginning of lithospheric thermal erosion: this indicates that a previous (although moderate) lithospheric thinning is needed for the beginning of melting in the plume. When the rifting area and the plume impact point on the lithosphere are very close (Δ=125 km) (Figure 5.4), the melt impinged at the base of the lithosphere causes a drop in viscosity values and a dramatic increase of strain rate values on the plate side where the plume

impacts. This determines a more pronounced asymmetric erosion of the mantle lithosphere with respect to the same case study in absence of melt generation, and is accompanied by a marked lithospheric delamination. The emplacement of plume material into the lithosphere occurs through many distinct batches, each of them distinguishable also by different degrees of partial melting (which could reflect into different phases of magmatic activity). However, the asymmetry of the generated rifting is not expressed in the topography, except for a less accentuated depression in the rifting structure, toward the plate side where the plume impinges the lithosphere (Figure 5.8).

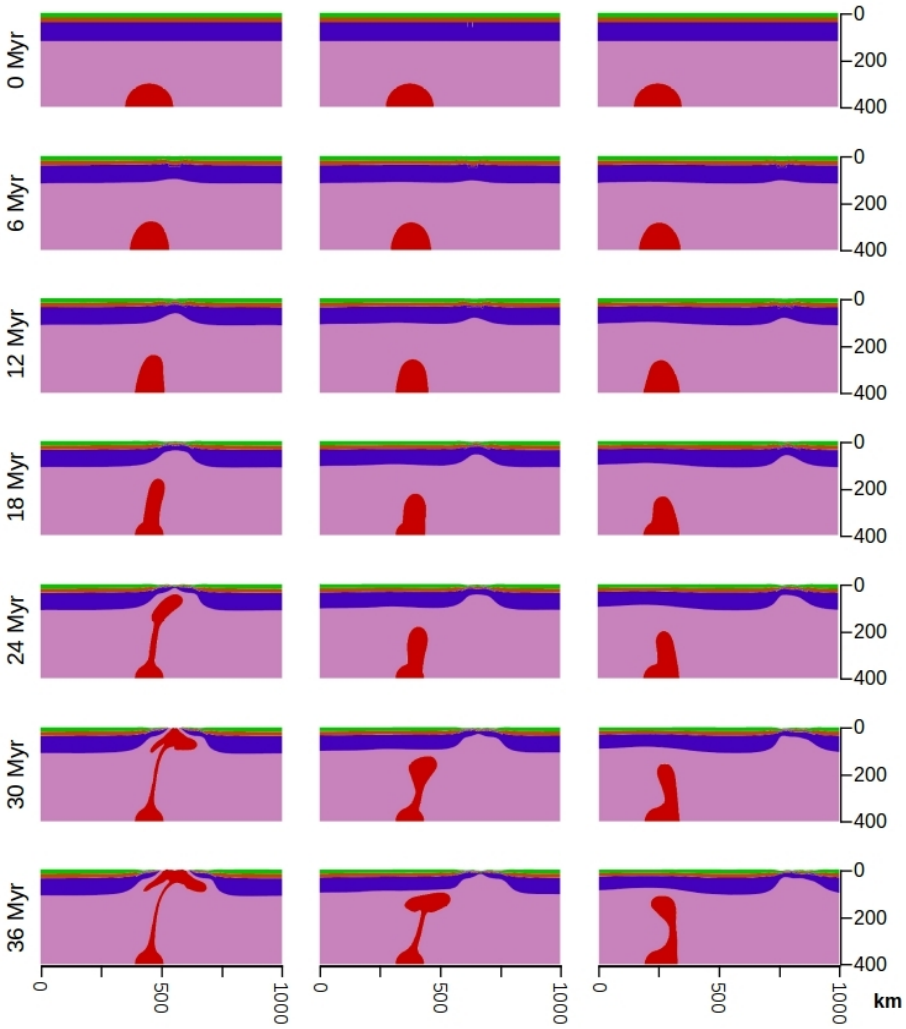

Figure 5.9 – Cross-section plots resulting from the simulation set where 1) the lithospheric mantle base temperature is 1200 °C and the model base temperature is 1400 °C, 2) melt is included in the model and 3) the plume-lithospheric weak seed distance (Δ) is 125 km (left column), 250 km (central column) and 500 km (right column). Dimensional values are expressed in km. Images are referred to the material deformation. Green: upper crust; orange: lower crust; violet: lithospheric mantle; pink: upper mantle; red: plume.

If the distance Δ is increased to a value of 250 km (Figure 5.5), the melt underplating starts at the plume impingement point, and subsequently propagates towards the extended lithospheric thinning area. However, in this simulation set the presence of melt does not cause a drop in viscosity, despite its abundance, except for very small intervals. This occurs because melts generated by plume material channeled into the rifting area are widely distributed along the lithosphere. As a consequence, the local volume of melt is smaller than in the previous case, and their temperature is above the solidus for a very limited time span. Thus, the viscosity does not drop sufficiently long to cause the initiation of other potential rifts. This response is also reflected by the topography, which is equal for the simulation sets with and without melt generation (Figure 5.8).

For Δ = 500 km, the strain concentrates in the first 11 Myr in proximity of the lithospheric weakness, leading to the necking of the lithosphere (Figure 5.7). At this time, we predict the first presence of melt at the Moho, with associated drop in viscosity. This leads to a fast strain transfer from the previous location of lithospheric thinning and extension to a new location, above the plume impingement point. The very high temperatures reached and the accumulation of melt in this location greatly contribute to the concentration of strain in this new rifting area. The process of lithosphere erosion becomes particularly efficient after 15 Myr, when the lithosphere has been almost completely penetrated by plume material. The activation of this rifting area implies the abandonment of the previous rifting location, that becomes progressively inactive. The importance of the melt contribution can also be noted from the topographic trend of the model free surface (Figure 5.8): in the melt simulation set, the model predicts two rift structures of similar depth, whereas in the no-melt simulations a very deep rift is associated with a moderate topographic swell.

When a colder mantle geotherm and plume temperature are adopted, in both the upper mantle and the plume the model predicts a marked increase in viscosity, and an associated decrease in plume uprising velocity. This contributes to a further cooling of the plume material before reaching the base of the lithosphere. As a consequence, the lithospheric erosion is not as effective as in the previous simulation seta, and occurs about 10 Myr after the onset of plate thinning (Figure 5.9). In addition, when the plume impacts the lithosphere, it is effectively channeled into the center of an already well delineated rift system, even though the decompression-related partial melting does not occur only along the rift axis, but is more concentrated along the plate side above the plume. Our model predicts an asymmetric melt distribution for Δ less than 250 km, despite that the low temperature and the increased viscosity do not favor any pronounced asymmetry of plate margins. If Δ is increased to a value of 500 km, the rifting is completely controlled by the presence of the lithospheric weakness, with the presence of a plume causing plate thinning at the impact point ($\beta_{lithosphere}$<1.4) and negligible topography swelling.

5.4 Discussion

In our model the effectiveness of thermo-mechanical erosion due to the plume impact over the lithosphere mostly depends on two parameters: 1) the relative lateral distance between plume and lithospheric thinning area, and 2) the upper mantle and plume temperature (hence, viscosity). If the effect of melts is not incorporated in the simulations, the lithospheric strength reduction related to plume erosion is generally modest, in agreement with findings by Brune et al. (2013). This leads to a controlling role of the preexisting lithospheric structure in determining the location of thinning and extension: we have observed that when models do not include the possibility of melting for mantle materials, the presence of zones of strain localization is pivotal for the

development of rifting basins, in agreement with Franke (2012) and Koptev et al. (2015). At short distances between lithospheric heterogeneities and plume, the lithospheric structure affects the pattern of the rising plume in the upper mantle, since it determines the location where the asthenospheric wedge that underlies the lithospheric rift occurs. In such conditions, the plume head flattens at the lithosphere-mantle boundary, in agreement with previous findings (Burov et al., 2007; Guillou-Frottier et al., 2012; Burov and Gerya, 2014; Koptev et al., 2015), resulting in delamination in the lithospheric mantle (e.g. Burov and Gerya, 2014) that becomes progressively asymmetric in the process. The lithosphere erosion is preferentially concentrated at the top of the plume impact point, and is accompanied by down-thrusting at both sides of the flattening plume head.

In cases where the lithospheric weakness plays a key role in the location of the rifting area, the contribution given by the buoyancy forces associated with the plume presence may strongly influence the characteristics of rifts during their evolution. According to Huismans et al. (2001), the forces associated with the plume impingement beneath the lithosphere may become predominant in the synrift-to-postrift phases. Our model shows that when the distance between plume and lithospheric extensional area is equal or less than 250 km, the plume presence causes fast lithospheric consumption, that favors the growth of the asthenospheric wedges beneath the rifting area. Furthermore, the asymmetric thickness variations of the lithosphere-asthenosphere boundary (LAB) caused by the plume (including the lithospheric down-thrusting at the sides of the plume head) may lead to a steady-state migration of the rifting and the creation of asymmetric margins, with one margin hyper-extended. Asymmetric margins are not uncommon (e.g. Gaina et al., 2007) and have been already reproduced in numerical models (e.g. Brune 2014), but we suggest that plumes may also play a role in their development and evolution. In addition, plume material may be channeled away from the lithosphere impingement point, across the lithosphere and toward the rifting area, and erode the lithosphere on the opposite rifting margin. The resulting erosive effect, coupled with the plate-related far field stresses, promotes the asymmetry of the two margins and the migration of the rifting area far from the plume. This integrates the results obtained by Brune et al. (2016), where a marked asymmetry developed in plate margins promotes rifting migration at further evolution stages.

The effects of melting on the rift evolution show a marked dependence on both the distance between the plume and lithospheric weak zones and the upper mantle thermal state, but this relationship is not simple to predict. When the plume is located in proximity of the lithospheric heterogeneity, plume material is directly channeled in the asthenospheric rifting wedge, with subsequent high temperature and upwelling velocity. It derives that temperatures predicted in the plume are high enough to allow extensive partial melting of mantle materials. In this framework the high amount of melt intruded at the crust-mantle boundary determines a marked viscosity drop and leads to a very effective lithospheric mantle delamination. This is mostly concentrated on the rifting margin where the plume directly impacts against the lithosphere. The consequences of this asymmetric distribution of lithospheric erosion are two-fold: 1) this may lead to an asymmetric distribution of volcanism, and 2) the very effective replacement of the lithosphere by hotter and less dense plume material may lead to a topographic swelling at the rifting margin where the plume is located.

Asymmetric distribution of volcanism along magmatic passive margins has been observed in previous studies (e.g. Holbrook et al., 2001). However, melt underplating strongly favors the possibility of magmatic activity concentrated along one of the two margins: when melt is not included, the plume material is directly channeled in the asthenospheric wedge with a minimum asymmetric erosion of the plate margins, due to the high viscosity of the lithosphere. Differently, when melt underplating occurs, the viscosity drop due to the loss of cohesion in the lithosphere

determines a strong concentration of strain in the plate margin where the plume is present. This, however, does not promote rifting migration when lithosphere weak zones and plume are very close, because plume material is still effectively channeled in the asthenospheric wedge which is connected to the lithospheric heterogeneity. Consequently, most erosional effects by the plume material are still confined to the initial extensional area. In addition, when melting is included in the model, temperatures reached in the crust are favorable for an extended anatexis, with subsequent silicic volcanism. Although poorly preserved in the stratigraphic record, silicic melts and volcanic products may constitute a large part of the eruptive stratigraphy (e.g. Bryan et al., 2002), and, at crustal levels, the presence of acidic melts contributes in decreasing rock strength (Arzi, 1978, Rosenberg and Handy, 2005, Lavecchia et al., 2016a, b).

When the distance between lithospheric heterogeneities and plume promotes a marked asymmetry in plate margins, our model indicates a spreading mechanism affecting the melt underplating and the subsequent eruptive and effusive activity. This results in a younging direction of magmatic bodies constituting the Seaward Dipping Reflectors (SDR, e.g. Abdelmalak et al., 2016) towards the rift center, and accompanying/post-dating the development of the passive margins. On the other hand, when melt underplating occurs along a passive margin where lithosphere is strongly thinned (Figure 5.5), temperatures reached at the Moho along the margins are relatively low. As a result, melt intruded at the base of the lithosphere may solidify in a short time span, thus not playing a determinant role for the geodynamic evolution of the margin.

When plume material does not directly interact with areas of lithospheric extension (Figure 5.7), our model shows a major role of melt underplating for the evolution of passive margins. The presence of melt may determine a strong decrease in lithospheric strength along the underplated intervals. In such conditions, the initial rift developed under the lithosphere structural control may be abandoned and the plume assumes a dominant role. The association between rifting areas and hotspots, with subsequent rift jumps and abandoned rifting branches, is observed in many locations, including Iceland (e.g. Garcia et al., 2003), South Atlantic (Brozena and White, 1990) and the Galapagos (Wilson and Hey, 1995). According to our findings, the process of rift jump is not linear, but follows a two-step process: during a first stage the plume erodes the lithosphere and reaches a depth favorable for the beginning of decompression melting; afterwards, the melt underplated at the crust-lithosphere boundary leads to a strength drop sufficient for the plate break-up to occur. This leads to an extended magmatism where the plume impacts the lithosphere, and the strength decrease in the lithosphere may favor a symmetric evolution of the plate margins (see Brune et al., 2016). However, here we point out the importance of 3D models to determine whether a plume-relate rift is not constrained only in proximity of the plume but may determine a plate-scale rifting system (e.g. Burov and Gerya, 2014).

5.5 Conclusions

The interaction between a structurally complex lithosphere and plumes is not simple to predict. A further source of complexity is added when the melt presence is taken into account during the study of the passive margins characteristics. Our study shows that the configuration of a rifting areas may be influenced by the topography of the lithosphere-asthenosphere boundary, thermal state of the mantle and plume presence at different stages of its evolution, and that the presence of melts may have a great impact on the resulting characteristics of passive margins.

The lateral distance between main areas of lithospheric heterogeneity and plumes is a parameter of primary importance of rifting evolution. Lithosphere weak zones determine the location for the initial plate breakup, that may persist in the same area for an extended period of time. Subsequently, our model predicts a close interaction between the rift area generated by

passive stresses and the presence of plumes. When the plume is close enough to be channeled into the rift, the effects of active and passive stress fields sum up, resulting in an acceleration of the lithosphere erosion. In the absence of mantle melting, the erosion is characterized by features depending on the initial distance between plumes and lithospheric heterogeneities: a small distance favors the development of symmetric passive margins, whereas a greater distance is more favorable for asymmetric margins. On the other hand, when a plume is not channeled into areas of lithospheric thinning, and in absence of melting, then its presence does not cause relevant variations over plate evolution.

Melts may cause substantial variations in the evolution of plate margins, when the melt presence exceeds a threshold sufficient to cause a strength drop in the lithosphere, but their role also depends on the relative position of plumes with respect to the rifting area. Melt underplating may favor the evolution of asymmetric passive margins, independently from the preexisting structure of the lithosphere, and appears a key factor in the erosion of the lithosphere acted by plumes: this effect may be so intense that well delineated rifts may be abandoned and new areas of lithospheric breakup may develop over intensely underplated lithospheric intervals, with consequent jumps in rift formation.

6. Conclusions and synthesis

With the results of the crustal and lithosphere-upper mantle numerical models presented in this thesis, I aim to enhance our knowledge on the processes leading to lithosphere extension and breakup. The results are mainly targeted to the study of initial stages of rifting, from initiation of lithospheric necking to dyke intrusion in the continental crust. In addition, I investigated the relationships between “active”, plume-related force fields, and “passive”, plate motion-related stresses. In this context, the findings are particularly relevant for the study of the Afar Rift and Main Ethiopian Rift. These areas are key sectors of the East African Rift system, and connect the Aden Gulf and Red Sea rift to N-NE to the Turkana and Kenya Rift to S-SW (e.g. Corti, 2009, and ref. therein). The area is subjected to plume impingement (e.g. Bastow et al., 2008; 2011; Chang and Van der Lee, 2011; Buiter, 2014, Burov and Gerya, 2014, and ref. therein), that played an important role in its geodynamic evolution, influencing the thermo-mechanical characteristics of the lithosphere and also constituting a magmatic source. In addition, the Afar plume-related magmatic phase is coeval with the Arabia-Eurasia collision phase along the Bitlis-Zagros main thrust, and started at an age of ≈40 Ma (Faccenna et al., 2013). As a result, spreading velocities that affect the rift branches vary from ≈5 mm/yr in the Main Ethiopian Rift (Mahatsente et al., 1999, Bastow et al., 2011, Buiter, 2014) to ≈15 mm/yr in the Afar Rift (McClusky et al., 2010, Buiter, 2014) are measured. The main question this thesis is focused on have been defined in Chapter 1, and are the following:

1. How was the rifting development history influenced by pre-existing lithosphere discontinuities?
2. What are the relationships between mantle plume and passive stress field?

The results obtained during my study help to give answers to these questions, which are provided in this Chapter.

This thesis focused on a series of numerical modelling experiments aimed to investigate the evolution of an heterogeneous continental lithosphere in an extensional geodynamic setting. The models were targeted to study the interaction between “passive” and “active” rifting components, investigating the contributions provided by lithospheric structure, plate-related strain rate or velocity fields, and plume impingement to the development of rifts, and also assessing the conditions that may lead to one dominant factor controlling the evolution of continental extension and breakup. A major emphasis has been given to the transient characteristics that lithosphere rheology may experience, not only due to thermal and petrological variations, but also to melt generation and emplacement. More in detail, I have investigated the space and time variations in rheological features that may be determined by both petrological variations and anatexis in the crust, and mantle material partial melting, accompanied by basaltic migration and underplating.

The results show that lithospheric structure may be pivotal for rifting development, especially during the first stages of continental extension, while plumes may exert a more important role for rift evolution, either in further focusing deformation along the lithosphere-controlled extension, or in determining a diversion of previous rifts. When melt presence is considered, the effectiveness of plume control may be enhanced and plumes may drive lithospheric thinning and breakup.

The initial location and subsequent evolution of continental extension and breakup is strongly controlled by the interaction between lithospheric structure and mantle plumes, and this control may be exerted for the entire rift evolution. This proves particularly important in the case of the Afar and Main Ethiopian rifts. In the East African area, the crystalline basement is constituted by formations piled up during the Panafrican orogeny Previous results indicate that a primary control on rifting location was exerted by inherited basement structures (e.g. Bosworth et al., 2005; Chorowicz et al., 1998; Chorowicz, 2005). The beginning of plume impingement started in the Lake Tana region (Ethiopian Plateau), and subsequently the plume head migrated southward, in response to Africa movement above the plume (e.g. Bonavia et al., 1995; Chorowicz et al., 1998, George et al., 1998). This model is questioned by other studies (e.g. Burke, 1996), stating that Africa was stationary during the last 30 Ma, and that the magmatism pattern may be better explained by the occurrence of two plume heads. In both cases, the lithosphere impinged by the plume has an extension of 1000 km (Chorowicz, 2005, and ref. therein), meaning that the Panafrican suture zones were located above the plume head. My modeling results show that when the plume head is located below or in proximity of lithospheric heterogeneities and weak zones, the lithosphere structure controls the initial location of rifting, even when the lithosphere is affected by extended partial melting and thus strongly weakened. However, in such a case the presence of thick layers of underplated crust may also invoke a melt control over further continental extension, thinning and breakup, depending on the position of the plume in relationship with the lithospheric structure.

In the studied extensional setting, I expect topographic swelling and magmatic phases adjacent to areas of lithosphere extension. Today the Ethiopian plateau is characterized by altitudes higher than 3000 m, and also the Somalian plateau, although characterized by smaller altitudes, is bounded by ≈ 3000 m crests (Chorowicz, 2005, and ref. therein). This does not match the modeling results, which show that the rift shoulder located above the plume head is characterized by a slow, but steady uplift, while the other rift shoulder is subjected to a constant subsidence. However, when the lithospheric weak zone is situated in proximity of the mantle plume, but not above it, this may cause the discrepancy between the observed and modeled topography. If the lithospheric heterogeneity had been located above the spreading plume head, the models could predict uplift of both rift shoulders. As a consequence, I suggest that the pre-existing weak zones in the lithosphere were located above the area subjected to plume impingement. In addition, a slight shift between the lithospheric weak zones and the first impact point of the plume head better fits the observations.

Partial melting of mantle material is an important source for volcanic activity in rifting areas. The models show that in presence of a shift between plume axis and lithospheric heterogeneities, crustal underplating subsequent to plume partial melting tends to first develop on the plate side above the plume impact point, and afterwards to spread laterally towards and beyond the rift axis. This is in agreement with the trend observed in the Ethiopian Plateau-Afar Rift-Somalian plateau area, where plume-related volcanic activity migrates southward (e.g. Bonavia et al., 1995). However, the models also show that plume melting (and thus magmatic activity) may propagate away from the rift axis, which is not observed in the Afar Rift area. This is a pivotal point, since partial melting of mantle material is the primary source for volcanic activity in the East Africas Rift System, as evidenced by previous studies (e.g Schilling et al., 1992; Keller et al., 1994; Rooney et al., 2007; Ayalew and Gibson, 2009) and results published as outcome of this thesis (Lavecchia et al., 2016a, b). Thus, I suggest that the migration of volcanic activity might be better explained by a variable topography of the lithosphere-asthenosphere boundary (LAB). In detail, the lithosphere in the Ethiopian Plateau, where the plume head impact point is located, might have been thicker than the lithosphere in the Somalian Plateau, and a progressive lithospheric thinning

south-southeastward may have led to some plume material channeling and feeding of the magmatic activity, in agreement with the volcanism migration pattern.

If far field stresses related to the Arabia-Eurasia subduction system may control the evolution of Afar Rift, they cannot control the extension in the Main Ethiopian Rift. In this area, extensional velocity is orthogonal to the rift axis during the initial spreading phases and acquires a strike slip component during the Pliocene-Quaternary boundary (Boccaletti et al., 1999). The spreading direction in the Main Ethiopian Rift, especially during the first phases of development, is parallel to the Bitlis-Zagros Main Thrust trend, making the relative far field stress ineffective. In addition, first magmatic activity in the region has been linked to the presence of mantle plumes (e.g. Rooney et al., 2007; Ayalew and Gibson, 2009). This indicates a primary control of the plume on the Main Ethiopian Rift development.

At present day, most strain in the Afar region is accommodated along magmatic segments, without evidence for a marked crustal thinning (e.g. Ebinger and Casey, 2001; Hofstetter and Beyth, 2003; Buck, 2004; 2006, Cornwell et al., 2006). The model results show that melt intruding the crust may cause a progressive, albeit moderate increase in crustal strength, and a switch from ductile to brittle behavior in host rocks. This increase is more pronounced if it is considered that melts may migrate when melt fraction in host rocks exceeds 7 vol% (see Chapter 3). Under these conditions, the melt-depleted host rocks will be constituted only by metamorphosed solid phase, with increased values of cohesion, and their resulting strength will be higher than the one obtained in my models. On the other hand, the partially molten, inner magmatic segment constitutes a weak crustal interval. This may have contributed to localization of the extension in the rift axial region by dyke filling. Furthermore, the increase in host rock strength in proximity of the magmatic segments may provide an alternative explanation for the observed off-axis volcanism in the Main Ethiopian Rift region, occurring in provious studies (e.g. Maccaferri, 2014). High temperatures that develop in the proximity of the intruded melts may also favor crustal anatexis: melt percentages obtained by partial melting of the crust can lead to increased seismic activity, but cannot explain the widespread acidic volcanism in the Afar area. Thus, I suggest that the genesis of silicic melts feeding volcanic activity and plutonism in the region must be ascribed to processes of fractioned crystallization affecting mafic, mantle-related melts, with minor contributions coming from crustal anatexis, in agreement with Rooney et al. (2007) and Ayalew and Gibson (2009).

In conclusion, I suggest that the plume did not control the focusing of the Afar Rift extension and breakup. Rather, deformation has occurred in response to the extensional far-field stresses resulting from the Neotethys closure along the Arabia-Eurasia margin, reactivating pre-existing structures developed during the Panafrican orogeny. This occurred simultaneously with the African Plume impinging the lithosphere, focusing mostly along the lithospheric heterogeneities. The resulting feedback effect strongly favored breakup and, today, causes the concentration of magmatic activity in the Afar Rift. However, in the Norther Main Ethiopian Rift (N-MER) area the plume played a more important role, and constituted the main cause for lithosphere extension and breakup. The presence of the largest mantle thermal anomaly in the N-MER may determine a further progression of the extensional tectonics and an evolution towards continental breakup and seafloor spreading conditions in the area. Based on these results, I expect a further evolution of the area into conditions of seafloor spreading; this is a process that already today affects the Danakil microplate, which is considered as an insulated, oceanic microplate (e.g. Eagles et al., 2002).

6.1 Outlook and suggestions for future research

The research carried out so far could be further developed to verify the assumptions about the key factors controlling the evolution of Afar region. The following points could be studied more in detail:

1. Construction of models in which the plume impingement of the lithosphere occurs simultaneously with the beginning of extension, in order to determine if, in such conditions, the lithosphere structure still plays the key role in determining the location of the onset of rifting.
2. A 3D simulation to better delineate the regional evolution of Afar Rift. In addition, such models would better reflect the Afar geometry.
3. The models discussed in this thesis include data for melting of mantle materials, relative to anhydrous peridotite. These can be expanded by adding and integrating data for hydrated peridotite.
4. Models where the initial LAB topography is not flat should be constructed to study if variations in lithospheric thickness may significantly influence the plume head spreading along the lithosphere (and subsequently magmatism).

References

Abbate E., Passerini P., and Zan L. (1995), Strike-slip faults in a rift area: transect in the Afar Triangle, East Africa. Tectonophysics, 241, 67–97.

Abdelmalak M., Planke S., Faleide J., Jerram D., Zastrozhnov D., Eide S., and Myklebust R. (2016), The development of volcanic sequences at rifted margins: New insights from the structure and morphology of the Vøring Escarpment, mid-Norwegian Margin. J. Geophys. Res., ISSN 2169-9313, doi: 10.1002/2015JB012788.

Acton G., Stein S., and Engeln J. (1991), Block rotation and continental extension in Afar: a comparison to oceanic microplate systems. Tectonics, 10, 501–526.

Andersen T., and Jamtveit B. (1990), Uplift of deep crust during orogenic extensional collapse: a model based on field studies in the Sogn–Sunnfjord region of western Norway. Tectonics, 9, 1097–1111.

Annen C., and. Sparks R. (2002), Effects of repetitive emplacement of basaltic intrusions on thermal evolution and melt generation in the crust, Earth Planet. Sci. Lett., 203, 937–955.

Annen C., Blundy J.D., and Sparks R. (2006), The genesis of intermediate and silicic magmas in deep crustal hot zones, J. Petrol., 47, 505–539, doi:10.1093/petrology/egi084.

Annen. C (2011), Implications of incremental emplacement of magma bodies for magma differentiation, thermal aureole dimensions and plutonism-volcanism relationships. Tectonophysics, 500, 3–10.

Arzi A. (1978), Critical phenomena in the rheology of partially melted rocks, Tectonophysics, 44, 173–184.

Audet P., and Bürgmann R. (2011), Dominant role of tectonic inheritance in supercontinent cycles. Nature Geosci., 4, 184–187, doi: 10.1038/NGEO1080.

Audin L., Quidelleur X., Coulie E., Courtillot V., Gilder S., Manighetti I., Gillot P., Tapponnier P., and Kidane T. (2004), Paleomagnetism and K–Ar and 40Ar/39Ar ages in the Ali Sabieh area (Republic of Djibouti and Ethiopia): constraints on the mechanism of Aden ridge propagation into southeastern Afar during the last 10 Myr. Geophys. J. Int., 158, 327–345.

Ayalew D., and Gibson S.A. (2009), Head-to-tail transition of the Afar mantle plume: Geochemical evidence from a Miocene bimodal basalt–rhyolite succession in the Ethiopian Large Igneous Province, Lithos, 112, 461–476.

Baldridge W., Keller G., Haak V., Wendlandt E., Jiracek G., and Olsen K. (1995), The Rio Grande Rift. In: Olsen K. (Ed.), Continental rifts: evolution, structure, tectonics. Dev. Geotecton., 25, 233-276.

Barberi F., and Varet J. (1977), Volcanism of Afar: small-scale plate tectonics implications. Bull. Geol. Soc. Am., 88, 1251–1266.

Barberi F., Bonatti E., and Marinelli G. (1974), Transverse tectonics during the split of continent: data from the Afar rift. Tectonophysics, 23, 17–19.

Barberi F., Borsi S., Ferrara G., Marinelli G., Santacroce R., Tazieff H., and Varet J. (1972), Evolution of the Danakil Depression (Afar, Ethiopia) in light of radiometric age determinations. J. Geol., 80, 720–729.

References

Barberi F., Santacroce R., and Varet J. (1975), Structural evolution of the Afar triple junction. In: Pilger A., and Rösler A. (Ed.), Afar Depression of Ethiopia, Proceedings of an International Symposium on the Afar Region and Related Rift Problems. Bad Bergzabern, F.R. Germany, April 1–6, 1974, 1. E. Schweizerbart Õsche Verlagsbuchhandlung, Stuttgart, 38–54.

Bassi G. (1991), Factors controlling the style of continental rifting; insights from numerical modelling, Earth Planet. Sci. Lett., 105, 430–452.

Bastow I., and Kleir D. (2011), The protracted development of the continent-ocean transition in Afar. Nature Geosci., 4, 248-250.

Bastow I., Keir D., and Daly E. (2011), The Ethiopia Afar Geoscientific Lithospheric Experiment (EAGLE): probing the transition from continental rifting to incipient seafloor spreading. In: Beccaluva L., Bianchini G., and Wilson M. (Eds.), Volcanism and Evolution of the African Lithosphere. Geol. Soc. Am. Spec. P., 478, 51–76.

Bastow I., Nyblade A., Stuart G., Rooney T., and Benoit M. (2008), Upper mantle seismic structure beneath the Ethiopian hotspot: rifting at the edge of the African low velocity anomaly. Geochem. Geophys. Geosyst., 9, Q12022.

Bastow I., Stuart G., Kendall J. and Ebinger C. (2005), Upper mantle seismic structure in a region of incipient continental breakup: Northern Ethiopian Rift. Geophys. J. Int., 162, 479–493.

Bellhasen N., Faccenna C., Funiciello F., Daniel J., and Jolivet L. (2004), Why did Arabia separate from Africa? Insights from 3-D laboratory experiments. Earth Planet. Sci. Lett., 216, 365-381.

Bergantz G.W. (1989), Underplating and partial melting: implications for melt generation and extraction. Science 245 (4922), 1093–1095.

Berhe S. (1986), Geologic and geochronologic constraints on the evolution of the Red Sea–Gulf of Aden and Afar Depression. J. Afr. Earth Sci., 5, 101–117.

Beutel E., van Wijk J., Ebinger C., Keir D., and Agostini A., (2010), Formation and stability of magmatic segments in the Main Ethiopian and Afar rifts. Earth Planet. Sci. Lett. 293, 225–235.

Bialas R., Buck W., and Qin R. (2010), How much magma is required to rift a continent? Earth Planet. Sci. Lett., 292, 68–78.

Björnnson A., Saemundsson K., Einarsson P., Tryggvason E., and Grönvold K. (1977), Current rifting episode in north Iceland, Nature, 266, 318–323.

Black R., Morton W., and Hailu T. (1974), Early structure around the Afar triple junction. Nature, 248, 496–497.

Black R., Morton W., and Rex D. (1975), Block tilting and volcanism within the Afar in the light of recent K/Ar age data. In: Pilger A., and Rösler A. (Eds.), Afar Depression of Ethiopia, Proceedings of an International Symposium on the Afar Region and Related Rift Problems. Bad Bergzabern, F.R. Germany, April 1–6, 1974, 1. E. Schweizerbart Õsche Verlagsbuchhandlung, Stuttgart, 296–299.

Boccaletti M., Getaneh A., Mazzuoli R., Tortorici L., and Trua T. (1995), Chemical variations in a bimodal magma system: the Plio-Quaternary volcanism in the Dera Nazret area (Main Ethiopian Rift, Ethiopia). Afr. Geosci. Rev. 2, 37–60.

Boccaletti M., Mazzuoli R., Bonini M., Trua T., and Abebe B. (1999), Plio-Quaternary volcanotectonic activity in the northern sector of the Main Ethiopian Rift: relationships with oblique rifting. J. Afr. Earth Sci. 29, 679–698.

Boher M., Abouchami W., Michard A., Albarede F., and Arndt N. (1992), Crustal growth in west Africa at 2.1 Ga. J. Geophys. Res., 97, 345–369.

Bohrson W., and Spera F. (2001), Energy-constrained open-system magmatic processes II: application of energy-constrained assimilation-fractional crystallisation (EC-AFC) model to magmatic systems, J. Petrol., 42(5), 1019–1041.

Bonavia F., Chorowicz J., and Collet B., (1995), Have wet and dry Precambrian crust largely governed Cenozoic intraplate magmatism from Arabia to East Africa? Geophys. Res. Lett., 22, 2337–2340.

Bosworth W., Huchon P., and McClay K. (2005), The Red Sea and Gulf of Aden Basins. J. Afr. Earth Sci., 43, 334-378.

Bott M, and Kusznir N. (1979), Stress distribution associated with compensated plateau uplift structures with application to the continental splitting mechanisms. Geophys. J. R. Astron. Soc., 56, 451-459.

Bott M. (1982), The mechanism of continental splitting. Tectonophysics, 81, 301-309.

Bott M. (1991), Ridge push and associated plate interior stress in normal and hot spot regions. Tectonophysics, 200, 17–32.

Braun J., and Beaumont C. (1989), A physical explanation of the relation between flank uplifts and the breakup unconformity at rifted continental margins, Geology, 17, 760–764.

Brown G., Schmidt D., and Huffman A. (1989), Shield area of western Saudi Arabia, Geology of the Arabian Peninsula. US Geol. Surv. Prof. P., 560-A.

Brown M. (2007), Crustal melting and melt extraction, ascent and emplacement in orogens: Mechanisms and consequences, J. Geol. Soc., 164, 709–730.

Brown M. (2010a), Melting of the continental crust during orogenesis: The thermal, rheological, and compositional consequences of melt transport from lower to upper continental crust, Can. J. Earth Sci., 47, 655–694.

Brown M. (2010b), The spatial and temporal patterning of the deep crust and implications for the process of melt extraction, Philos. Trans. R. Soc. London, Ser. A, 368, 11–51.

Brown M. (2013), Granite: From genesis to emplacement, Geol. Soc. Am. Bull., 125, 1079–1113.

Brozena J., and White R. (1990), Ridge jumps and propagations in the South Atlantic Ocean. Nature, 348, 149-152.

Brune S., Heine C., Pèrez-Gussinyè M., and Sobolev S. (2014), Rift migration explains continental margin asymmetry and crustal hyperextension. Nature Commun., 5:4014, doi: 10.1038/ncomms5014.

Brune S., Popov A., and Sobolev S. (2013), Quantifying the thermo-mechanical impact of plume arrival on continental break-up. Tectonophysics, 604, 51-59, doi: 10.1016/j.tecto.2013.02.009.

Brune S.,Heine C. Clift,, P.D. and Pèrez-Gussinyè M. (2016), Rifted margin architecture and crustal rheology: reviewing Iberia-Newfoundland, central South Atlantic, and South China Sea. Mar. Pet. Geol., 79, 257-281, doi: 10.1016/j.marpetgeo.2016.10.018.

Bryan S., Riley T., Jerram D., Stephens C., and Leat P. (2002), Silicic volcanism: an undervalued component of large igneous provinces and volcanic rifted margins. Geol. Soc. Am. Spec. Pap., 362, 99-120.

Bryan S., Ukstins Peate I., Peate D., Self S., Jerram D., Mawby M., Marsh J., and Miller J. (2010), The largest volcanic eruptions on Earth. Earth Sci. Rev., 102, 207–229, doi:10.1016/j.earscirev.2010.07.001.

Buck W. (1991), Modes of continental lithospheric extension, J. Geophys. Res., 96, 20,161–20,178, doi:10.1029/91JB01485.

Buck W. (2004), Consequences of asthenospheric variability on continental rifting. In: Karner G., Taylor B., Driscoll N., and Kohlstedt D. (Eds.), Rheology and Deformation of the Lithosphere at Continental Margins, 1–31, Columbia Univ. Press, Palisades, N.Y.

References

Buck W. (2006), The role of magma in the development of the Afro-Arabian Rift System. In: Yirgu G., Ebinger C., and Maguire P. (Eds.) The Afar volcanic province within the East African Rift system, Geol. Soc. London, Spec. Publ., 259, 43–54.

Buiter S. (2014), How plumes help to break plates. Nature, 513, 36-37.

Buiter S., and Torsvik T. (2014), A review of Wilson Cycle plate margins: a role for mantle plumes in continental break-up along sutures? Gondwana Res. 26, 627-653, doi: 10.1016/j.gr.2014.02.007.

Bunger A., Menand T., Cruden A., Zhang X., and Halls H. (2013), Analytical predictions for a natural spacing within dyke swarms, Earth Planet. Sci. Lett., 375, 270–279.

Bunter M., Debretsion T., and Woldegiorgis L. (1998), New developments in the pre-rift prospectivity of the Eritrean Red Sea. J. Pet. Geol., 21, 373–400.

Burke K. (1996), The African plate. South Afr. J. Geol., 99 , 339–409.

Burov E, and Gerya T. (2014), Asymmetric three-dimensional topography over mantle plumes. Nature, 513, 85-89, doi:10.1038/nature13703.

Burov E., and Cloetingh S. (2009), Controls of mantle plumes and lithospheric folding on modes of intraplate continental tectonics: Differences and similarities, Geophys. J. Int., 178, 1691–1722.

Burov E., Guillot-Frottier L., d'Acremont E., Le Pourhiet L., and Cloetingh S. (2007), Plume head-lithosphere interactions near intra-continental plate boundaries. Tectonophysics, 434, 15-38, doi: 10.1016/j.tecto.2007.01.002.

Caggianelli A., and Prosser G. (2001), An exposed cross-section of late Hercynian upper and intermediate continental crust in the Sila nappe (Calabria, southern Italy), Period. Min., 70(3), 277–301.

Caggianelli A., and Prosser G. (2002), Modelling the thermal perturbation of the continental crust after intraplating of thick granitoid sheets: A comparison with the crustal sections in Calabria (Italy), Geolog. Mag., 139(6), 699–706.

Camp V., and Roobol M. (1992), Upwelling asthenosphere beneath western Arabia and its regional implications. J. Geophys. Res., 97, 15255–15271.

Carmichael R. (1990), Practical Handbook of Physical Properties of Rocks and Minerals, 741 pp., CRC-Press, Boca Raton, Fla.

Cashman K., and Ferry L. (1988), Crystal size distribution (CSD) in rocks and the kinetics and dynamics of crystallization—III. Metamorphic crystallization, Contrib. Mineral. Petrol., 99, 401–415.

Chang S., and Van der Lee S. (2011), Mantle plumes and associated flow beneath Arabia and East Africa. Earth Planet. Sci, Lett., 302, 448–454.

Chase C. (1978), Plate kinematics: the Americas, East Africa, and the rest of the world. Earth Planet. Sci. Lett., 37, 355–368.

Chessex R., Delaloye M., Muller J., and Weidmann M. (1975), Evolution of the volcanic region of Ali Sabieh (T.F.A.I.) in the light of K–Ar age determination. In: Pilger A., and Rösler A. (Eds.), Afar Depression of Ethiopia, Proceedings of an International Symposium on the Afar Region and Related Rift Problems. Bad Bergzabern, F.R. Germany, April 1–6, 1974, 1. E. Schweizerbart Õsche Verlagsbuchhandlung, Stuttgart, 220–227.

Chorowicz J., Collet B., Bonavia F., Mohr P., Parrot J.F., and Korme T., (1998), The Tana basin, Ethiopia: intra-plateau uplift, rifting and subsidence. Tectonophysics, 295, 351–367.

Chorowicz, J (2005), The East African rift system. J Afr. Sci., 43, 379-410, doi: 10.1016/j.jafrearsci.2005.07.019.

Christensen J., Rosenfeld J., and Depaolo D. (1989), Rates of tectonometamorphic processes from rubidium and strontium isotopes in garnet, Science, 244(4911), 1465–1469.

Christensen J.N., Selverstone J., Rosenfeld J., and DePaolo D. (1994), Correlation by Rb-Sr geochronology of garnet growth histories from different structural levels within the Tauern Window, Eastern Alps, Contrib. Mineral. Petrol., 18, l–12.

Civetta L., De Fino M., Gasparini P., Ghiara M., La Volpe L., and Lirer L. (1975), Geology of central-eastern Afar (Ethiopia). In: Pilger A., and Rösler A. (Eds.), Afar Depression of Ethiopia, Proceedings of an International Symposium on the Afar Region and Related Rift Problems. Bad Bergzabern, F.R. Germany, April 1–6, 1974, 1. E. Schweizerbart Õsche Verlagsbuchhandlung, Stuttgart, 201–206.

Civetta L., De Fino M., La Volpe L., and Lirer L. (1974), Geochemical trends in the alkali basaltic suite of the Assab range (Ethiopia). Chem. Geol., 13, 149–162.

Clauser C. (2009), Heat transport processes in the Earth's crust, Surv. Geophys., 30, 163–191.

Clauser C., and Huenges E. (1995), Thermal conductivity of rocks and minerals, in Rock Physics and Phase Relations: A Handbook of Physical Constants, AGU Ref. Shelf 3, edited by T. J. Ahrens, pp. 105–126, AGU, Washington, D. C.

Cloetingh S., and Wortel R. (1986), Stress in the Indo-Australian plate. Tectonophysics, 132, 49-67.

Cloetingh S., Burov E., Matenco L., Beekman F., Roure F., and Ziegler P.A. (2013a), The Moho in extensional tectonic settings: Insights from thermo-mechanical models, Tectonophysics, 609, 558–604.

Cloetingh S., Burov E., and Francois T. (2013b), Thermo-mechanical controls on intra-plate deformation and the role of plume-folding interactions in continental topography, Gondwana Res., doi:10.1016/j.gr.2012.11.012.

Cloetingh S., Gallart J., de Vicente G., and Matenco L. (2011), TOPO-EUROPE: From Iberia to the Carpathians and analogues, Tectonophysics, 502, 1–27.

Cloetingh S., van Wees J., van der Beek P., and Spadini G. (1995), Role of pre-rift rheology in kinematics of extensional basin formation: constraints from thermomechanical models of Mediterranean and intracratonic basins. Mar. Pet. Geol., 12, 793–807.

Coffin M., and Eldholm O. (1994), Large igneous provinces: crustal structure, dimensions, and external consequences. Rev. Geophys., 32, 1–36.

Coleman R. (1974), Geologic background of the Red Sea. In: Burke C., and Drake C., (Eds.), The Geology of Continental Margins. Springer, Berlin, 813–819.

Coleman R. (1993), Geologic evolution of the Red Sea. Oxford Monogr. Geol. Geophys., 24. Oxford Univ. Pr., Oxford, 186 pp.

Coleman R., Gregory R., and Brown G., (1983), Cenozoic volcanic rocks of Saudi Arabia. USGS Open-File Rep., 83-788.

Collet B., Taud H., Parrot J., Bonavia F., and Chorowicz J. (2000), A new kinematic approach for the Danakil Block using a digital elevation model representation. Tectonophysics, 316, 343–357.

Coltice N., Phillips B., Bertrand H., Ricard Y., and Rey P.(2007), Global warming of the mantle at the origin of flood basalts over supercontinents. Geology 35, 391–394.

Condie, K.(2002), Continental growth during a 1.9 Ga superplume event. J. Geodyn., 34, 249–264.

Cornwell D., Mackenzie G., England R., Maguire P., Asfaw L., and Oluma B. (2006), Northern Main Ethiopian Rift crustal structure from new high-precision gravity data. In: Yirgu G., Ebinger C., Maguire P. (Eds.), The Afar Volcanic Province within the East African Rift System. Geol. Soc. Lond. Spec. Publ., 259, 307–321.

Corti G. (2008) Control of rift obliquity on the evolution and segmentation of the main Ethiopian rift. Nature Geosci., 1, 258–262. doi: 10.1038/ngeo160.

References

Corti G. (2009), Continental rift evolution: From rift initiation to incipient break-up in the Main Ethiopian Rift, East Africa. Earth Sci. Rev., 96, 1–53, doi: 10.1016/j.earscirev.2009.06.005.

Daniels K., Bastow I., Keir D., Sparks R., and Menand T. (2014), Thermal models of dyke intrusion during development of continent-ocean transition, Earth Planet. Sci. Lett., 385, 145–153.

Daradich A., Mitrovica J., Pysklywec R., Willett S., and Forte A. (2003), Mantle flow, dynamic topography, and rift-flank uplift of Arabia. Geology, 31, 901–904.

Davis M., and Kusznir N. (2004), Depth-dependent lithospheric stretching at rifted continental margins. In: Karner, G., Taylor, B., Driscoll, N., Kohlstedt, D. (Eds.), Rheology and Deformation of the Lithosphere at Continental Margins. Columbia Univ. Press, pp. 92–137.

De Chabalier J., and Avouac J. (1994), Kinematics of the Asal rift, Djibouti, determined from the deformation of the Fieale volcano. Science, 265, 1677-1681.

Debayle E., Lévêque J., and Cara M. (2001), Seismic evidence for a deeply rooted low-velocity anomaly in the upper mantle beneath the northeastern Afro/Arabian continent. Earth Planet. Sci. Lett., 193, 423–436.

Deer W., Howie R., and Zussman J. (2013), An Introduction to the Rock-Forming minerals. Mineral. Soc., London, UK, pp. 498.

Del Moro A., Fornelli A., and Piccarreta G. (2000), Tectonothermal history of the Hercynian continental crust of the Serre (southern Calabria, Italy) monitored by Rb/Sr biotite resetting, Terra Nova, 12, 239–244.

Delibrias G., Marinelli G., and Stieltjes L. (1975), Spreading rate of the Asal Rift: a geological approach, Stuttgart. In: Pilger A., and Rösler A. (Eds.), Afar Depression of Ethiopia, Proceedings of an International Symposium on the Afar Region and Related Rift Problems. Bad Bergzabern, F.R. Germany, April 1–6, 1974, 1. E. Schweizerbart Õsche Verlagsbuchhandlung, Stuttgart, 201–206.

Dewey J. (1988), Extensional collapse of orogens. Tectonics, 7, 1123–1139.

Dewey J., and Bird J. (1970), Mountain belts and the new global tectonics. J. Geophys. Res, 75, 225–264.

Dingwell D. (1995), Viscosity and anelasticity of melts. In: Ahrens, T. (Ed.), Mineral Physics and crystallography. A handbook of physical constants, AGU Reference shelf2. Am. Geophys. Union, Washington DC, 209-217.

Dixon T., Stern R., and Hussein I. (1987), Control of Red Sea rift geometry by precambrian structures. Tectonics, 6, 551–571.

Dugda M., Nyblade A., and Julia J. (2007), Thin lithosphere beneath the Ethiopian Plateau revealed by a joint inversion of Rayleigh wave group velocities and receiver functions. J. Geophys. Res. 112, b08305. doi: 10.1029/2006jb004918.

Dugda M., Nyblade A., Julia J., Langston C., Ammon C., and Simiyu S. (2005), Crustal structure in Ethiopia and Kenya from receiver function analysis: implications for rift development in eastern Africa. J. Geophys. Res. 110, B01303. doi: 10.1029/2004JB003065.

Dunbar J., and Sawyer D. (1989), How pre-existing weaknesses control the style of continental breakup, J. Geophys. Res., 94, 7278–7292, doi:10.1029/JB094iB06p07278.

Dziewonski A., Lekic V., and Romanowicz B. (2010), Mantle anchor structure: an argument for bottom up tectonics. Earth Planet. Sci. Lett., 299, 69–79.

Eagles G., Gloaguen R., and Ebinger C. (2002), Kinematics of the Danakil microplate. Earth Planet. Sci. Lett., 203, 607-620.

Ebinger C., and Casey M. (2001), Continental breakup in magmatic provinces: an Ethiopian example. Geology 29, 527–530. doi: 10.1130/0091-7613(2001)029b0527:CBIMPAN2.0.CO;2.

Ebinger C., and Sleep N. (1998), Cenozoic magmatism throughout east Africa resulting from impact of a single plume. Nature, 395, 788–791.

Ebinger C., Jackson J., Foster A., Hayward N., McKenzie D., Kusznir N., Louden K., Watts A., Menzies M., and Roberts A. (1999), Extensional basin geometry and the elastic lithosphere, Philos. Trans. R. Soc. London, Ser. A, 357, 741–765.

Ebinger C., Yemane T., WoldeGabriel G., Aronson J., Walter R. (1993), Late Eocene–Recent volcanism and faulting in the southern main Ethiopian rift. J. Geol. Soc., Lond., 150, 99–108.

England P., and Thompson A. (1984), Pressure–temperature–time paths of regional metamorphism I. Heat transfer during the evolution of regions of thickened continental crust. J. Petrol. 25, 894–928.

Faccenna C., Becker T., Jolivet L., and Keskin M. (2013), Mantle convection in the Middle East: reconciling Afar upwelling, Arabia indentation and Aegean trench rollback. Earth Planet. Sci. Lett., 375, 254-269, doi: 10.1016/j.epsl.2013.05.043.

Fischer R., and Gerya T. (2016), Early Earth plume-lid tectonics: a high resolution 3D numerical modelling approach. J. Geodyn., 100, 198-214, doi: 10.1016/j.jog.2016.03.004.

Fitton J., Mahoney, J., Wallace P., and Saunders A. (2004), Leg 192 synthesis: origin and evolution of the Ontong Java plateau. Proc. Ocean Drilling Program. Scientific Results 192, 1–18.

Forsyth D., and Uyeda S. (1975), On the relative importance of the driving forces of plate motion. Geophys. J. R. Astron. Soc., 43, 163-200.

Forte A., and Mitrovica J. (2001), Deep-mantle high-viscosity flow and thermochemical structure inferred from seismic and geodynamic data. Nature, 410, 1049–1056.

Franke D. (2012), Rifting, lithosphere breakup and volcanism: Comparison of magma-poor and volcanic rifted margins, Mar. Pet. Geol., 43, 63-87, doi: 10.1016/j.marpetgeo.2012.11.003

Furlong K., and Fountain D. (1986), Continental Crustal Underplating: Thermal Considerations And Seismic-Petrologic Consequences. J. Geophys. Res., 91, B8, 8285-8294.

Furman T., Bryce J., Rooney T., Hanan B., Yirgu G., and Ayalew D. (2006), Heads and tails: 30 million years of the Afar plume. In: Yirgu G., Ebinger C., and Maguire P. (Eds.), The Afar volcanic province within the East African Rift System: Geol. Soc. Spec. Publ., 259, 95–119.

Gaidies F., Pattison D., and de Capitani C. (2011), Toward a quantitative model of metamorphic nucleation and growth, Contrib. Mineral. Petrol., 162, 975–993.

Gaina C., Muller R., Brown B., Ishihara T., and Ivanov S. (2007), Breakup and early seafloor spreading between India and Antarctica. Geophys. J. Int., 170, 151–169.

Garcia S., Arnaud N., Angelier J., Bergerat F., and Homberg C. (2003), Rift jump process in Northern Iceland since 10 Ma from 40Ar/39Ar geochronology. Earth Planet. Sci. Lett., 214, 529-544.

George R., Rogers N., and Kelley S. (1998), Earliest magmatism in Ethiopia: evidence for two mantle plumes in one flood basalt province. Geology, 26, 923–926.

Gerya T. (2010), Introduction to Numerical Geodynamic Modelling, 345 pp., Cambridge Univ. Press, U. K.

Ghebreab W. (1998), Tectonics of the Red Sea region reassessed. Earth Sci. Rev., 45, 1–44.

Ghebreab W., Carter A., Hurford A., and Talbot C. (2002), Constraints for timing of extensional tectonics in the western margin of the Red Sea in Eritrea. Earth Planet. Sci. Lett., 200, 107–119.

Gleason G. and Tullis J. (1995), A flow law for dislocation creep of quartz aggregates determined with the molten salt cell. Tectonophysics 247, 1–23.

Gouin P. (1979), Earthquake history of Ethiopia and the Horn of Africa. Int. Dev. Res. Cent., Ottawa, Ontario, Publ. 118e, 259 p.

Grand S. (2002), Mantle shear-wave tomography and the fate of subducted slabs. R. Soc. London Philos. Trans., ser.A, 360, 2475-2491.

Greenwood W. (1972), The Hail Arch: a key to the Arabian shield during evolution of the Red Sea Rift. Geol. Soc. Am., Abstr. Prog., 4, 520.

Griffiths R., and Campbell I. (1990), Stirring and structure in starting mantle plumes. Earth Planet. Sci. Lett., 99, 66–78.

Guidarelli M., Stuart G., Hammond J., Kendall J., Ayele A., and Belachew M. (2011), Surface wave tomography across Afar, Ethiopia: crustal structure at a rift triple-junction zone. Geophys. Res. Lett. 38, L24313. doi: 10.1029/2011GL046840.

Guillou L., and Jaupart C. (1995), On the effect of continents on mantle convection. J. Geophys. Res., 100, 24217–24238.

Guillou-Frottier L., Burov E., Cloetingh S., Le Goff I.,. Deschamps Y,. Huet B, and Bouchot V. (2012), Plume-induced dynamic instabilities near cratonic blocks: Implications for P-T-t paths and metallogeny. Glob. Planet. Change , 90-91, 37-50.

Hansen S., and Nyblade A. (2013), The deep seismic structure of the Ethiopian/Afar hotspot and the African superplume. Geophys. J. Int., 194, 118-124.

Hansen S., Schwartz S., Al-Amri A., and Rodgers A. (2006), Combined plate motion and density-driven flow in the asthenosphere beneath Saudi Arabia: evidence from shear-wave splitting and seismic anisotropy. Geology, 34, 869–872.

Hawkesworth C., Turner S., McDermott F., Peate D., and van Calsteren P. (1997), U-Th Isotopes in Arc Magmas: Implications for Element Transfer from the Subducted Crust Science, 276, 551–555.

Hayward N., and Ebinger C. (1996), Variations in the along-axis segmentation of the Afar Rift system, Tectonophysics, 15, 244–257.

Hempton M. (1987), Constraints on Arabian plate motion and extensional history of the Red Sea. Tectonics, 6, 687–705.

Hill R. (1991), Starting plumes and continental break-up. Earth Planet. Sci. Lett., 104, 398–416.

Hjartardóttir A., Einarsson P., Bramham E., and Wright T. (2012), The Krafla fissure swarm, Iceland, and its formation by rifting events, Bull. Volcanol., 74, 2139–2153, doi:10.1007/s00445-012-0659-0.

Hoffman C., Courtillot V., Feraud P., Rochette P., Yirgu E., Ketefo E., and Pik R. (1997), Timing of the Ethiopian flood basalt event: implications for plume birth and global change. Nature, 389, 838-841.

Hofstetter A., and Beyth M. (2003), The Afar Depression: interpretation of the 1960–2000 earthquakes. Geophys. J. Int., 155,715–732.

Holbrook W., Larsen H., Korenaga J., Dahl-Jensen T., Reid I., Kelemen P., Hopper J., Kent G., Lizarralde D., Bernstein S., Detrick R. (2001), Mantle thermal structure and active upwelling during continental breakup in the North Atlantic. Earth Planet. Sci. Lett., 190, 251-266.

Holbrook W., Purdy G., Collins J., Sheridan R., Musser D., Glover L., Talwani M., Ewing J., Hawman R., and Smithson S. (1992), Deep velocity structure of rifted continental crust,

U.S. Mid-Atlantic Margin, from wide-angle reflection/refraction data, Geophys. Res. Lett., 19, 1699–1702, doi:10.1029/92GL01799.

Holland T., and Powell R. (1998), An internally consistent thermodynamic data set for phases of petrological interest, J. Metamorph. Geol., 16, 309–343.

Holness M., and Sawyer E. (2008), On the pseudomorphing of melt-filled pores during the crystallization of migmatites, J. Petrol., 49, 1343–1363.

Houseman G., McKenzie D., and Molnar P. (1981), Convective instability of a thickened boundary layer and its relevance for the thermal evolution of continental convergent belts. J. Geophys. Res., 86, 6115–6132.

Huismans R., Buiter S., and Beaumont C. (2005), Effect of plastic-viscous layering and strain softening on mode selection during lithospheric extension, J. Geophys. Res., 110, B02406, doi:10.1029/2004JB003114.

Huismans R., Podladchikov Y., and Cloetingh S. (2001), Transition from passive to active rifting: Relative importance of asthenospheric doming and passive extension of the lithosphere. J. Geophys. Res., 106, B6, 11271-11291.

Incropera F., DeWitt D., Bergman T., and Lavine A. (2006), Fundamentals of heat and mass transfers, 997 pp., Wiley, Hoboken, N. J.

Ito G., and van Keken P. (2007), Hot spots and melting anomalies. In: Bercovici D., and Schubert G. (Eds.), Treatise on geophysics vol.7: Mantle dynamics. Elsevier, 371-435.

Jessop A., and Trevor L. (1978), Heat flow and heat generation in the superior province of the Canadian shield, Tectonophysics, 50(1), 55–77.

Ji S., and Zhao P. (1993), Flow laws of multiphase rocks calculated from experimental data on the constituent phases, Earth Planet. Sci. Lett., 117, 181–187.

Ji S., Zhao P., and Bia X. (2003), Flow laws of multiphase materials and rocks from end-member flow laws, Tectonophysics, 370, 129–145.

Kachanov L. (2004), Fundamentals of the Theory of Plasticity. Dover Publ. INC., N.Y., pp. 512.

Karato S. (2008), Deformation of Earth Materials, 463 pp., Cambridge Univ. Press, U.K.

Karato S., and Wu P. (1993), Rheology of the upper mantle: a synthesis. Science, 260, 771-778.

Kazmin V. (1971), Precambrian of Ethiopia. Nature, 230, 176–177.

Kazmin V., and Garland C. (1973), Evidence of Precambrian block-faulting in the western margin of the Afar depression, Ethiopia. Geol. Mag., 110, 55–57.

Kazmin V., Shifferaw A., and Balcha T. (1978), The Ethiopian basement: stratigraphy and possible manner of evolution. Geologische Rundschau, 67, 531–546.

Kazmin V., Shifferaw A., and Balcha T. (1978), The Ethiopian basement: stratigraphy and possible manner of evolution. Int. J. Earth Sci. 67, 531–546.

Keir D., Ebinger C., Stuart G., Daly E., and Ayele A. (2006), Strain accommodation by magmatism and faulting as rifting proceeds to breakup: Seismicity of the northern Ethiopian rift, J. Geophys. Res., 111, B05314, doi:10.1029/2005JB003748.

Keir D., Kendall J., Ebinger C., and Stuart G. (2005), Variations in late syn-rift melt alignment inferred from shear-wave splitting in crustal earthquakes beneath the Ethiopian rift. Geophys. Res. Lett. 32, L23308. http://dx.doi.org/10.1029/2005GL024150.

Keller G., Prodehl C., Mechie J., Fuchs K., Khan M., Maguire P., Mooney W., Achauer U., Davies P., Meyer R., Braile L., Nyambok I., and Thompson G. (1994), The East African rift system in the light of KRISP 90. Tectonophysics, 236, 465– 483.

Kenea N., Ebinger C., and Rex D. (2001), Late Oligocene volcanism and extension in the southern Red Sea Hills, Sudan. J. Geol. Soc. Lond., 158, 285–294.

Kirby S. (1985), Rock mechanics observations pertinent to the rheology of the continental lithosphere and the localization of strain along the shear zones, Tectonophysics, 119, 1–27.

References

Kirstein L., Peate,D., Hawkesworth C., Turner S., Harris C., and Mantovani M. (2000), Early Cretaceous basaltic and rhyolitic magmatism in southern Uruguay associated with the opening of the South Atlantic. J. Petrol. 41, 1413–1438.

Koptev A. Calais E., Burov E., Leroy S., and Gerya T. (2015), Dual continental rift systems geerated by plume-lithosphere interactions. Nature Geosci., 8, 388-392, doi:10.1038/NGEO2401

Koptev A., Burov E., Calais E., Leroy S., Gerya T., Guillou-Frottier L., and Cloetingh S. (2015a), Contrasted continental rifting via plume-craton interaction: applications to Central East African Rift. Geosci. Frontiers, 7 221-236, doi: 10.1016/j.gsf.2015.11.002.

Koptev A., Calais E., Burov E., Leroy S., and Gerya T. (2015b), Dual continental rift systems geerated by plume-lithosphere interactions. Nature Geosci., 8, 388-392, doi:10.1038/NGEO2401

Kronenberg A., Kirby S., and Pinkston J. (1990), Basal slip and mechanical anisotropy of biotite, J. Geophys. Res., 95, 19,257–19,278, doi:10.1029/JB095iB12p19257.

Kruhl J., and Vernon R. (2005), Syndeformational emplacement of a tonalitic sheet-complex in a late-Variscan thrust regime: Fabrics and mechanism of intrusion, Monte'E Senes, Northeastern Sardinia, Italy, Can. Mineral., 43, 387–407.

Kruhl J., Erdmann S., and Büttner S. (2007), Brittle-ductile microfabrics in naturally deformed cordierite: Evidence for significant short-term strain-rate variations, J. Struct. Geol., 29, 355–374.

Kusky T., Abdelsalam M., Stern R., and Tucker R. (2003), Evolution of the East African and related orogens, and the assembly of Gondwana (Preface). Precambrian Res., 123, 81–85.

Lachenbruch A. (1968), Preliminary geothermal model of the Sierra Nevada, J. Geophys. Res., 73, 6977–6990, doi:10.1029/JB073i022p06977.

Laporte D., and Watson E. (1995), Experimental and theoretical constraints on melt distribution in crustal sources: The effect of crystalline anisotropy on melt interconnectivity, Chem. Geol., 124, 161–184.

Laube N., and Springer J. (1998), Crustal melting by ponding of mafic magmas: A numerical model, J. Volcanol. Geotherm. Res., 81, 19–35.

Lavecchia A., Clark S., Beekman F., Cloetingh S., and Burov E. (2016a), Thermal perturbation, mineral assemblages and rheology variations induced by dyke emplacement in the crust. Tectonics, 35. doi:10.1002/2016TC004125.

Lavecchia A., Beekman F., Clark S.R., and Cloetingh S. (2016b), Thermo-rheological aspects of crustal evolution during continental breakup and melt intrusion: The Main Ethiopian Rift, East Africa. Tectonophysics, 686, 51–62, doi: 10.1016/j.tecto.2016.07.018.

Le Pichon X., and Gaulier J. (1988), The rotation of Arabia and the Levant fault system. Tectonophysics, 153, 271–294.

Lenardic A., Moresi L., Jellinek A., and Manga M. (2005), Continental insulation, mantle cooling, and the surface area of oceans and continents. Earth Planet. Sci. Lett., 234, 317–333.

Lépine J., and Hirn A. (1992), Seismotectonics in the Republic of Djibouti, linking the Afar Depression and the Gulf of Aden. Tectonophysics, 209, 65–86.

Li C., van der Hilst R., Engdahl R., and Burdick S. (2008), A new global model for P wave speed variations in Earth's mantle. Geochem. Geophys. Geosyst., 9, 5, 21.

Lin S., and van Keken P. (2005), Multiple volcanic episodes of flood basalts caused by thermochemical mantle plumes. Nature, 436, 250–252.

Logg A., Mardal K., and Wells G. (Eds.) (2012), Automated Solution of Differential Equations by the Finite Element Method, 723 pp., Springer, London.

Luth W., Jahns R., and Tuttle O. (1964), The granite system at pressures of 4 to 10 kilobars, J. Geophys. Res., 69, 759–773, doi:10.1029/JZ069i004p00759.

Maccaferri F., Rivalta E., Keir D., and Acocella V. (2014), Off-rift volcanism in rift zones determined by crustal unloading, Nature Geosci., 7, 297–300, doi:10.1038/NGEO2110.

Mackenzie, G., Thybo, H., Maguire, P., 2005. Crustal velocity structure across the Main Ethiopian Rift: results from 2-dimensional wide-angle seismic modelling. Geophys. J. Int., 162, 994–1006, doi: 10.1111/j.1365-246X.2005.02710.x.

Mahatsente R., Jentzsch G., and Jahr T. (1999), Crustal structure of the Main Ethiopian Rift from gravity data: 3-dimensional modeling. Tectonophysics 313, 363–382.

Mahatsente R., Jentzsch G., and Jahr T. (1999), Crustal structure of the Main Ethiopian Rift from gravity data: 3-dimensional modeling. Tectonophysics 313, 363–382.

Makris J., and Ginzburg A. (1987), The Afar depression: transition between continental rifting and sea-floor spreading. Tectonophysics, 141, 199-214.

Malkin B., and Shemenda A. (1991), Mechanism of rifting: considerations based on results of physical modeling and on geological and geophysical data. Tectonophysics 199, 191–210.

Manighetti I., Tapponnier P., Courtillot V., and Gallet Y. (2001), Strain transfer between disconnected, propagating rifts in Afar. J. Geophys. Res., 106, 13613–13665.

Manighetti I., Tapponnier P., Gillot P., Jacques E., Courtillot V., Armijo R., Ruegg J., and King G. (1998), Propagation of rifting along the Arabia–Somalia plate boundary: into Afar. Journal of Geophysical Research, 103, 4947–4974.

Marchildon N., and Brown M. (2002), Grain-scale melt distribution in two contact aureole rocks: Implications for controls on melt localization and deformation, J. Metamorph. Geol., 20, 381–396.

McClusky S., Reilinger R., Ogubazghi G., Amleson A., Healeb B., Vernant P., Sholan J., Fisseha S., Asfaw L., Bendick R., and Kogan L. (2010), Kinematics of the southern Red Sea–Afar Triple Junction and implications for plate dynamics. Geophys. Res. Lett., 37, L05301, doi: 10.1029/2009GL041127.

McKenzie D. (1978), Some remarks on the development of sedimentary basins, Earth Planet. Sci. Lett., 40, 25–32.

McKenzie D., and Morgan W. (1969), Evolution of triple junctions. Nature, 224, 125–13.

McKenzie D., Davies D., and Molnar P. (1970), Plate tectonics of the Red Sea and east Africa. Nature, 226, 243–248.

Menzies M., Klemperer S., Ebinger C., and Baker J. (2002), Characteristics of volcanic rifted margins. In: Menzies M., Klemperer S., Ebinger C., and Baker J. (Eds.), Volcanic Rifted Margins. Geol. Soc. Am. Spec. Paper, 362, 1–14.

Merle O. (2011), A simple continental rift classification. Tectonophysics, 513, 88-95, doi: 10.1016/j.tecto.2011.10.004.

Michaut C., and Jaupart C. (2006), Ultra-rapid formation of large volumes of evolved magma, Earth Planet. Sci. Lett., 250, 38–52, doi:10.1016/j.epsl.2006.07.019.

Mohr P. (1967), The Ethiopian Rift System. Bull. Geophys. Observatory, Addis Ababa, 11, 1–65.

Mohr P. (1983), Ethiopian flood basalt province. Nature ,303, 577–584.

Mohr P. (1991), Nature of the crust beneath magmatically active continental rifts, Tectonophysics, 213, 269–284.

Molly E. (1959), Platinum deposits of Ethiopia. Econ. Geol. 54, 467–477.

Montelli R., Nolet G., Dahlen F., and Masters G. (2006), A catalogue of deep mantle plumes: new results from finite-frequency tomography. Geochem. Geophys. Geosyst. 7, Q11007.

Montelli R., Nolet G., Dahlen F., Masters G., Engdahl E., and Hung S. (2004), Finite-frequency tomography reveals a variety of plumes in the mantle. Science, 303, 338–343.

Moore W., Schubert G., and Tackley P. (1999), The Role of Rheology in Lithospheric Thinning by Mantle Plumes. Geophys. Res. Lett., 26, 8, 1073-1076.

Morgan W. (1971), Convection plumes in the lower mantle. Nature, 230, 42–43.

Morley C. (1988), Variable extension in Lake Tanganyika. Tectonics 7, 785–801.

Morton W., and Black R. (1975), Afar Depression of Ethiopia. In: Pilger, A., and Rösler, A. (Ed.), Afar Depression of Ethiopia, Proceedings of an International Symposium on the Afar Region and Related Rift Problems, Bad Bergzabern, F.R. Germany, April, 1–6, 1974, 1. E. SchweizerbartÕsche Verlagsbuchhandlung, 55–61.

Natali C., Beccaluva L., Bianchini G., and Siena F. (2011), Rhyolites associated to Ethiopian CFB: Clues for initial rifting at the Afar plume axis, Earth Planet. Sci. Lett., 312, 59–68.

Natarov S., and Conrad C. (2012), The role of Poiseuille flow in creating depth-variation of asthenospheric shear, Geophys. J. Int., 190, 1297–1310.

Nelson W., Furman T., and Hanan B. (2008), Sr, Nd, Pb and Hf evidence for two-plume mixing beneath the East African Rift System. Geochim. Cosmochim. Acta, 72, A676.

Nelson W., Furman T., van Keken P., and Lin S. (2007) Two plumes beneath the East African Rift System: a geochemical investigation into possible interactions in Ethiopia. Eos. Trans. AGU 88 (52) Fall Meet. Suppl., Abstract V42B-04.

Olsen K., and P. Morgan (1995), Introduction: progress in understanding continental rifts. In: Olsen K. (Ed.), Continental Rifts: Evolution, Structure, Tectonics. Developments in Geotectonics, vol. 25. Elsevier, Amsterdam, 3–26.

Park Y., Nyblade A., Rodgers A., and Al-Amri A. (2007), Upper mantle structure beneath the Arabian Peninsula and northern Red Sea from teleseismic body wave tomography: implication for the origin of Cenozoic uplift and volcanism in the Arabian Shield. Geochem., Geophys., Geosyst., 8, Q06021.

Park Y., Nyblade A., Rodgers A., and Al-Amri A. (2008), S wave velocity structure of the Arabian Shield upper mantle from Rayleigh wave tomography. Geochem. Geophys. Geosyst., 9, Q07020.

Passerini P., Marcucci M., Sguazzoni G., Zan L., and Haga A. (1991), Strike-slip faults parallel to crustal spreading axes: data from Iceland and the Afar Depression. Terra Nova, 3, 607–618.

Paterson S., Fowler Jr. T., Schmidt K., Yoshinobu A., Yuan E., and Miller R. (1998), Interpreting magmatic fabric patterns in plutons. Lithos 44, 53–82.

Patiño Douce A., and Johnston A. (1991), Phase equilibria and melt productivity in the pelitic system: implications for the origin of peraluminous granitoids and aluminous granulites. Contrib. Mineral. Petrol. 107, 202–218.

Pattison D., and Tinkham D. (2009), Interplay between equilibrium and kinetics in metamorphism of pelites in the Nelson aureole, British Columbia, J. Metamorph. Geol., 27, 249–279.

Phillips B., and Coltice N. (2010), Temperature beneath continents as a function of continental cover and convective wavelength. J. Geophys. Res., 115, B04408–13, 1–13, doi: 10.1029/2009JB006600.

Philpotts A., and Ague J. (2009), Principles of Igneous and Metamorphic Petrology. Camb. Univ. Press, Cambridge,UK, p. 667.

Pik R., Marthy B., Carignan J., and Lave J. (2003), Stability of the upper Nile drainage network (Ethiopia) deduced from (U-Th)/He thermochronometry: implications for uplift and erosion of the Afar plume dome. Earth Planet. Sci. Lett., 215, 73–88.

Platt J., and England P. (1993), Convective removal of lithosphere beneath mountain belts: thermal and mechanical consequences. Am. J. Sci., 293, 307–336.

Poupinet G. (1979), On the relation between P-wave travel time residuals and the age of the continental plates. Earth Planet. Sci. Lett., 43, 149–161.

Purcell P. (1976), The Marda fault zone, Ethiopia. Nature, 261, 569–571.

Ranalli G. (1995), Rheology of the Earth. Chapman and Hall, London, UK, p. 414.

Richards M., Duncan R., and Courillot V. (1989), Flood basalts and hot-spot tracks: Plume heads and tails. Science, 246, 103–107.

Ritsema J., and Allen R. (2003), The elusive mantle plume. Earth Planet. Sci. Lett., 207, 1-12.

Ritter J, Jordan M., Christensen U., and Achauer U. (2001), A mantle plume below the Eifel volcanic fields, Germany. Earth Planet. Sci. Lett. 186, 7–14.

Romanowicz B., and Gung Y. (2002), Superplumes from the core-mantle boundary to the lithosphere: implications for heat flux. Science 296, 513–516.

Rooney T., Furman T., Bastow I., Ayalew D., and Yirgu G. (2007), Lithospheric modification during crustal extension in the Main Ethiopian Rift. J. Geophys. Res. 112, B10201. doi: 10.1029/2006JB004916.

Roscoe R. (1952), The viscosity of suspensions of rigid spheres, Brit. J. Appl. Phys., 3, 267–269.

Rosenberg C., and Handy M. (2005), Experimental deformation of partially melted granite revisited: Implications for the continental crust, J. Metamorph. Geol., 23, 19–28.

Rudnick R., and Gao S. (2003), Composition of the continental crust, in Treatise on Geochemistry, vol. III, edited by H. D. Holland and K.K. Turekian, pp. 1–64, Elsevier.

Ruegg J. (1975), Main results about the crustal and upper mantle structure of the Djibouti region (T. F. A. I.). In: Pilger A., and Rösler A. (Eds.), Afar Depression of Ethiopia, Proceedings of an International Symposium on the Afar Region and Related Rift Problems. Bad Bergzabern, F.R. Germany, April 1–6, 1974, 1. E. Schweizerbart Õsche Verlagsbuchhandlung, Stuttgart, 120–134.

Ruegg J., and Kasser M. (1987), Deformation across the Asal-Ghoubbet Rift, Djibouti, uplift and crustal extension 1979-1986. Geophys. Res. Lett., 14, 745-748.

Ryan P., and Dewey J. (1997), Continental eclogites and the Wilson cycle. J. Geol. Soc. Lond., 154, 437–442.

Rybacki E, and Dresen G. (2000), Dislocation and diffusion creep of synthetic anorthite aggregates. J. Geophys. Res. 105, 260, 17–36.

Rychert C., Hammond J., Harmon N., Kendall J., Keir D., Ebinger C., Bastow I., Ayele A., Belachew M. , and Stuart G. (2012), Volcanism in the Afar Rift sustained by decompression melting with minimal plume influence, Nature Geosci., 5, 406–409.

Sawyer E. (2001), Melt segregation in the continental crust: Distribution and movement of melt in anatectic rocks, J. Metamorph. Geol., 19, 291–309.

Schilling J. (1973), Afar mantle plume: rare earth evidence. Nature Phys. Sci., 242, 2–6.

Schilling J., Kingsley R., Hanan B., and McCully B. (1992), Nd-Sr-Pb isotopic variations along the Gulf of Aden: evidence for Afar mantle plume-continental lithosphere interaction. J. Geophys. Res., 97, 10927–10966.

Schubert G., Turcotte D., and Olson P. (2001), Mantle convection in the Earth and planets. Cambridge University Press, UK, pp. 940.

Searle R. (1975), The dispersion of surface waves across southern Afar. In: Pilger A., and Rösler A. (Eds.), Afar Depression of Ethiopia, Proceedings of an International Symposium on the Afar Region and Related Rift Problems. Bad Bergzabern, F.R. Germany, April 1–6, 1974, 1. E. Schweizerbart Õsche Verlagsbuchhandlung, Stuttgart, 113–120.

Sengor A., and Burke K. (1978), Relative timing of rifting and volcanism on Earth and its tectonic applications. Geophys. Res. Lett., 5, 419-421.

Sengor A., and Yilmaz Y. (1981), Tethyan evolution of Turkey: a plate tectonic approach. Tectonophysics, 75, 181–241.

Shaw H. (1965), Comments on viscosity, crystal settling, and convection in granitic magmas, Am. J. Sci., 263, 120–152.

Shelton G., and Tullis J. (1981), Experimental Flow Laws for Crustal Rocks, Eos Trans, vol. 62, 396 pp., AGU, Washington, D. C.

Shelton G., and Tullis J. (1981), Experimental flow laws for crustal rocks. EOS Trans. Am. Geophys. Union 62, 396.

Sibson R. (1974), Frictional constraints on thrust, wrench and normal faults, Nature, 249, 542–544.

Sichler B. (1980), La biellette danakile: un modéle pour l'évolution géodynamique de l'Afar. Bulletin Société géologique de France, 7, XXII, 6, 925–933.

Sicilia D., Montagner J., Cara M., Stutzmann E., Debayle E., Lépine J., Lévêque J., Beucler E., Sebai A., Roult G., Ayel A., and Sholan J. (2008), Upper mantle structure of shear-waves velocities and stratification of anisotropy in the Afar hotspot region. Tectonophysics, 462, 1–4, 164–177.

Simmons N., Forte A., and Grand S. (2007), Thermochemical structure and dynamics of the African superplume: Geophys. Res. Lett., 34, 2, doi: 10.1029/2006GL028009.

Sleep N., Ebinger C., and Kendall J. (2002), Defection of mantle plume material by cratonic keels In: Fowler C., Ebinger C., and Hawkesworth C. (Eds.), The Early Earth: Physical, Chemical and Biological Development, Geol. Soc. Lond. Spec. Pub. 199, 135-150.

Sobolev S., Sobolev A., Kuzmin D., Krivolutskaya N., Petrunin A., Arndt N., Radko V., and Vasiliev Y. (2011), Linking mantle plumes, large igneous provinces and environmental catastrophes. Nature Lett., 477, 312-316; doi: 10.1038/nature10385.

Solano J., Jackson M., Sparks R., Blundy J., and Annen C. (2012), Melt segregation in deep crustal hot zones: A mechanism for chemical differentiation, crustal assimilation and the formation of evolved magmas, J. Petrol., 53, 1999–2026, doi:10.1093/petrology/egs041.

Sonder L., Wernicke B., and Christiansen R. (1987), A Physical Model for Cenozoic Extension of Western North America, Geol. Soc. London, Spec. Publ., 28, 187–201.

Spear F. (1993), Metamorphic Phase Equilibria and Pressure-Temperature-Time Paths Mineral, 799 pp., Mineral. Soc. Am., Washington, D.C.

Spear F., and Cheney J. (1989), A petrogenetic grid for pelitic schists in the system SiO 2 -Al 2 O 3 -FeO-MgO-K 2 O-H 2 O, Contrib. Mineral. Petrol., 101, 149–164.

Spohn T., and Schubert G. (1983), Convective thinning of the lithosphere: A mechanism for this initiation of continental rifting. J. Geophys. Res., 87, 4669–4681.

Stampfli G., Mosar J., Favre P., Pillevuit A., and Vannay J. (2001), Permo-Mesozoic evolution of the western Tethys realm: the Neo-Tethys East Mediterranean Basin connection. In: Ziegler P., Cavazza W., Robertson A., and Crasquin-Soleau S. (Eds.), Peri-Tethys Memoir 6: Peri-Tethyan Rift/Wrench Basins and Passive Margins, Memoires du Museum National d'Histoire Naturelle de Paris, 186, 51–108.

Stein R., Briole P., Ruegg J., Tapponier P. and Gasse F. (1991), Contemporary Holocene and Quaternary deformation of the Asal rift, Djibouti. Implications for the mechanism of slow spreading ridges. J. Geophys. Res., 96, 789-806.

Stern R. (1994), Arc assembly and continental collision in the Neoproterozoic East African orogen: implications for the consolidation of Gondwanaland. Annu. Rev. Earth Planet. Sci., 22, 319–351.

Symmes G., and Ferry J. (1992), The effect of whole-rock MnO content on the stability of garnet in pelitic schists during metamorphism, J. Metamorph. Geol., 10, 221–237.

Takahashi E. (1986), Melting of a Dry Peridotite KLB-1 up to 14 GPa: Implications on the Origin of Peridotitic Upper Mantle. J. Geophys. Res., 91, B9, 9367-9382.

Takahashi E., Shimazaki T., Tsuzaki Y., and Yoshida H. (1993), Melting study of a peridotite KLB-1 to 6.5 GPa, and the origin of basaltic magmas. Phil. Trans. R. Soc. Lond, 342, 105-120.

Tapponnier P. and Varet J. (1974), La zone de Mak'arrasou en Afar: un équivalent émergé des failles transformantes océaniques. Comptes rendus, Académie des Sciences, Paris 278 (Ser. D), 209–212.

Tapponnier P., Armij R., Manighett I., and Courtillot V. (1990), Bookshelf faulting and horizontal block rotations between overlapping rifts in southern Afar. Geophys. Res. Lett., 17, 1–4.

Tarling D. (1970), Paleomagnetism and the origin of the Red Sea and Gulf of Aden. Phil. Trans. R. Soc. Lond. Series A, 267, 19–226.

Tazieff H., Varet J., Barberi F., and Giglia G. (1971), Tectonic significance of the Afar (or Danakil) depression. Nature, 235, 144–147.

Tefera M., Chernet T. and Haro W. (1996), Explanation of the geological map of Ethiopia. Ethiopian Institute of Geological Surveys, Addis Ababa, 3, 79.

Tesfaye S., Harding D. and Kusky T. (2003), Early continental breakup boundary and migration of the Afar triple junction, Ethiopia. Geol. Soc. Am. Bull., 115, 9, 1053-1067.

Thieulot C. (2011), FANTOM. Two- and three-dimensional numerical modelling of creeping flows for the solution of geological problems. Phys. Earth Planet. Int., 188, 47-68, doi:10.1016/j.pepi.2011.06.011.

Thompson R., Gibson S., and Dickin A. (2001), Early Cretaceous basalt and picrite dykes of the southern Etendeka region, NW Namibia: windows into the role of the Tristan mantle plume in Paraná–Etendeka magmatism. J. Petrol. 42, 2049–2081.

Trubitsyn V., Mooney W., and Abbott D. (2003), Cold cratonic roots and thermal blankets: how continents affect mantle convection. Int. Geol. Rev., 45, 479–496.

Turcotte D., and Emerman S. (1983), Mechanisms of active and passive rifting. Tectonophysics, 94, 39-50.

Ueki K., and Iwamori H. (2013), Thermodynamic model for melting of peridotite. Geochem. Geophys. Geosyst., 14, 342-366, doi:10.1029/2012GC004143.

Ueki K., and Iwamori H. (2014), Thermodynamic calculations of the polybaric melting phase relations of spinel lherzolite. Geochem. Geophys. Geosyst., 15, 5015–5033, doi: 10.1002/2014GC005546.

Ukstins I., Renne P., Wolfenden E., Baker J., Ayalew D., and Menzies M. (2002), Matching conjugate volcanic rifted margins: 40Ar/39Ar chronostratigraphy of pre- and syn-rift bimodal flood volcanism in Ethiopia and Yemen. Earth Planet. Sci. Lett. 198, 289–306. doi: 10.1016/S0012-821X(02)00525-3.

Vail J. (1976), Outline of the geochronology and tectonic units of the basement complex of northeast Africa. Proc. R. Soc. Lond., A 350, 127–141.

Vail J. (1985), Pan African (Late Precambrian) tectonic terrains and the reconstruction of the Arabian Nubian shield. Geology, 13, 839–842.

Vanderhaeghe O. (2001), Melt segregation, pervasive melt migration and magma mobility in the continental crust: the structural record from pores to orogens. Phys. Chem. Earth A 26 (4–5), 213–223.

Varet J. (1978), Geology of central and southern Afar (Ethiopia and Djibouti Republic). In: Gasse F. (Ed.): CNRS, Paris, 118.

Vellutini P. (1990), The Manda-Inakir Rift, Republic of Djibouti: a comparison with the Asal Rift and its geodynamic interpretation. Tectonophysics, 172, 141–153.

Vielzeuf D., and Holloway J. (1988), Experimental determination of the fluid-absent melting relations in the pelitic system. Consequences for crustal differentiation, Contrib. Mineral. Petrol., 98, 257–276.

Vilà M., Fernàndez M. , and I. Jimènez-Munt (2010), Radiogenic heat production variability of some common lithological groups and its significance to lithospheric thermal modelling, Tectonophysics, 490, 152–164.

Wang Z., and Ji S. (1999), Deformation of silicate garnets: Brittle-ductile transition and its geological implications, Can. Mineral., 37, 525–541.

Wasylenki L., Baker M., Kent A., and Stolper E. (2003), Near-solidus Melting of the Shallow Upper Mantle: Partial Melting Experiments on Depleted Peridotite. J. Petrol., 44, 7, 1163-1191.

Whaler K., and Hautot S. (2006), The electrical resistivity structure of the crust beneath the northern Main Ethiopian Rift. In: Yirgu, G., Ebinger, C., Maguire, P. (Eds.), The Afar Volcanic Province Within the East African Rift System. Geol. Soc. Lond. Spec. Publ. 259, pp. 293–305.

White R., and McKenzie D. (1989), Magmatism at rift zones: the generation of volcanic continental margins and flood basalts. J. Geophys. Res., 94, 7685–7729.

Wilson D., and Hey R. (1995), History of rift propagation and magnetization intensity for the Cocos-Nazca spreading center. J. Geophys. Res., 100(B6), 10,041–10,056, doi: 10.1029/95JB00762.

Wilson L. (1981), Ascent and Eruption of Basaltic Magma on the Earth and Moon, J. Geophys. Res., 86, 2971–3001, doi:10.1029/JB086iB04p02971.

Wilson M. (1989), Igneous Petrogenesis, A Global Tectonic Approach. Unwin Hyman, London, pp. 466.

Wilson M. (1993), Plate-moving mechanisms: constraints and controversies. J. Geol. Soc. Lond., 150, 923–926.

Wolfenden E., Ebinger C., Yirgu G., Deino A., and Ayalew D. (2004), Evolution of the northern Main Ethiopian rift: birth of a triple junction. Earth Planet. Sci. Lett. 224, 213–228, doi: 10.1016/j.epsl.2004.04.022.

Wolfenden E., Ebinger C., Yirgu G., Renne P. and Kelley S. (2005), Evolution of a volcanic rifted margin: Southern Red Sea, Ethiopia. Geol. Soc. Am. Bull., 117, 7-8, 846-864.

Woodruff F., and Savin S. (1989), Miocene deepwater oceanography. Paleoceanography, 4, 87–140

Wright T., Ebinger C., Biggs J., Ayele A., Yirgu G., Keir D., and Stork A. (2006), Magma-maintained rift segmentation at continental rupture in the 2005 Afar dyking episode, Nature, 42, 291–294.

Wright T., Freysteinn S., Pagli C., Belachew M., Hamling I., Brandsdóttir B., Keir D., Pedersen R., Ayele A., Ebinger C., Einarsson P., Lewi E., and Calais E. (2012), Geophysical constraints on the dynamics of spreading centres from rifting episodes on land. Nature Geosci., 5, 242-250, doi: 10.1038/NGEO1428.

Wright T., Sigmundsson F., Pagli C, Belachew M., Hamling I., Brandsdóttir B., Keir D., Pedersen R., Ayele A., Ebinger C., Einarsson P., Lewi E., and Calais E. (2012), Geophysical constraints on the dynamics of spreading centres from rifting episodes on land, Nature Geosci., 5, 242–250, doi:10.1038/NGEO1428.

Zanettin B. (1993), On the evolution of the Ethiopian volcanic province. In: Abbate E., Sagri M., and Sassi F. (Eds.), Geology and Mineral Resources of Somalia and Surrounding Regions, Istituto Agronomico per L'Oltremare, Firenze, Relazioni e Monografie Agrarie Subtropicali e Tropicali Nuova Serie, 113, 279–310.

Zanettin B., Justin-Visentin E., and Piccirillo E. (1978), Volcanic succession, tectonics and magmatology in central Ethiopia. Atti Mem. Accad. Patavina Sci. Lett. Arti, 90, 5–19.

Zhou M., Malpas J., Song X., Robinson P., Sun M., Kennedy A., Lesher C., and Keays R. (2002), A temporal link between the Emeishan large igneous province (SW China) and the end-Guadalupian mass extinction. Earth Planet. Sci. Lett., 196, 113–122. doi: 10.1016/S0012-821X(01)00608-2.

Ziegler P. (1978), North Sea rift and basin development. In: Ramberg I., and Neumann E. (Eds.), Tectonics and Geophysics of Continental Rifts, D. Reidel, Dordrecht, 249-277.

Ziegler P. (1982), Geological Atlas of Western and Central Europe. Elsevier, Amsterdam, pp. 130.

Ziegler P. (1992), European Cenozoic rift system. In: Ziegler P. (Ed.), Geodynamics of Rifting, Volume I. Case history studies on rifts: Europe and Asia. Tectonophysics, 208, 91-111.

Ziegler P. (1993), Plate moving mechanisms: their relative importance. J. Geol. Soc. Lond., 150, 927-940.

Ziegler P., and Cloetingh S. (2004), Dynamic processes controlling evolution of rifted basins. Earth Sci. Rev., 64, 1–50.

Zoth G., and Hänel R. (1988), Appendix. In Hänel R., Rybach L., and Stegena L. (Eds.), Handbook of Terrestrial Heat Flow Density Determination. 449–466, Kluwer, Dordrecht, 449-466.

About the author

The author of this thesis was born on May 14, 1985 in Terlizzi, Italy. In 2008 he earned his Bachelor's degree in Geological Sciences, field of study Lithic-mineral resources: assessment and qualification, from Università degli Studi di Bari, Italy, followed in 2012 by a Master's degree (cum laude) in Geological and Geophysical siences, field of study Geologic process modeling, from the same institution. In October 2012 he started his PhD at Simula Research Laboratory, financed by Simula School of Research and Innovation, and since 2014 in the Tectonics Research Group of the Department of Earth Sciences of Utrecht University.